MISSIONE 4
ISTRUZIONE
RICERCA

National Recovery and Resilience Plan (NRRP)
Mission 4, Component 2 (M4C2) – Investment 1.1: Fund for the National Research Programme (NRP) and Research Projects of Significant National Relevance (PRIN)
Call PRIN 2022 PNRR – Directorial Decree no.1409, 14/09/2022

Enhancing our understanding of Subsidence RISK induced by groundwater exploitation towards sustainable urban development

CUP: B53D23033400001

DEL 2.2

Present-day land subsidence risk in Italy

Authors: F. Cigna, R. Paranunzio (CNR-ISAC), R. Bonì (IUSS), P. Teatini (UNIPD)

Version 1.0, Issue date: 30/09/2024
Dissemination level: Public

How to cite this document

CIGNA F., PARANUNZIO R., BONÌ R. & TEATINI P. (2024). *PRIN 2022 PNRR SubRISK+ Deliverable DEL 2.2: Present-day land subsidence risk in Italy*, Version 1.0, Issue date: 30/09/2024, pp. 67. Public Report. Available at: https://www.subrisk.eu/deliverables/

Acknowledgements

The authors would like to thank Dr C. Zoccarato and Prof. M. Zanini at the University of Padua for the fruitful discussions on building vulnerability to land subsidence and differential displacement.

Revision history

Revision no.	*Authors*	*Date*	*Description*
1.0	CIGNA F., PARANUNZIO R., BONÌ R. & TEATINI P.	30/09/2024	First release

Executive summary

Groundwater plays a key role in addressing global water needs. Around 20% of the world's aquifer systems are over-exploited, with outputs (withdrawal and natural discharge) exceeding recharge, resulting in resource depletion, storage loss and compaction. The induced land subsidence causes direct/indirect impacts on urban landscapes (ground depressions, earth fissures, structure damages, increased flood risk, loss of land to water bodies) and economic loss, yet these are often overlooked, and so are considerations on how climate change, population and urban growth may further exacerbate them.

The PRIN 2022 PNRR project *SubRISK+* (https://www.subrisk.eu) [2023–2025] innovates in this field, by providing new Earth Observation (EO)-derived products and tools aiming to: 1) enhance our understanding of subsidence and its impact; 2) empower the community to recognize the human-related behavioural, socio-economic and demographic drivers of this geohazard and its cascading effects on urban environments and ecosystems; and 3) strengthen our ability to consciously use natural resources to make a step-change towards sustainable development.

This report summarizes the results of SubRISK+ Work Package (WP) n.2 (*WP2: National scale risk assessment*), aimed to develop a land subsidence risk assessment methodology at the national scale based on satellite-derived ground displacement observations and land cover data. The methodology exploits interferometric radar datasets from the European Ground Motion Service (EGMS) of the Copernicus Programme, along with urban settlement characteristics from the Global Human Settlement Layer (GHSL) and the World Settlement Footprint (WSF) datasets. These are used to estimate present-day distribution and levels of hazard and exposure-vulnerability across the 15 metropolitan cities of Italy and, in turn, classify and map risk levels.

Over a cumulative investigated area of 54,378 km^2 for the 15 metropolitan cities of Italy and a total urbanized area amounting to 2,665 km^2, about 1.44 km^2 of land revealed high risk levels associated with differential displacement (either subsidence or uplift), mainly concentrated in narrow sectors exhibiting significant angular distortions (and, in some cases, an additive threat due to horizontal strain) occurring over very high exposure-vulnerability infrastructure (private/public buildings) within the cities of Napoli (e.g. Pozzuoli and Bagnoli), Catania, Roma and Messina. In these zones, there is a high likelihood of already occurred/incipient structural damage at urban infrastructure; site inspections to verify the structural health of the buildings and ad hoc mitigation measures are recommended at single-building scale. On the other hand, a medium risk level was identified across the vast majority of the metropolitan areas' land (1351 km^2), where potential structural damage might occur at the urban infrastructure involved; in these areas, tailored monitoring of ground deformation and derived stress indices is recommended at the building block scale. Finally, low risk level is identified across the remaining 1133 km^2, where an acceptable risk level is found and no specific actions are required.

The generated maps provide a baseline risk assessment overview for the 15 metropolitan cities in relation to the process of differential displacement induced by land subsidence/uplift and, as such, could provide valuable inputs for land subsidence-related risk management and mitigation workflows for national land management and urban authorities.

Table of contents

1 INTRODUCTION 5

2 DATA & METHODS 6

2.1 Input datasets 6

2.1.1 Administrative boundaries and population 6

2.1.2 Urban settlement datasets 7

2.1.3 Ground displacement observations 9

2.2 Risk assessment methodology 9

2.2.1 Exposure-Vulnerability (EV) 10

2.2.2 Hazard (H) 11

2.2.3 Risk (R) 13

3 RESULTS 14

3.1 Overview of differential displacement risk in Italy 14

3.2 City-specific differential displacement risk mapping 17

3.2.1 Torino 18

3.2.2 Milano 21

3.2.3 Genova 24

3.2.4 Venezia 27

3.2.5 Bologna 30

3.2.6 Firenze 33

3.2.7 Roma 36

3.2.8 Napoli 39

3.2.9 Bari 42

3.2.10 Reggio Calabria 45

3.2.11 Palermo 48

3.2.12 Messina 51

3.2.13 Catania 54

3.2.14 Sassari 58

3.2.15 Cagliari 61

4 CONCLUSIONS 64

REFERENCES 66

1 INTRODUCTION

SubRISK+: Enhancing our understanding of Subsidence RISK induced by groundwater exploitation towards sustainable urban development is a collaborative research project funded in 2023–2025 in the framework of the Italian National Recovery and Resilience Plan (NRRP), Mission 4, Component 2 (M4C2) – Investment 1.1: Fund for the National Research Programme (NRP) and Research Projects of Significant National Relevance (PRIN) [Call "PRIN 2022 PNRR", D.D. no.1409, 14/09/2022], and led by the National Research Council (CNR) of Italy – Institute of Atmospheric Sciences and Climate (ISAC), in collaboration with the University School for Advanced Studies (IUSS) of Pavia – Department of Science, Technology and Society (STS), and the University of Padua (UNIPD) – Department of Civil, Environmental and Architectural Engineering (ICEA).

The high-level goals of SubRISK+ are to enhance the understanding of land subsidence and its impact in urban environments; empower the community to recognize the human-related behavioural, socio-economic and demographic drivers of this geohazard and its cascading effects; and strengthen our ability to use consciously natural resources to make a step-change towards sustainable development. Full details on the scientific objectives, planned and achieved outcomes, project partners and stakeholders, news and publications of SubRISK+ are openly available in the project website at: https://www.subrisk.eu

This report summarizes the results of SubRISK+ Work Package (WP) n.2 (*WP2: National scale risk assessment*), aimed to develop a land subsidence risk assessment methodology at the national scale based on satellite-derived ground displacement observations and land cover data. Section 2 describes the used input datasets (section 2.1) and the developed risk assessment methodology (section 2.2). Present-day risk assessment results are then presented in section 0, which provides: the detailed statistics on present-day hazard, exposure-vulnerability and risk for the 15 metropolitan cities of Italy as a whole (section 3.1), as well as city-specific mapping of hazard, exposure-vulnerability and resulting risk zoning (section 3.2). The digital versions of the value-added risk maps for the 15 cities are publicly available through SubRISK+ project website within the '*Control Room*' (https://controlroom.subrisk.eu), which enables open access to SubRISK+ mapping products.

2 DATA & METHODS

2.1 Input datasets

The input datasets of the analysis include: (i) administrative boundaries and population data, (ii) land cover datasets generated using satellite optical imagery, and (iii) ground displacement observations derived from satellite radar data. Each dataset and its main characteristics are described in the following sections.

2.1.1 Administrative boundaries and population

The administrative boundaries of the 15 metropolitan cities of Italy (Figure 1) were sourced from the National Institute of Statistics (ISTAT; https://www.istat.it/en), which acts as the primary source of official statistics for Italy. On a yearly basis, ISTAT provides updated digital versions of the administrative boundaries of Italian towns, provinces and regions, and the associated unique identification codes enabling their link with census records and other key statistics.

Figure 1 – Location of the 15 metropolitan cities of Italy.

The 2023 version of the geographical database was exploited for the analysis, in its GIS-ready vector format (shapefile), with WGS84 / UTM zone 32N (EPSG:32632) projected coordinates. For each metropolitan city, the dataset provides – among others – the following attributes: COD_REG (unique

ID of the region), COD_PROV (unique ID of the province), and COD_CM (unique ID of the metropolitan city); for each town, in addition to the latter, the dataset includes other attributes, such as PRO_COM (unique ID of the town), and COMUNE (name of the town). A summary of the areal extent and number of towns belonging to each metropolitan city is provided in Table 1, along with the censed number of inhabitants in 2023.

Table 1 – Information on the 15 metropolitan cities of Italy: area, number of towns and inhabitants according to the 2023 census.

COD_REG	*Region*	*COD_CM*	*Metropolitan City*	*Area [km²]*	*No. of towns*	*Inhabitants*
1	Piedmont	201	**Torino**	6,827	312	2,198,237
7	Liguria	210	**Genova**	1,834	67	813,626
3	Lombardy	215	**Milano**	1,575	133	3,219,391
5	Veneto	227	**Venezia**	2,473	44	833,703
8	Emilia-Romagna	237	**Bologna**	3,702	55	1,011,659
9	Tuscany	248	**Firenze**	3,514	41	984,991
12	Lazio	258	**Roma**	5,363	121	4,216,553
15	Campania	263	**Napoli**	1,179	92	2,969,571
16	Puglia	272	**Bari**	3,863	41	1,223,102
18	Calabria	280	**Reggio Calabria**	3,210	97	517,202
19	Sicily	282	**Palermo**	5,009	82	1,200,957
		283	**Messina**	3,266	108	598,811
		287	**Catania**	3,574	58	1,071,914
20	Sardinia	290	**Sassari**	4,286	66	315,460
		292	**Cagliari**	4,704	72	543,147

2.1.2 Urban settlement datasets

The two sources of land cover information that were exploited are:

(i) The Global Human Settlement Layer (GHSL), in particular, the Settlement Characteristics GHS-BUILT-C R2023A dataset [1], derived from a composite of Copernicus Sentinel-2 2018 imagery and other GHS R2023A data. The dataset delineates the boundaries of the human settlements and identifies their inner characteristics in terms of the morphology of the built environment and the functional use: built spaces (residential and non-residential, with associated height class) and open spaces (water surfaces, low to high vegetation surfaces, and roads) are distinguished within the human settlements (while the remainder is classified as no data). The layer is openly available in raster format with 10 m spatial resolution, in the World Mollweide (EPSG:54009) projected system.

(ii) The World Settlement Footprint (WSF®) Evolution dataset [2], generated from the analysis of Landsat-5/7 data, their derived spectral indices and temporal statistics. The dataset outlines the extent of settlement (and non-settlement) areas on a yearly basis, from 1985 to 2015, and is openly available in raster format with a spatial resolution of 30 m, referenced to the WGS84 (EPSG:4326) geographic system.

An overview of the two datasets over the Italian territory is provided in Figure 2 and Figure 3.

Figure 2 – Overview of the Global Human Settlement Layer (GHSL) – BUILT-C R2023A dataset over the Italian territory (source: https://human-settlement.emergency.copernicus.eu/ghs_buC2023.php).

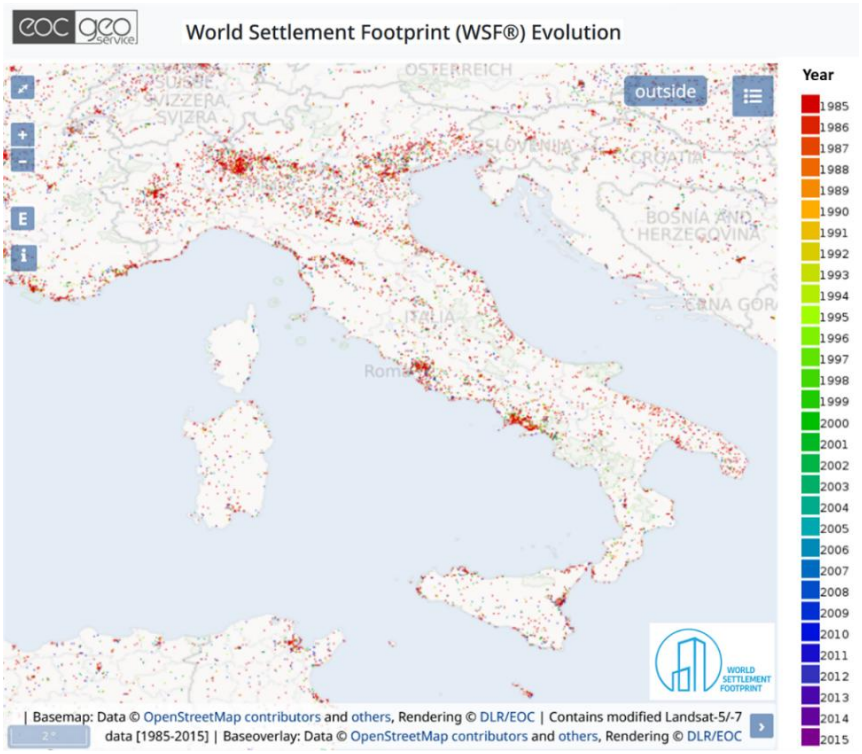

Figure 3 – Overview of the World Settlement Footprint (WSF®) Evolution dataset over the Italian territory (source: https://geoservice.dlr.de/web/maps/eoc:wsfevolution).

2.1.3 Ground displacement observations

Satellite-derived observations of ground displacement were sourced from the Copernicus European Ground Motion Service (EGMS; https://land.copernicus.eu/en/products/european-ground-motion-service). This provides millimetre precision estimates of ground displacement based on multi-temporal Interferometric Synthetic Aperture Radar (InSAR) [3] processing of Copernicus Sentinel-1 radar imagery, updated annually and openly available to the user community [4].

The EGMS Ortho 2018–2022 (vector) datasets were exploited for the analysis. These are point-wise layers depicting displacement along the vertical [5] and east-west [6] directions, which were derived from the combination of information provided by ascending and descending orbits of the EGMS Calibrated datasets (line-of-sight estimates, referenced to a model derived from global navigation satellite system data; [7]). Ortho datasets are resampled to a 100 m grid, and distributed in raster (geotiff) and vector (comma-separated values) formats. A displacement time series is associated with each point, with a temporal sampling following the satellite constellation revisit (12 or 6 days).

An overview of the dataset over the Italian territory is provided in Figure 4.

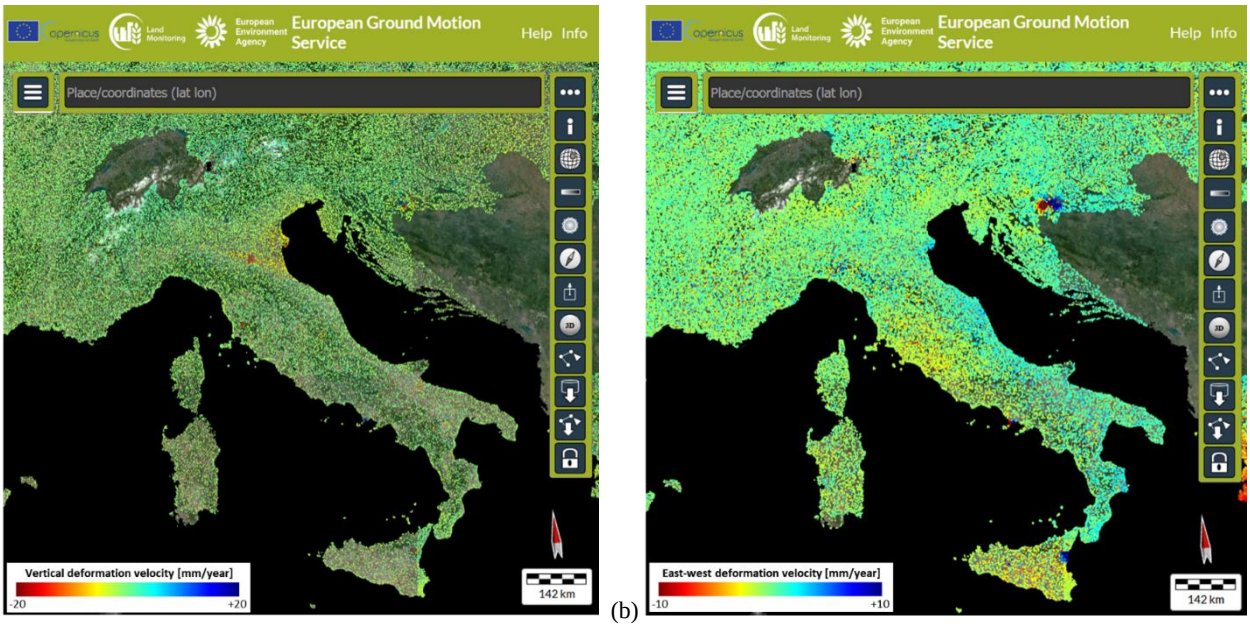

Figure 4 – Overview of the European Ground Motion Service (EGMS) Ortho datasets over the Italian territory: (a) vertical, and (b) east-west deformation velocities (source: https://egms.land.copernicus.eu).

2.2 Risk assessment methodology

The methodology builds upon a matrix-based risk assessment approach that was recently developed and demonstrated by SubRISK+ coordinator for three metropolitan cities in Central Mexico [8–10]. This method geospatially combines information on the type and distribution of the elements at risk (urban infrastructure) with InSAR-based ground displacement observations and derived stress metrics, with the aim to identify highly vulnerable urban infrastructure that might be impacted by differential displacement. Such an approach has been increasingly exploited across the scientific

community, with a growing number of applications in the USA, Nigeria, India and other countries (e.g. [11–13]), proving its adaptability across different geographical contexts.

2.2.1 Exposure-Vulnerability (EV)

Exposure and vulnerability of urban infrastructure are assessed based on its spatial distribution, type, height and age. Data on the type (residential, non-residential), height (≤ 3 m, 3-6 m, 6-15 m, 15-30 m, or > 30 m) and age (pre-/post-1985) of built-up surfaces are derived from the two urban settlement datasets (see section 2.1.2): building upon type and height of buildings extracted from the GHS-BUILT-C settlement characteristics (Figure 5a), and then complementing with information on building age as derived from the WSF Evolution layer (Figure 5b).

A combined Exposure-Vulnerability (EV) metric is therefore established based on the integration of GHS-BUILT-C and WSF Evolution data (Figure 5c), with values ranging between low (EV1) and very high (EV4). The metric assumes increasing levels of potential damage that could affect the buildings exposed to the hazard, when moving from lower to taller buildings, from residential to non-residential structures (the latter are assumed more likely to have loose foundations), and newer to older constructions (the latter are potentially more vulnerable with respect to new constructions complying with recent structural engineering regulations; e.g. [14]). Following the geospatial integration of the two layers, the EV metric is then spatially mapped across each metropolitan city, at the 10 m spatial resolution (Figure 5d).

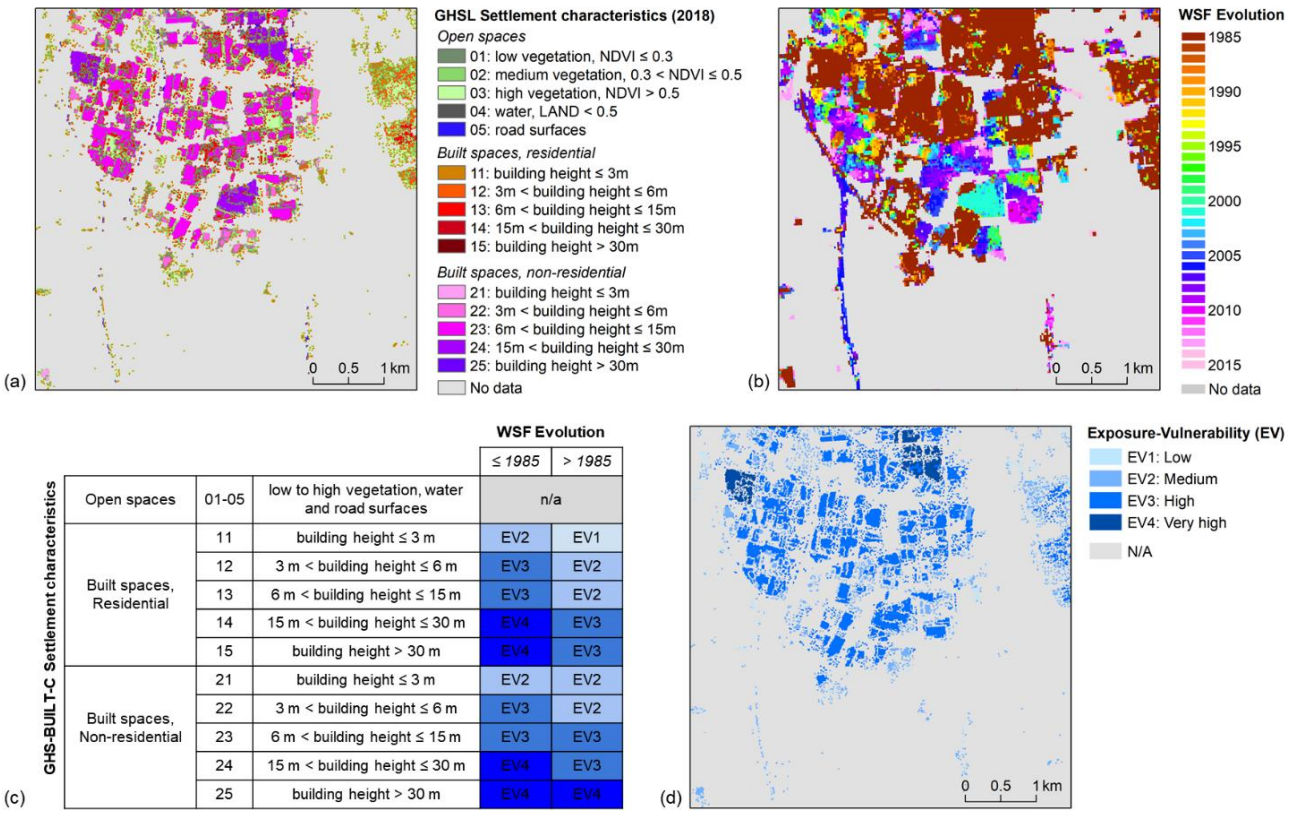

Figure 5 – Example of Exposure-Vulnerability (EV) assessment and mapping using SubRISK+ methodology: (a) GHSL Settlement Characteristics [1], *(b) WSF Evolution* [2], *(c) EV metric assessment approach, and (d) resulting EV map.*

2.2.2 Hazard (H)

The differential settlement occurring at the margins of subsiding areas (often above discontinuities in bedrock geology and aquifer system structure) is the primary cause for the development of surface fissures/faulting, cracks and damage in urban infrastructure (e.g., [15]). The associated hazard levels induced on urban infrastructure can therefore be estimated through the computation of the angular distortion (β) [16] and horizontal strain (ε) [17], as derived from the EGMS satellite InSAR datasets (see section 2.1.3). These two parameters are widely exploited in geotechnical engineering (e.g. [18]) and are among the main subsidence-related intensity parameters determining the building damage severity, together with construction year, type, characteristics and maintenance state of the superstructures and their foundations (e.g. [19]).

The computation of these two parameters starts by accounting for the vertical (V_U) and east-west (V_E) displacement velocity data provided by the EGMS Ortho layers for the 2018–2022 period (Figure 6a-b). By assuming that the estimated velocities have affected the observed areas for a period of 10 years, the total displacement values along the vertical and east-west directions, d_U and d_E respectively, and the total angular distortion and horizontal strain, β and ε (Figure 6c-d), are calculated at each map pixel as follows:

Total vertical displacement $d_U = V_U \times 10$ Total east-west displacement $d_E = V_E \times 10$

Total angular distortion $\beta = \frac{d_{U_j} - d_{U_i}}{l}$ Total horizontal strain $\varepsilon = \frac{d_{E_j} - d_{E_i}}{l}$

where d_{Uj} and d_{Ui} (and d_{Ej} and d_{Ei}) are the vertical (and east-west) displacements of adjacent points j and i, and l is their planar distance (in this case, this equals the spatial resolution of the EGMS Ortho datasets, i.e. 100 m).

To understand the meaning of β and ε, it is worth considering, for example, that β = 0.22% (i.e. 1/450) refers to a total of 22 cm differential displacement occurred over a period of 10 years across a 100 m horizontal distance. Similarly, ε = 0.15% (i.e. 1/670) refers to a total of 15 cm differential displacement over 10 years across a 100 m distance.

Hazard levels are identified according to a scale ranging from low (H1) to very high (H4) (Figure 6e), indicating an increasing probability of occurrence of fissuring/fracturing and associated damage of the urban infrastructure. The threshold values adopted for β and ε account for geotechnical practice (e.g. [14]) and past InSAR-based structural health applications (e.g. [8–10,20–22]). With regard to β, the thresholds adopted to classify the total distortion over the 10 year-long period are: 1/3000 (equivalent to 0.033%), 1/1500 (0.067%), and 1/500 (0.200%). A safety factor of 20% might be applied to slightly lower these thresholds, and thus ensure a more conservative hazard assessment. As for ε, the threshold adopted to categorize the strain cumulated over the 10 year-long period is: ±0.03% (namely 0.03%, applied to the absolute value of the strain, independently of its direction).

Following [10], hazard scores based on β are geospatially complemented with information on presence/absence of significant ε that potentially could also threaten the structures (Figure 6e): an increase in the hazard score obtained by classifying β is considered whenever the value of ε exceeds the adopted threshold. The hazard level is finally mapped across each metropolitan city, at the 100 m spatial resolution provided by the EGMS Ortho datasets (Figure 6f).

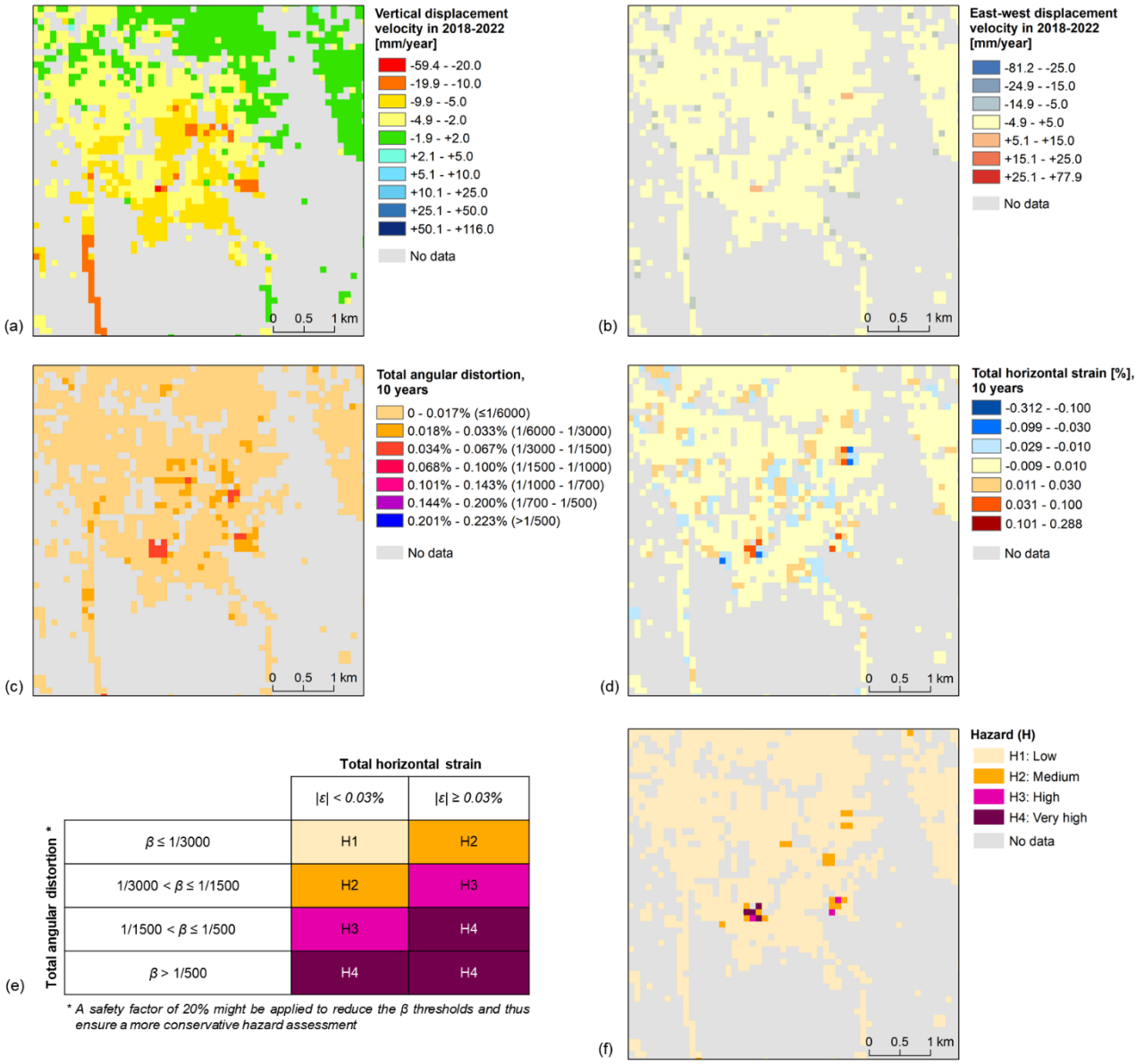

Figure 6 – Example of Hazard (H) assessment and mapping using SubRISK+ methodology: (a) EGMS Ortho vertical [5] *and (b) EGMS Ortho east-west* [6] *displacement velocity datasets, (c) total angular distortion and (d) horizontal strain over a period of 10 years, (e) H level assessment approach, and (f) resulting H map.*

2.2.3 Risk (R)

Hazard and exposure-vulnerability information are finally integrated via implementation of a tailored risk matrix, enabling the classification of risk levels into (Figure 7a):

Low (R1) this is considered an acceptable risk level, and no specific actions are required

Medium (R2) this is a relevant risk level, suggesting that potential structural damage might occur at the urban infrastructure involved; therefore, tailored monitoring of ground deformation and derived stress indices is recommended at the building block scale

High (R3) this is the highest risk level, indicating a high likelihood of already occurred/incipient structural damage at urban infrastructure; site inspections to verify the structural health of the buildings and ad hoc mitigation measures are recommended at single-building scale

The integration is tied to the 10 m spatial resolution of the exposure-vulnerability layer (see section 2.2.1), yet by acknowledging that hazard information is embedded at a broader resolution (see section 2.2.2), meaning that homogeneous H levels will be considered across multiple EV pixels. An example of the resulting risk map is provided in Figure 7b.

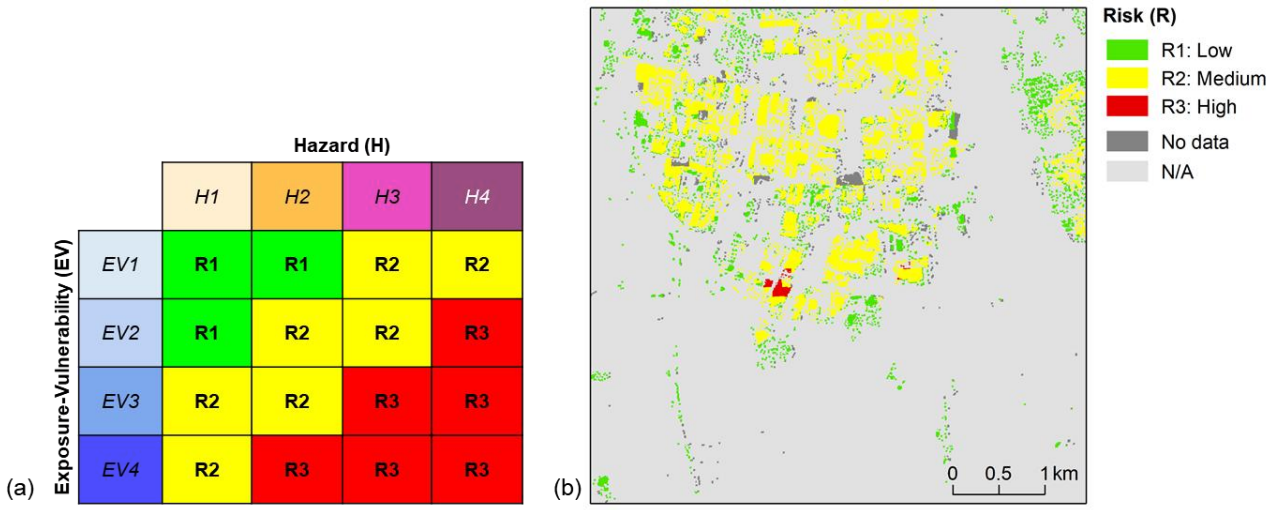

Figure 7 – Example of Risk (R) assessment and mapping using SubRISK+ methodology: (a) risk matrix, and (b) resulting R map.

3 RESULTS

3.1 Overview of differential displacement risk in Italy

Built-up spaces (either residential or non-residential buildings) within the 15 metropolitan cities of Italy embrace limited proportions of the respective total extents, with percentages ranging between 1.8% (Sassari) and 21.3% (Napoli); on the other hand, open spaces within the human settlements (low to high vegetated, water and road surfaces) and other rural land outside the human settlements span the vast majority of the administrative areas (Figure 8a). In terms of areal coverage, the greatest built-up spaces are found in Roma (442 km^2), Torino (311 km^2) and Milano (277 km^2), followed by Napoli (251 km^2), Bari (206 km^2), and the remainder 10 cities encompassing less than 200 km^2. It is only to built-up spaces that the Exposure-Vulnerability metric was assigned; the resulting statistical overview is provided in Figure 8b.

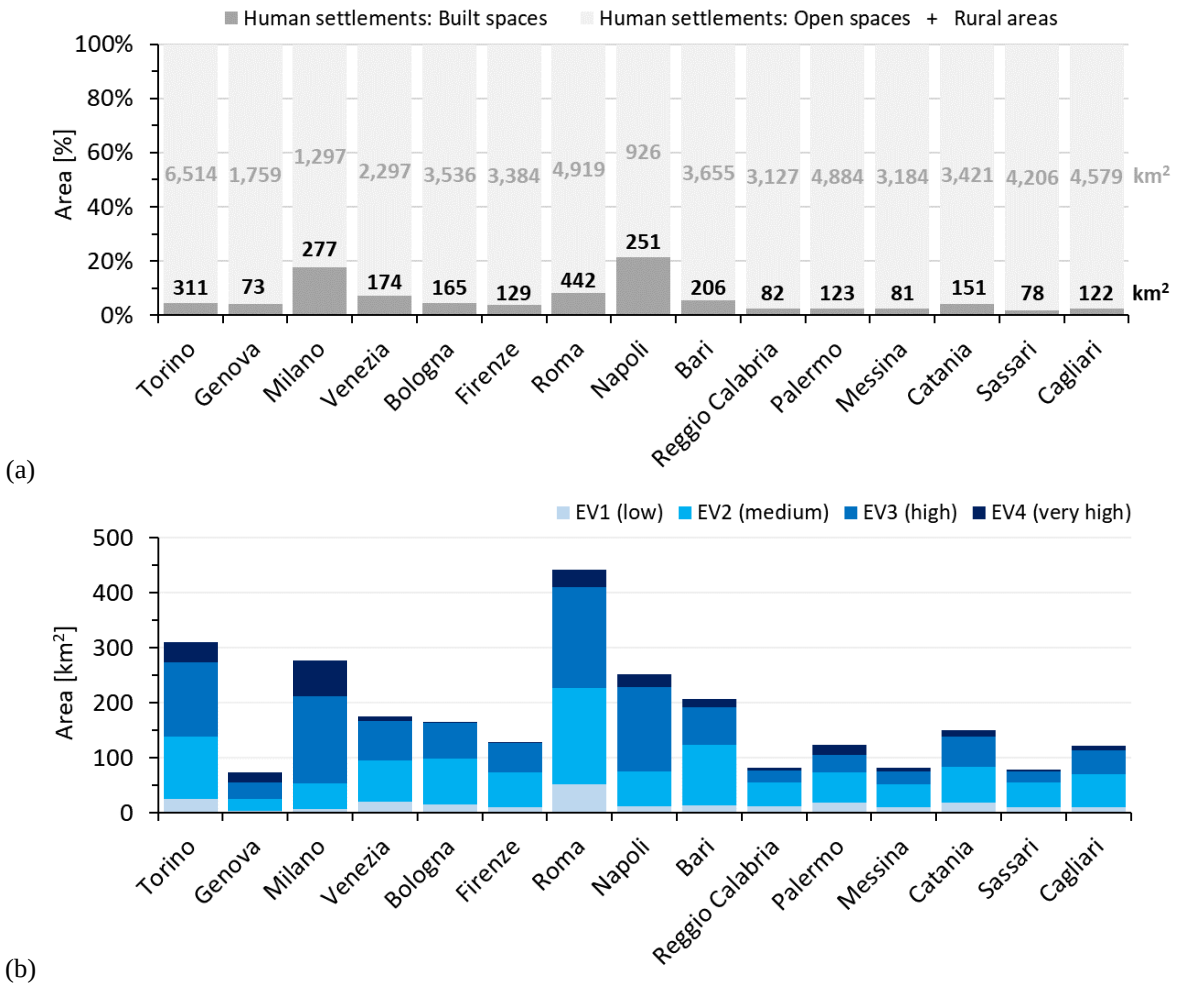

Figure 8 – (a) Built-up and unbuilt land within the 15 metropolitan cities of Italy (according to the GHS-BUILT-C R2023A - GHS Settlement Characteristics [1] layer), displayed using a percentage scale (100% refers to the total extent of each city), with labels indicating areas in km^2; and (b) Extent of the four Exposure-Vulnerability (EV) levels within each city, derived by following the method described in section 2.2.1.

The proportion of low exposure-vulnerability buildings (EV1) within the 15 metropolitan cities is generally between 2% (found at Milano, for ~6 km^2 out of its 277 km^2 built-up spaces) and 14% (Palermo, for ~18 km^2 out of 123 km^2 built-up spaces). Medium exposure-vulnerability buildings (EV2) typically cover between 17% (Milano, for ~48 km^2 out of its 277 km^2 built-up spaces) and 58% (Sassari, for ~45 km^2 out of its 78 km^2 built-up spaces). Similar proportions are found for high exposure-vulnerability buildings (EV3), extending between 24% (Sassari, for ~19 km^2 out of its 78 km^2 built-up spaces) and 61% (Napoli, for ~152 km^2 out of its 251 km^2 built-up spaces). The amount of buildings associated with the highest exposure-vulnerability metric (EV4) range between 1% (Bologna, for ~2 km^2 out of its 165 km^2 built-up spaces) and 25% (Genova, for ~18 km^2 out of its 73 km^2 built-up spaces). In terms of absolute extent (Figure 8b), the metropolitan cities highlighting the largest extents of EV4 buildings are Milano (~65 km^2), Torino (~37 km^2), Roma (~33 km^2) and Napoli (~23 km^2).

Ground displacement datasets for the 15 cities provide information for proportions of their administrative extents ranging between 16.5% (Messina) and 66.2% (Napoli) (Figure 9a); their coverage mostly follows the spatial distribution of built-up spaces, as the latter typically encompass a number of good reflectors to the radar signal, hence the ideal land cover for satellite interferometric methods to perform (see section 2.1.3). The hazard assessment for the 15 cities depicts low hazard levels (H1) across more than 98.5% of the mapped land within each city (Figure 9b); overall, the greatest proportion of medium (H2) to very high (H4) hazard zones is found in Genova, where hazard is deemed significant across more than 1.3% of the mapped area (~6.5 out of 488 km^2). In terms of absolute extent, Napoli (~8.5 km^2) and Palermo (~7.0 km^2) provide the greatest extents of H2 to H4 hazard zones, while the lowest extents are found in Milano (~0.4 km^2) and Sassari (~0.9 km^2). The greatest hazard levels (H3, high; and H4, very high) are generally limited to narrow sectors of the 15 cities, and encompass a total of 9.1 (H3) and 1.4 (H4) km^2 across the whole 15 cities. The largest extents mapped are 1.8 (H3) and 0.25 (H4) km^2 in Napoli, and 1.5 (H3) and 0.43 (H4) km^2 in Torino.

The 'baseline' (present-day) risk assessment achieved via geospatial integration of exposure-vulnerability and hazard maps provides mapping coverage spanning between 86% (Sassari) and 98% (Milano) of the built-up spaces; indeed, the total extent of the mapped risk areas slightly differs from the total extent of the mapped exposure-vulnerability zones, due to the presence of some built-up spaces with no hazard information available. Low risk (R1) zones generally cover a large proportion of the mapped areas (30-50%), with peaks at Reggio Calabria (65%) and Sassari (67%); similarly, medium risk (R2) areas typically extend ~40-60%, with peaks at Napoli (71%) and Milano (81%) (Figure 10). A total of 1133 km^2 R1 and 1351 km^2 R2 areas are found overall across the 15 metropolitan cities.

On the other hand, a total of 1.44 km^2 high risk (R3) zones is found overall across the 15 cities. Their extent is generally limited to less than 0.01% of the administrative land of each city (less than 0.02 km^2), usually restricted to narrow/small sectors. More significant extents are found in Messina (0.03 km^2), Roma (0.07 km^2), Catania (0.09 km^2) and Napoli (1.16 km^2), onto areas where the most vulnerable urban infrastructure is affected by the greatest differential settlements and induced structural stress (see section 0). Examples of such locations are in Pozzuoli and Bagnoli, within the metropolitan city of Napoli, where significant angular distortion with added stress coming from horizontal strain occurs in highly dense residential and non-residential built-up areas where building height exceeds 15 m.

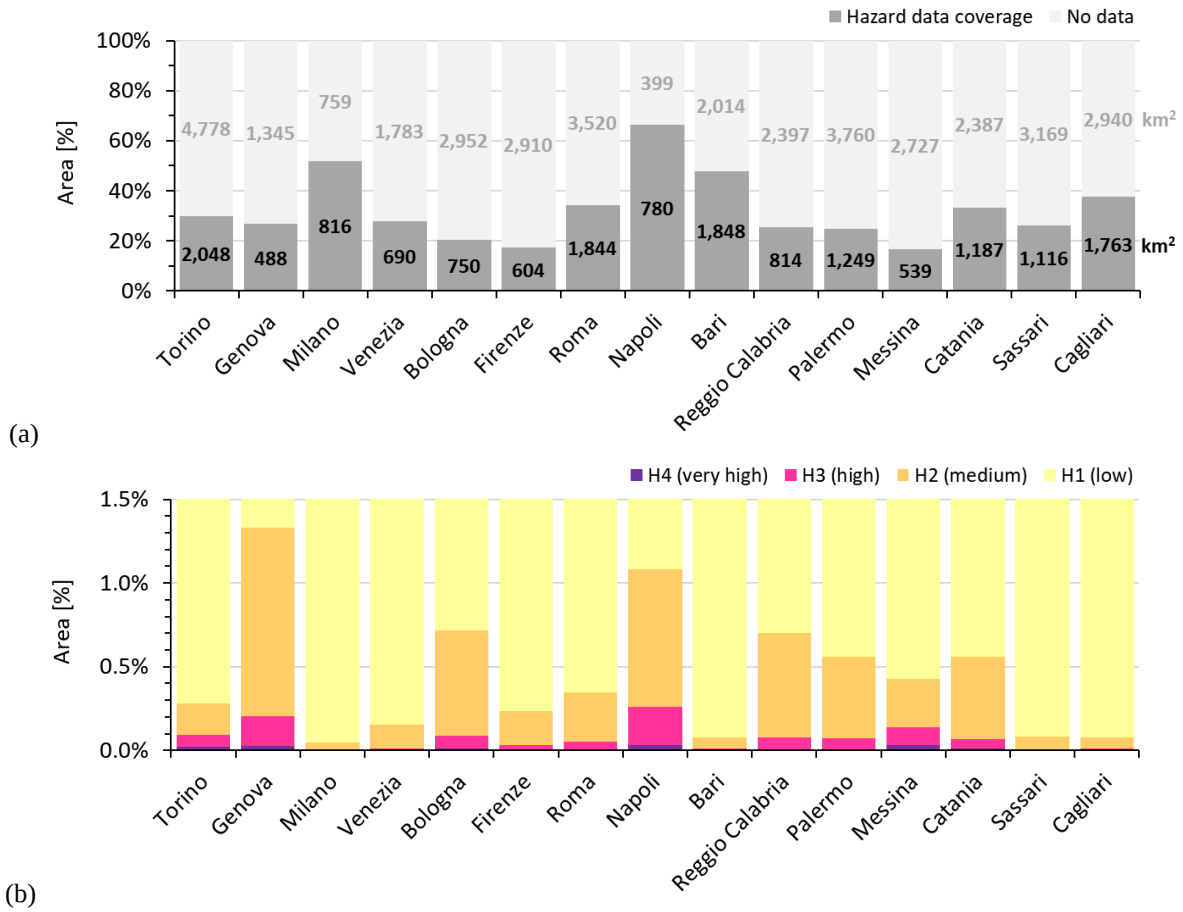

Figure 9 – (a) Hazard (H) data coverage and no data within the 15 metropolitan cities of Italy (based on the EGMS Ortho InSAR dataset [5]), displayed using a percentage scale based on the respective total extent of each city; and (b) Extent of the four Hazard (H) classes within each city, displayed using a percentage scale (100% refers to the total extent of the hazard data within each city), and derived by following the method described in section 2.2.2.

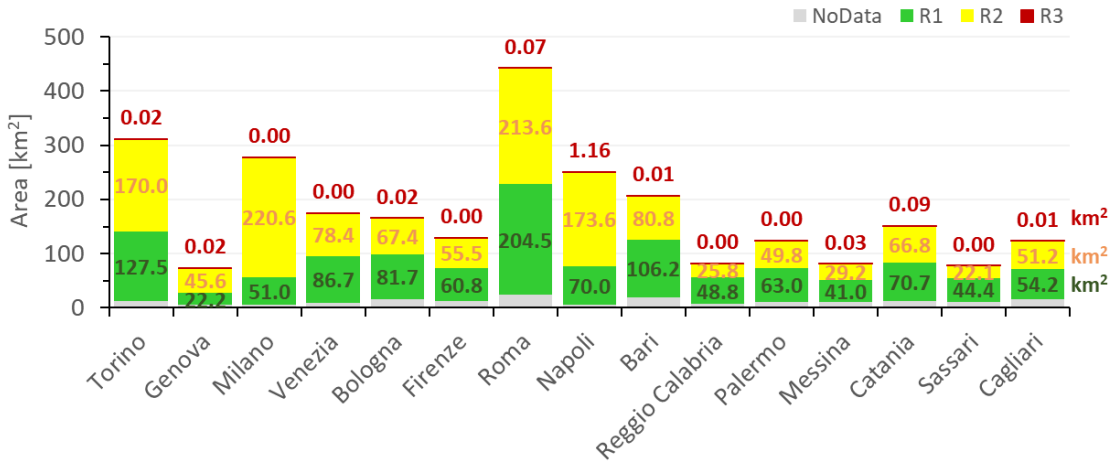

Figure 10 – Extent of the three Risk (R) classes within each of the 15 metropolitan cities of Italy, derived by following the method described in section 0.

3.2 City-specific differential displacement risk mapping

The following sub-sections provide the full set of maps of the main input datasets (GHS-BUILT-C R2023A - GHS Settlement Characteristics, WSF Evolution, EGMS InSAR displacement datasets) and the resulting value-added maps (exposure-vulnerability, hazard and risk) generated for each of the 15 metropolitan cities of Italy.

As specified in section 3.1, exposure-vulnerability, hazard and risk maps refer to the process of differential displacement induced by ground instability (either purely vertical, or also encompassing east-west components), as estimated by the InSAR datasets for the 2018–2022 period.

The EGMS InSAR displacement velocity, hazard, exposure-vulnerability and resulting risk maps are meant to be explored through SubRISK+ *'Control Room'* (https://controlroom.subrisk.eu), where their digital versions are available for open visualization and browsing (Figure 11).

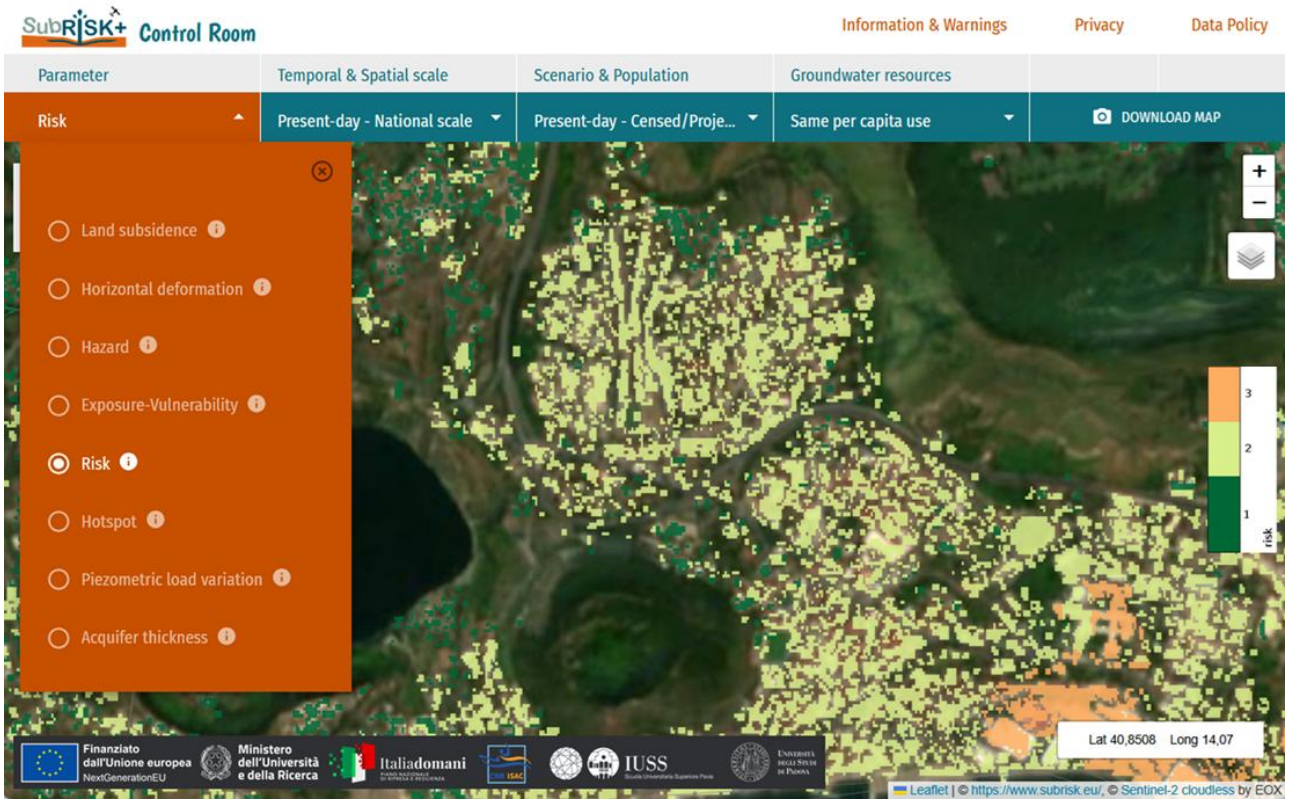

Figure 11 – SubRISK+ Control Room, the web platform enabling access to the value-added risk mapping products generated at the different spatial scales: example showing the differential displacement risk over an area within the metropolitan city of Napoli.

3.2.1 Torino

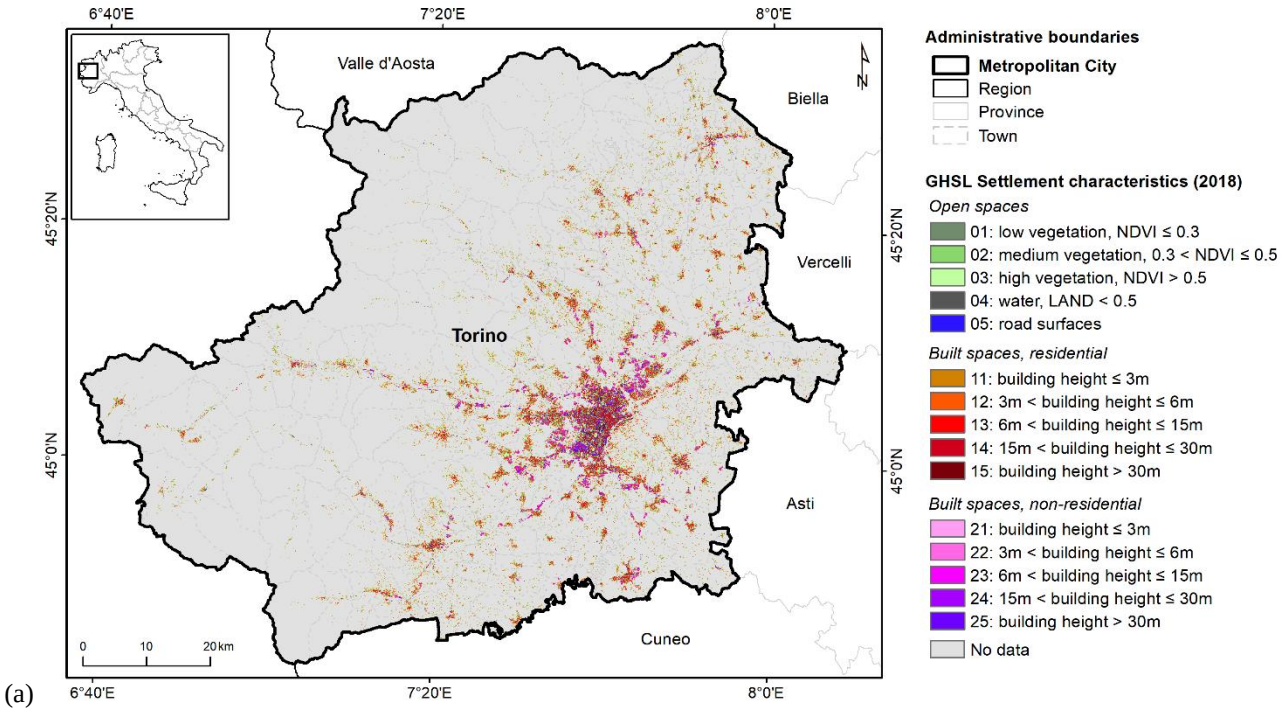

(a)

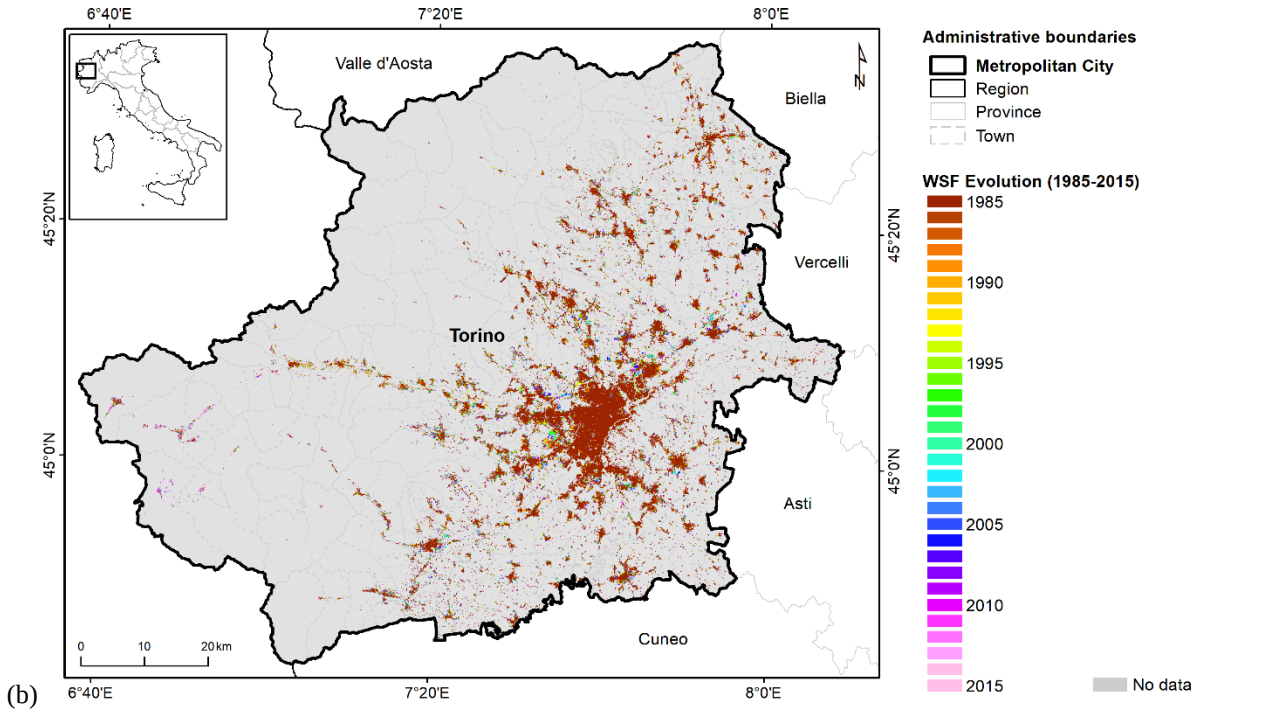

(b)

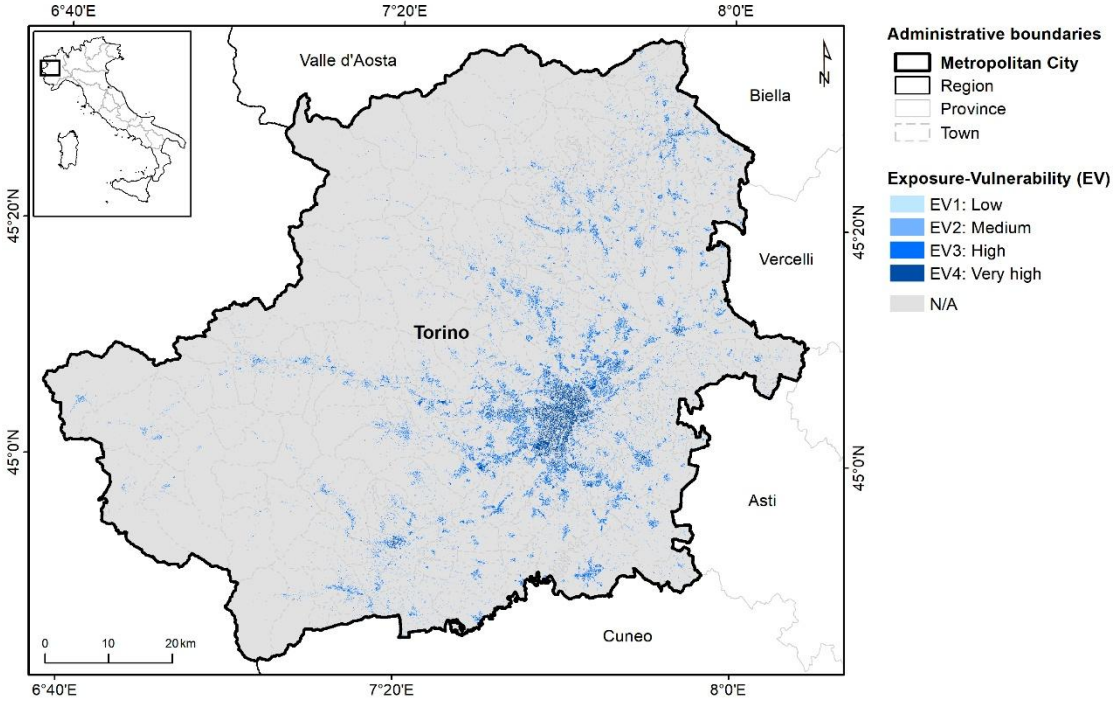

(c)

Figure 12 – Exposure-vulnerability mapping in the metropolitan city of Torino: (a) GHS-BUILT-C R2023A - GHS Settlement Characteristics [1], (b) WSF Evolution 2015 [2]*, and (c) resulting exposure-vulnerability map.*

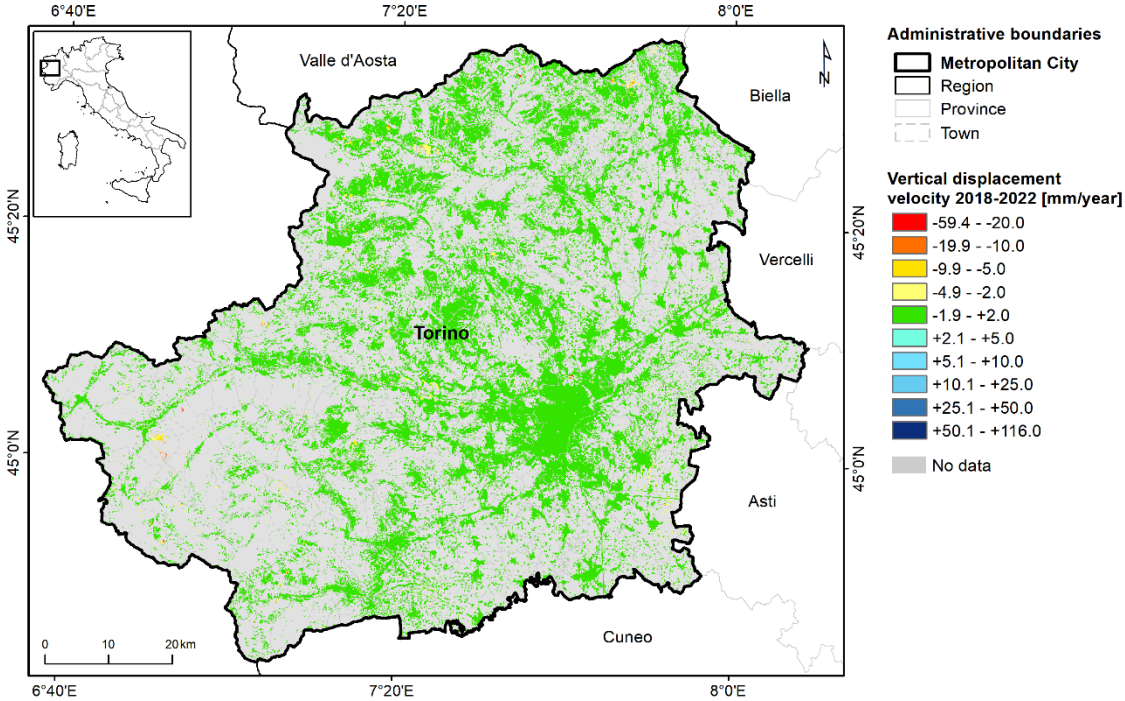

(a)

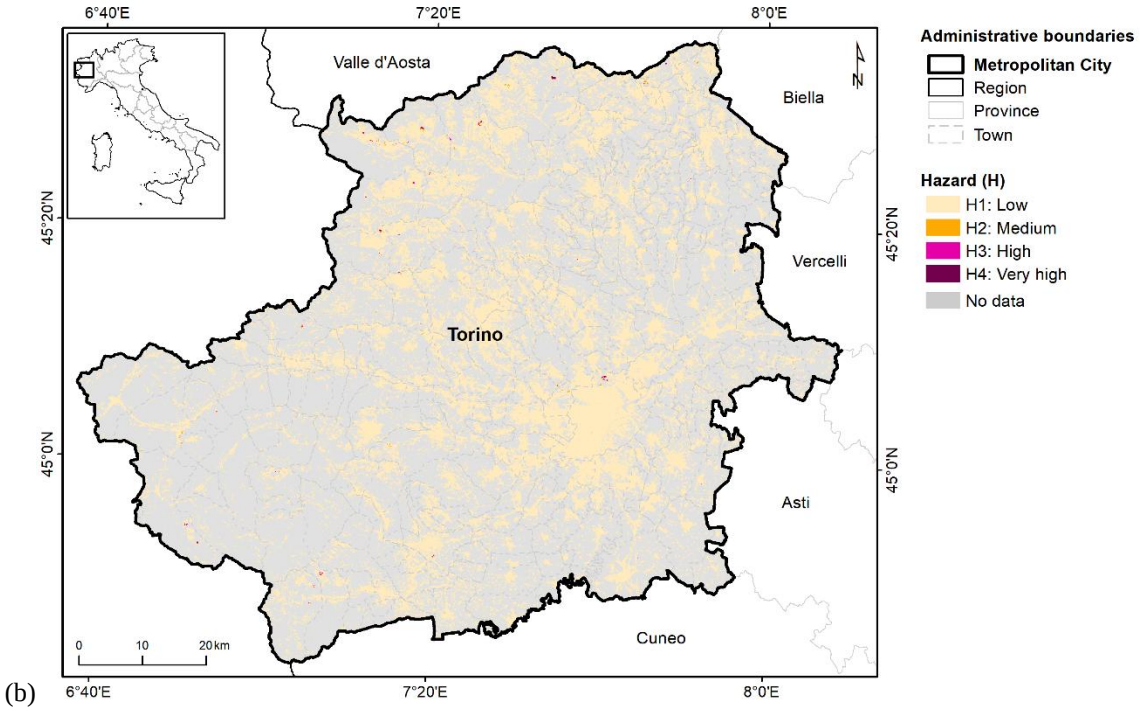

(b)

Figure 13 – Differential displacement hazard mapping in the metropolitan city of Torino: (a) vertical ground displacement velocity in 2018–2022 based on EGMS Ortho InSAR datasets [5]*, and (b) resulting hazard map.*

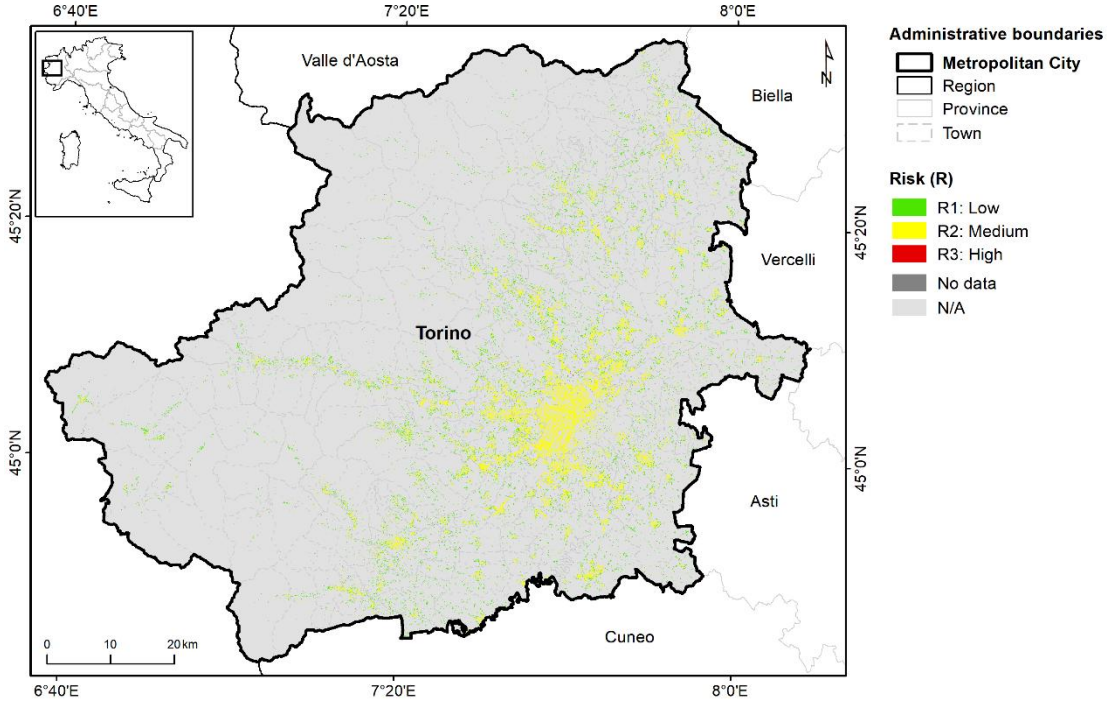

Figure 14 – Differential displacement risk mapping in the metropolitan city of Torino, based on 2018–2022 satellite InSAR observations.

3.2.2 Milano

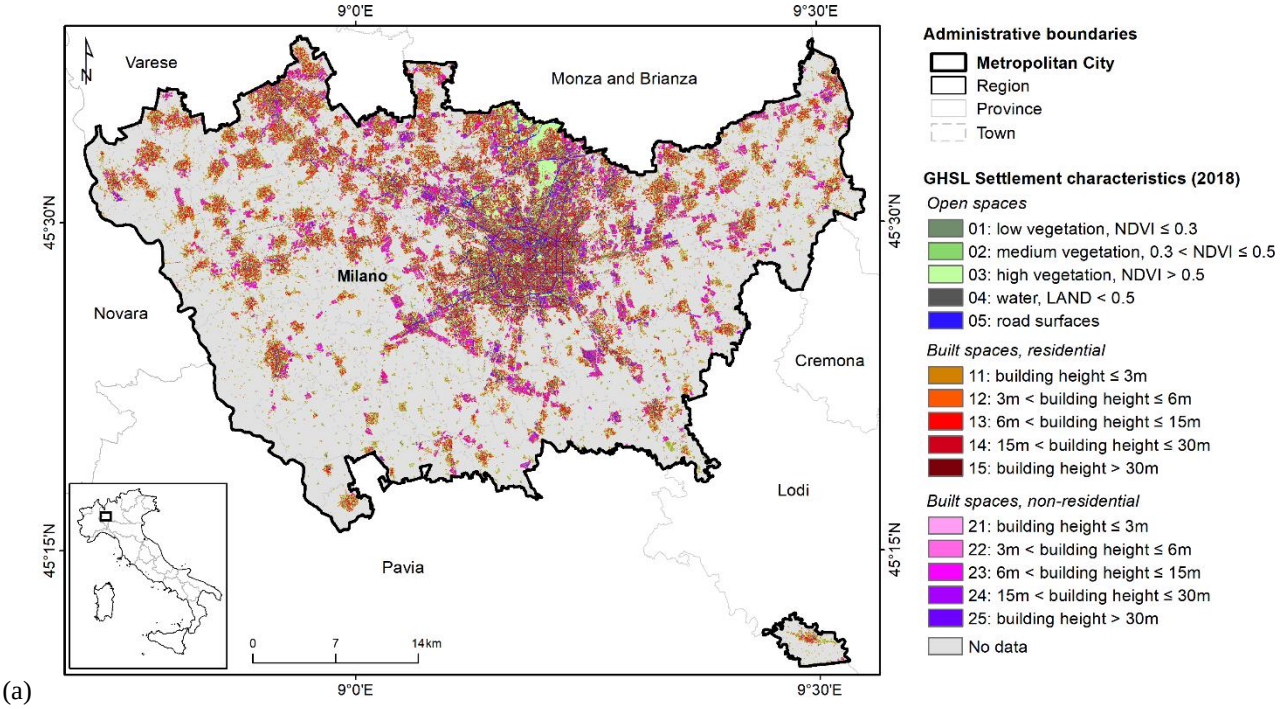

(a)

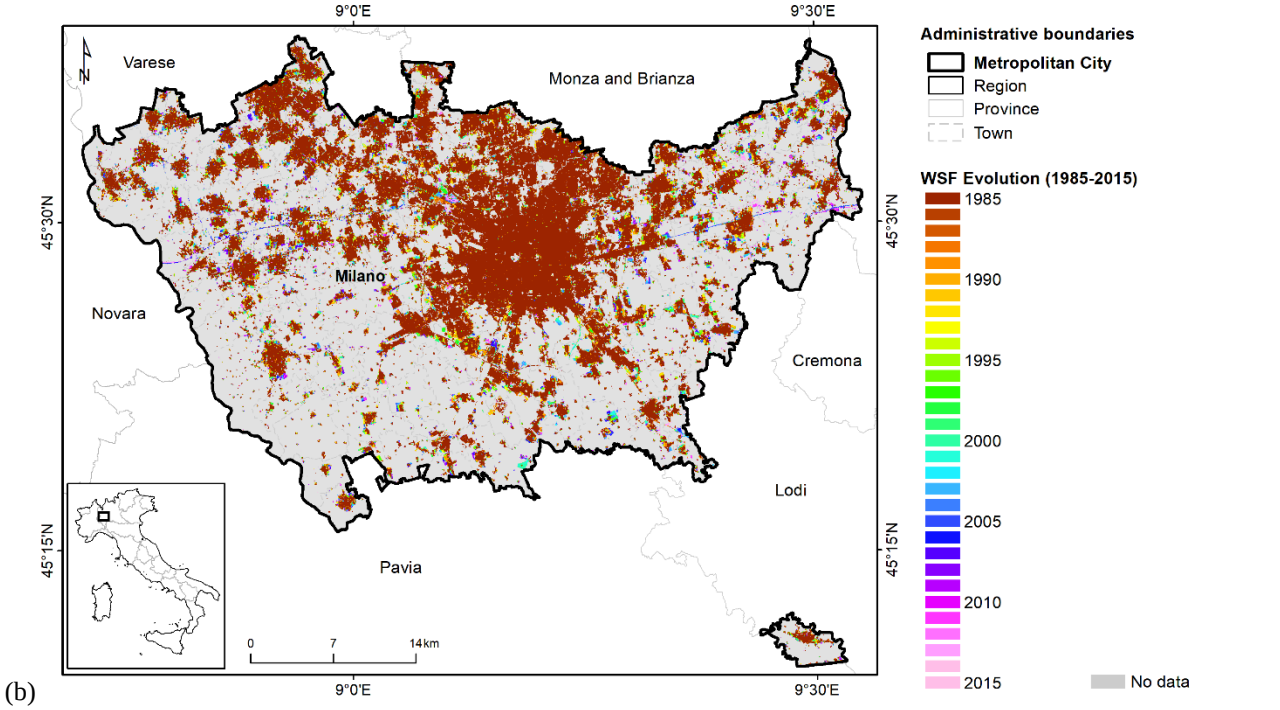

(b)

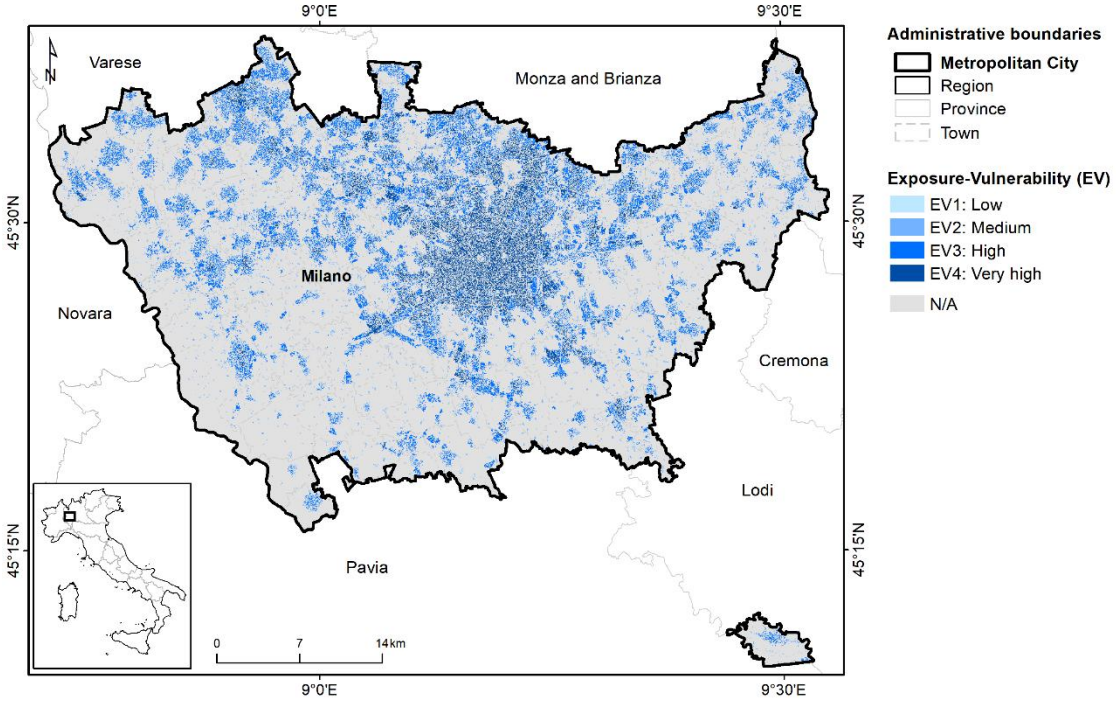

(c)

Figure 15 – Exposure-vulnerability mapping in the metropolitan city of Milano: (a) GHS-BUILT-C R2023A - GHS Settlement Characteristics [1], (b) WSF Evolution 2015 [2]*, and (c) resulting exposure-vulnerability map.*

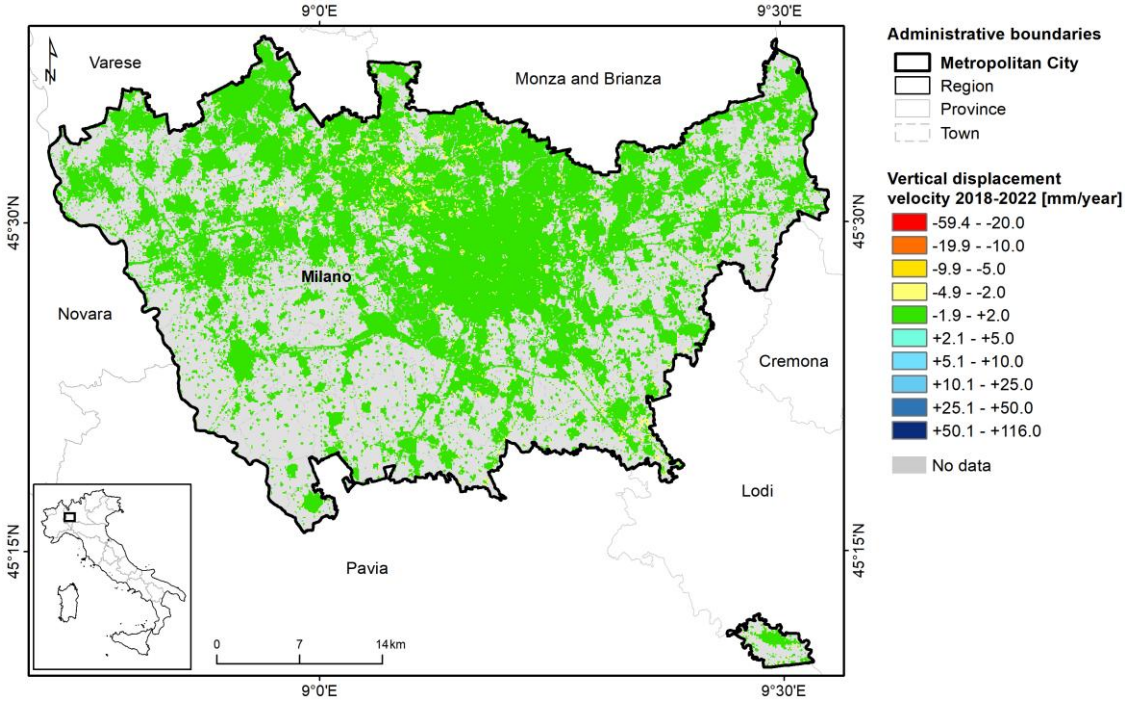

(a)

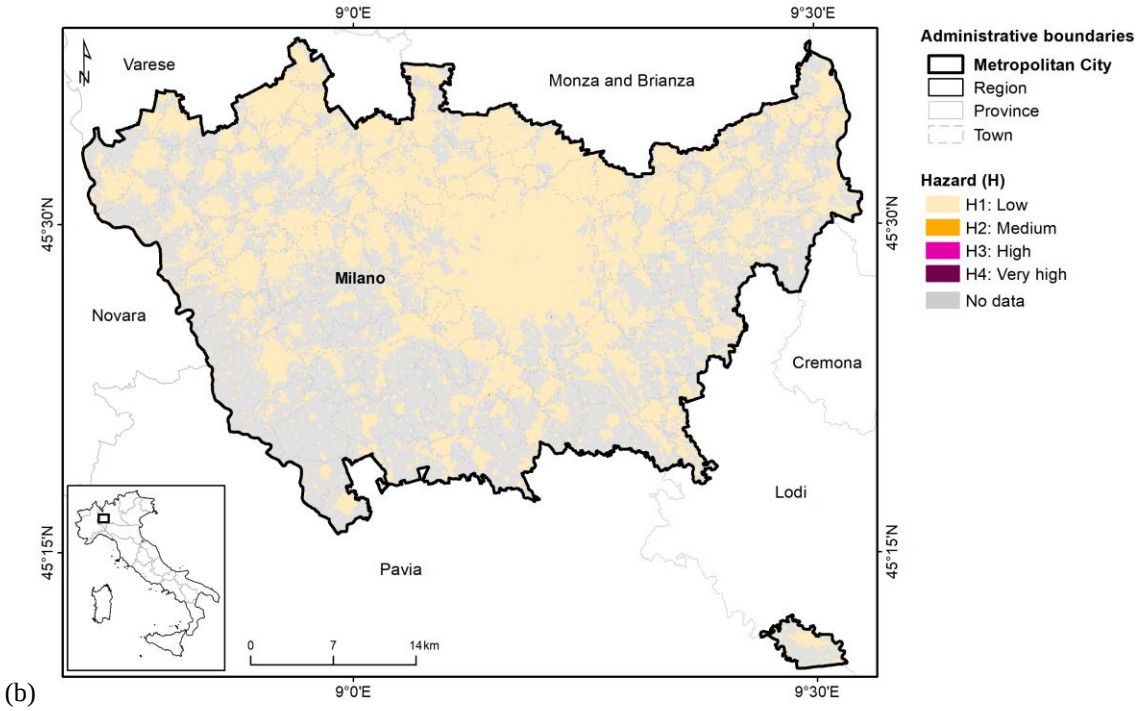

(b)

Figure 16 – Differential displacement hazard mapping in the metropolitan city of Milano: (a) vertical ground displacement velocity in 2018–2022 based on EGMS Ortho InSAR datasets [5]*, and (b) resulting hazard map.*

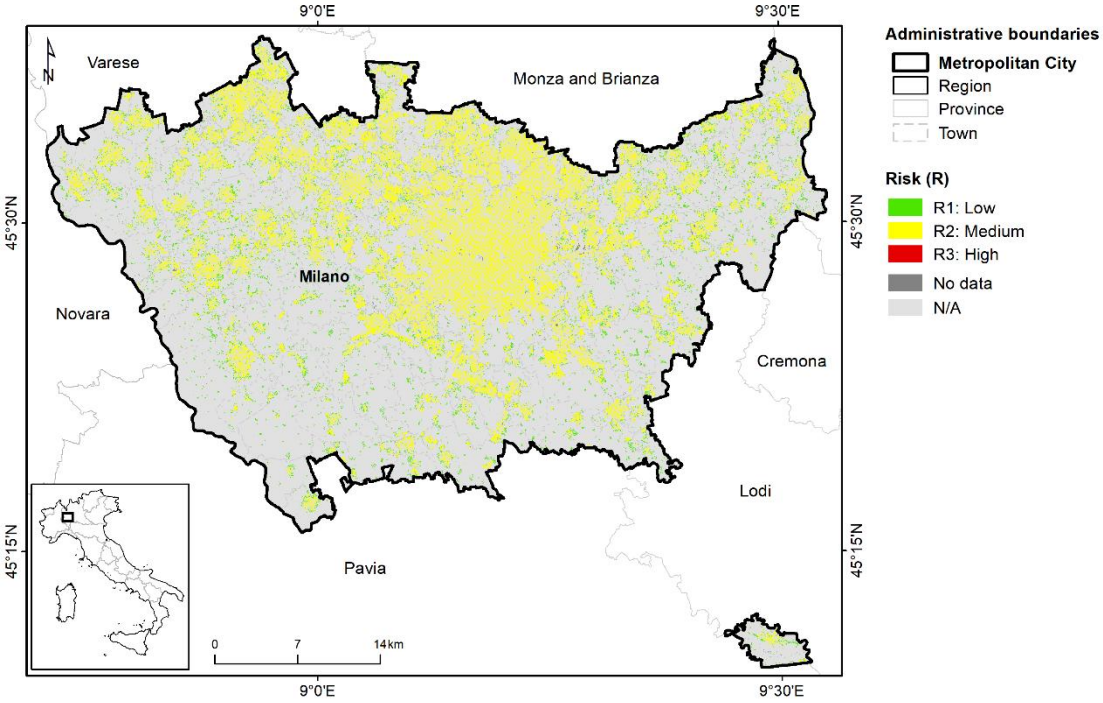

Figure 17 – Differential displacement risk mapping in the metropolitan city of Milano, based on 2018–2022 satellite InSAR observations.

3.2.3 Genova

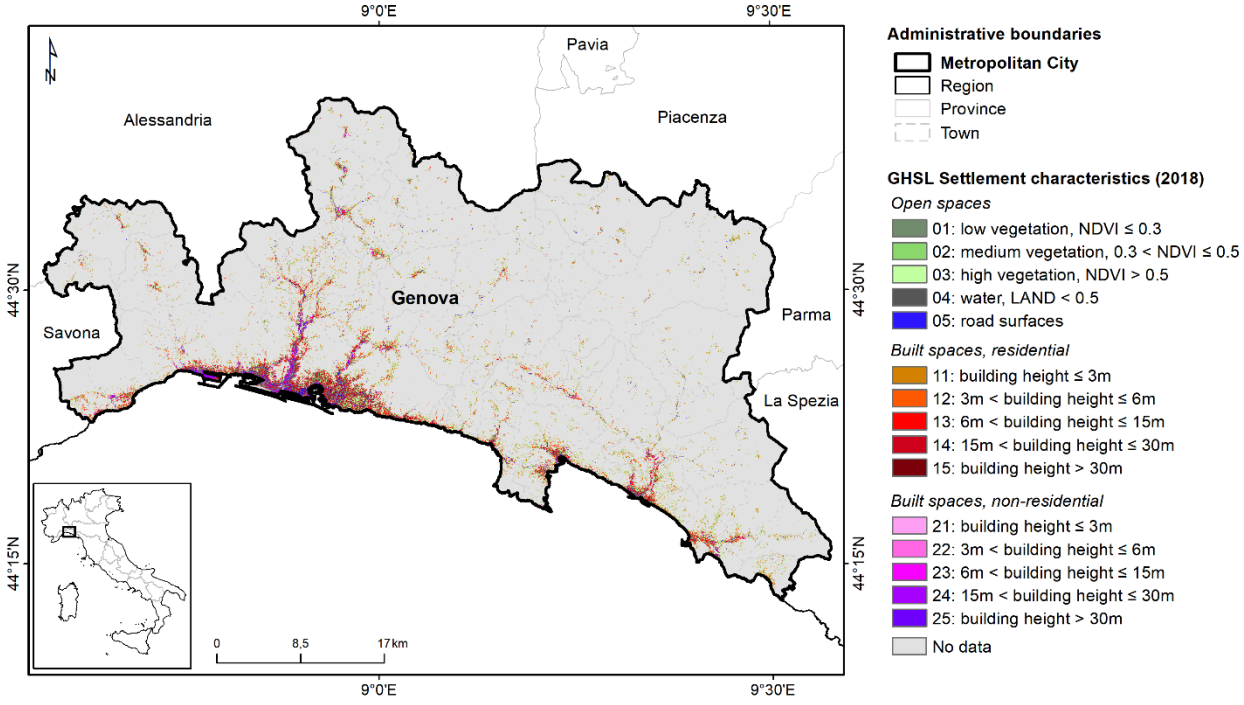

(a)

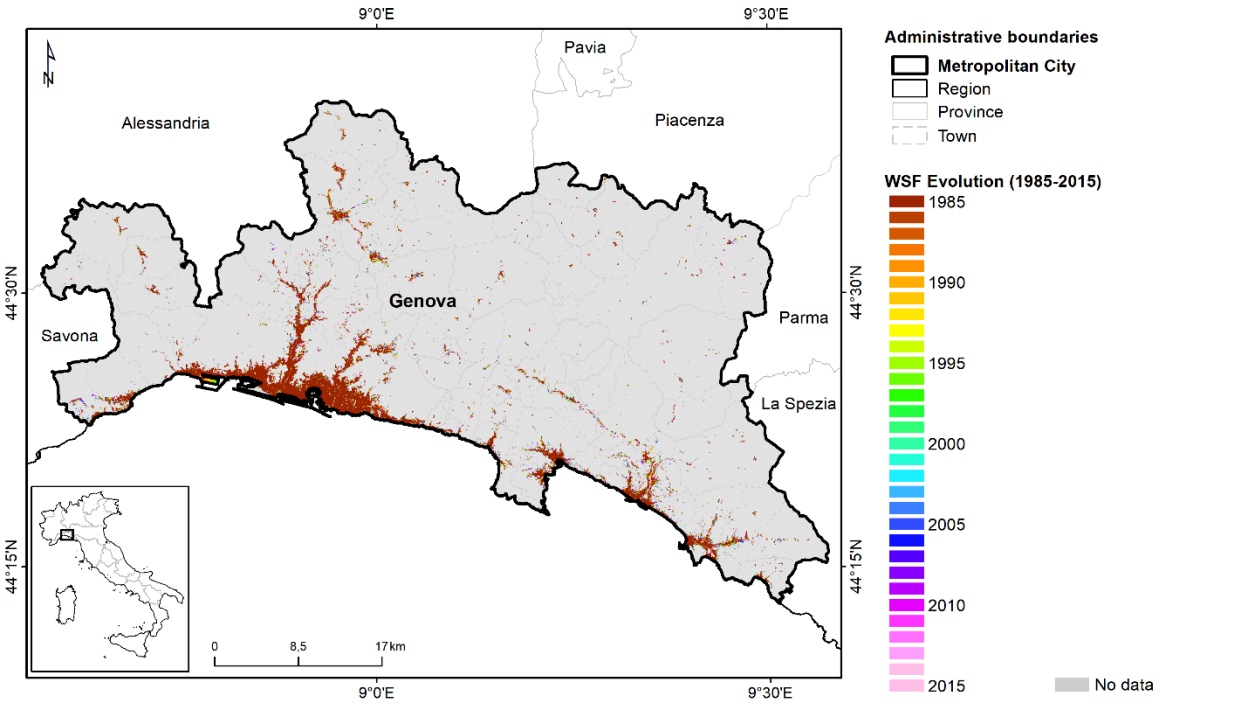

(b)

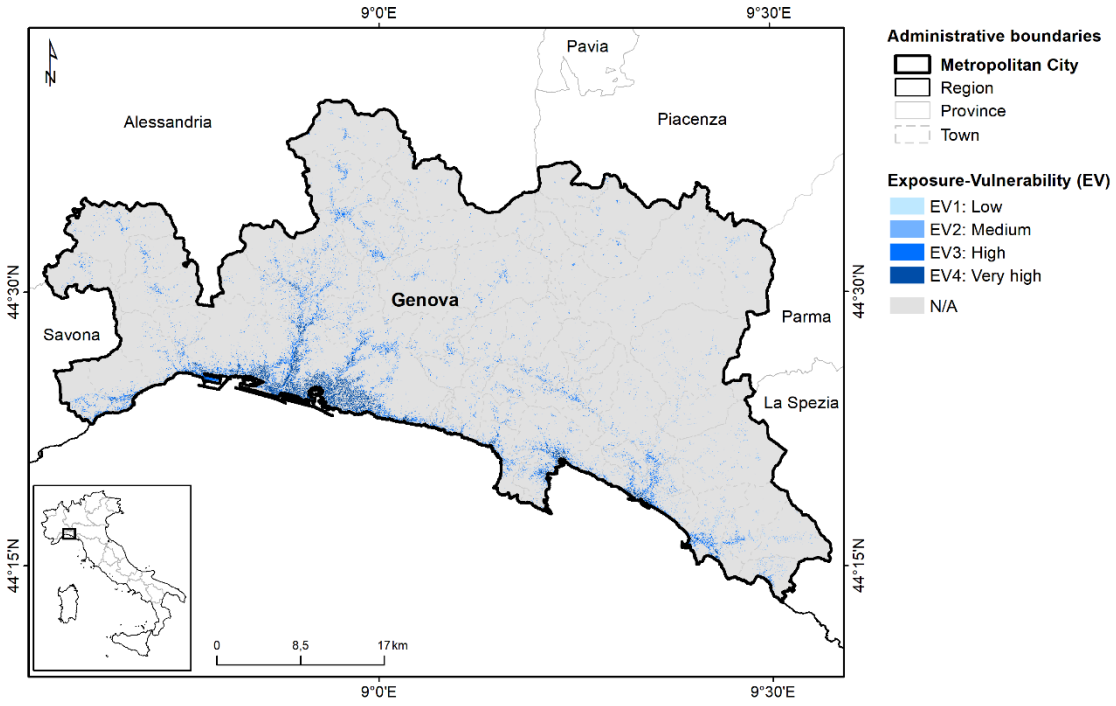

(c)

Figure 18 – Exposure-vulnerability mapping in the metropolitan city of Genova: (a) GHS-BUILT-C R2023A - GHS Settlement Characteristics [1], (b) WSF Evolution 2015 [2]*, and (c) resulting exposure-vulnerability map.*

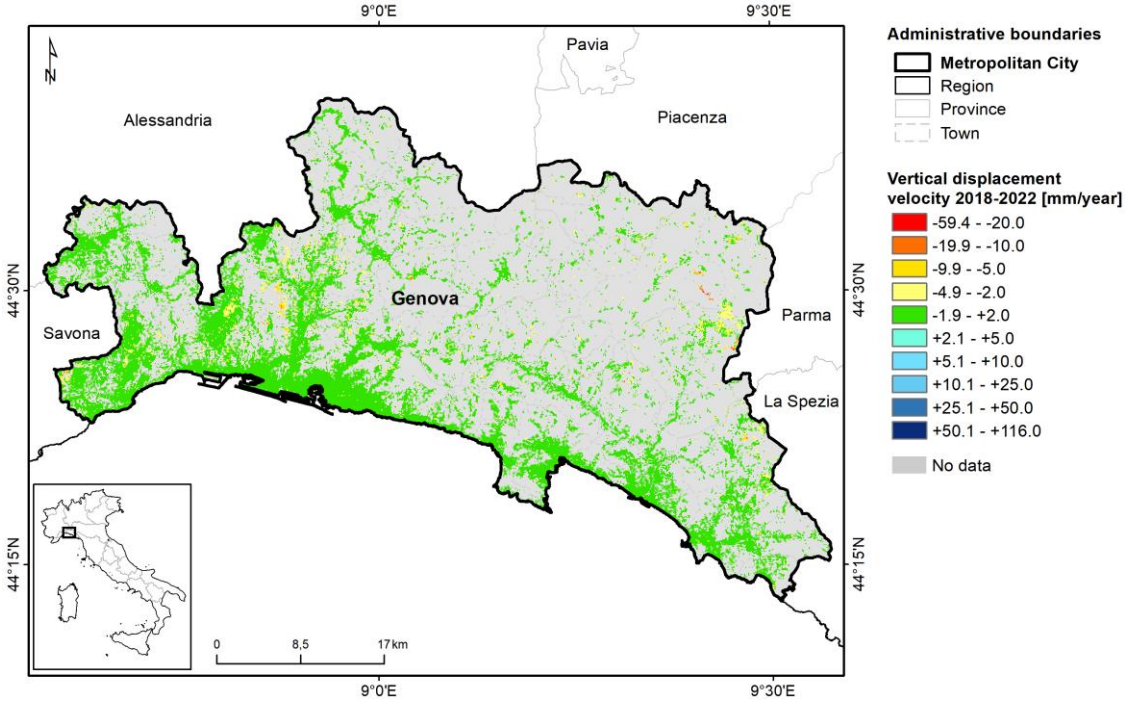

(a)

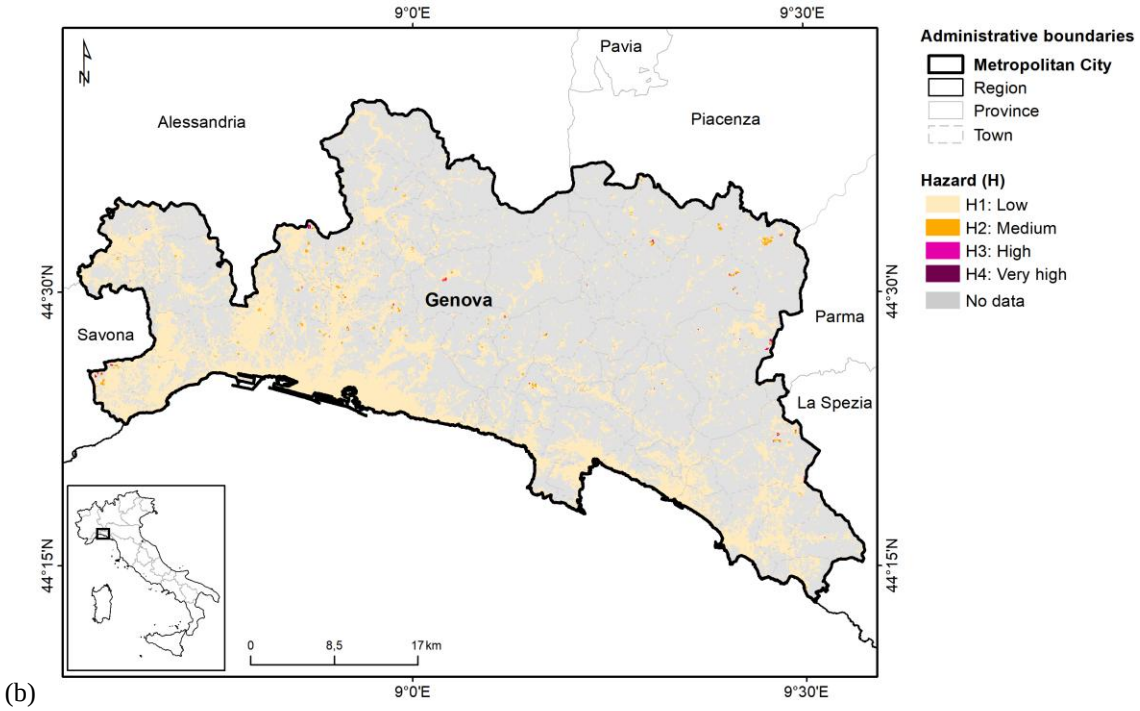

(b)

Figure 19 – Differential displacement hazard mapping in the metropolitan city of Genova: (a) vertical ground displacement velocity in 2018–2022 based on EGMS Ortho InSAR datasets [5]*, and (b) resulting hazard map.*

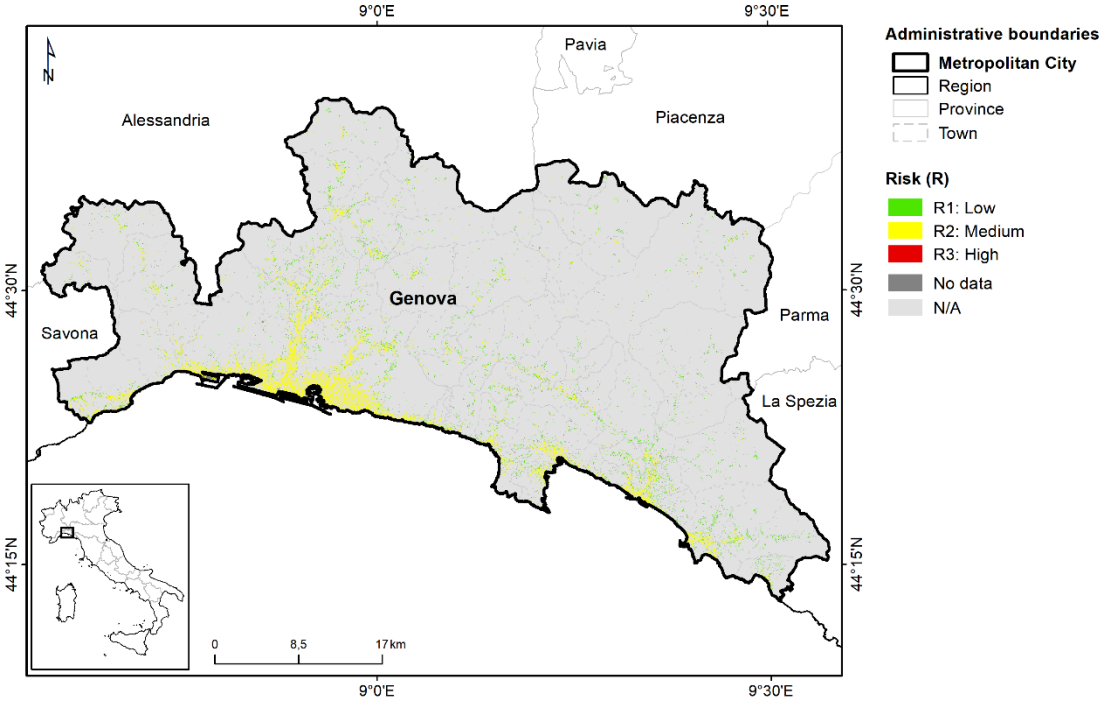

Figure 20 – Differential displacement risk mapping in the metropolitan city of Genova, based on 2018–2022 satellite InSAR observations.

3.2.4 Venezia

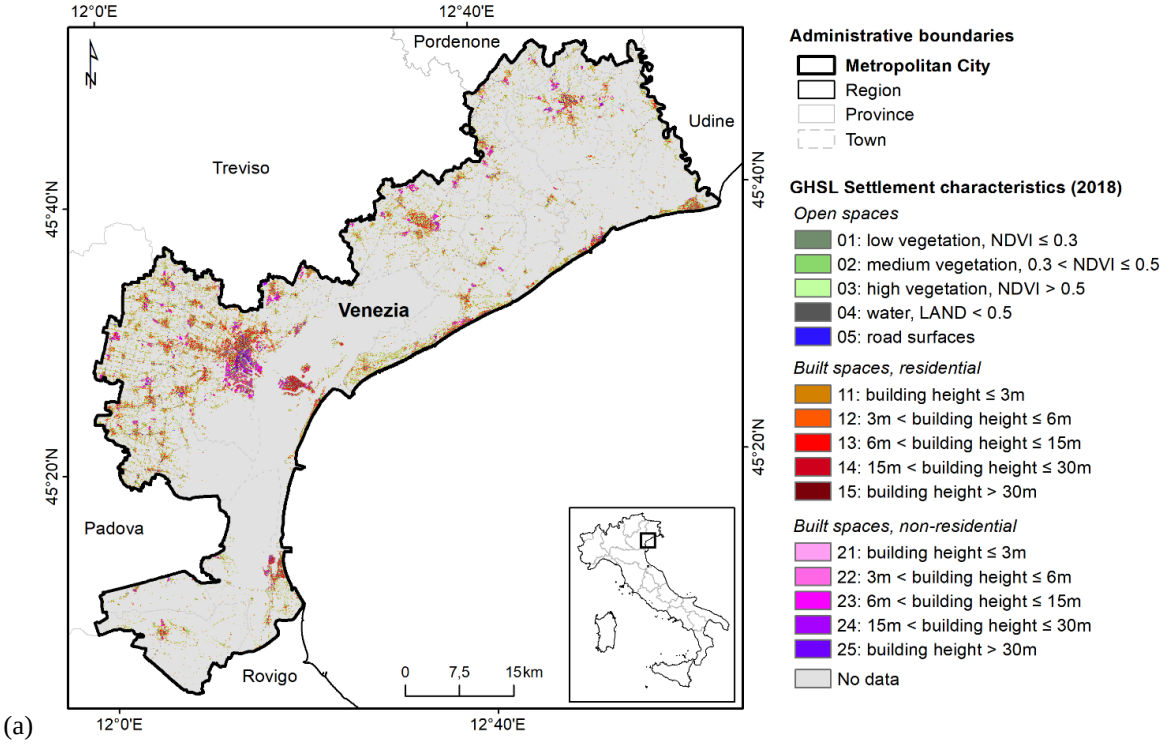

(a)

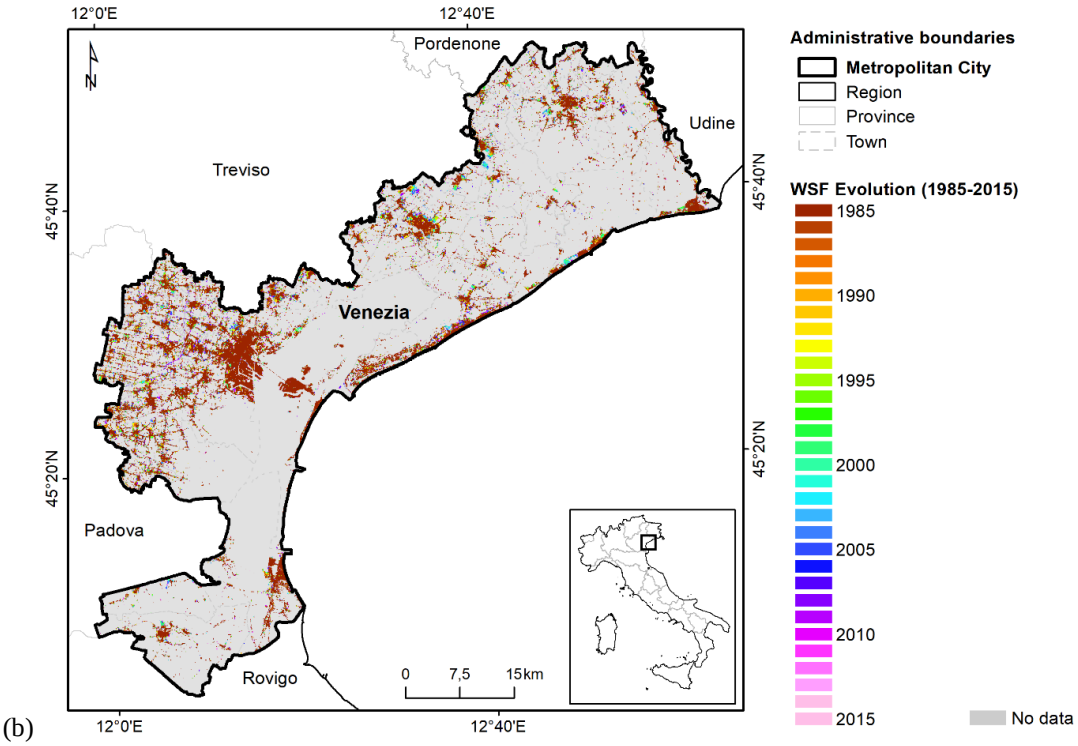

(b)

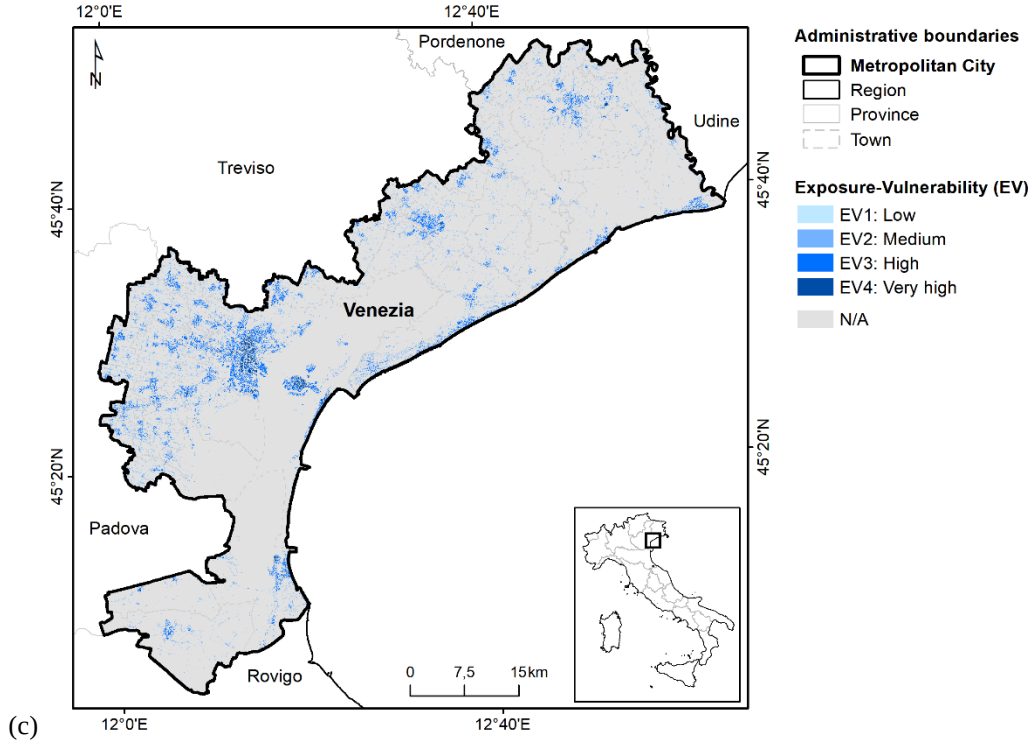

(c)

Figure 21 – Exposure-vulnerability mapping in the metropolitan city of Venezia: (a) GHS-BUILT-C R2023A - GHS Settlement Characteristics [1], (b) WSF Evolution 2015 [2]*, and (c) resulting exposure-vulnerability map.*

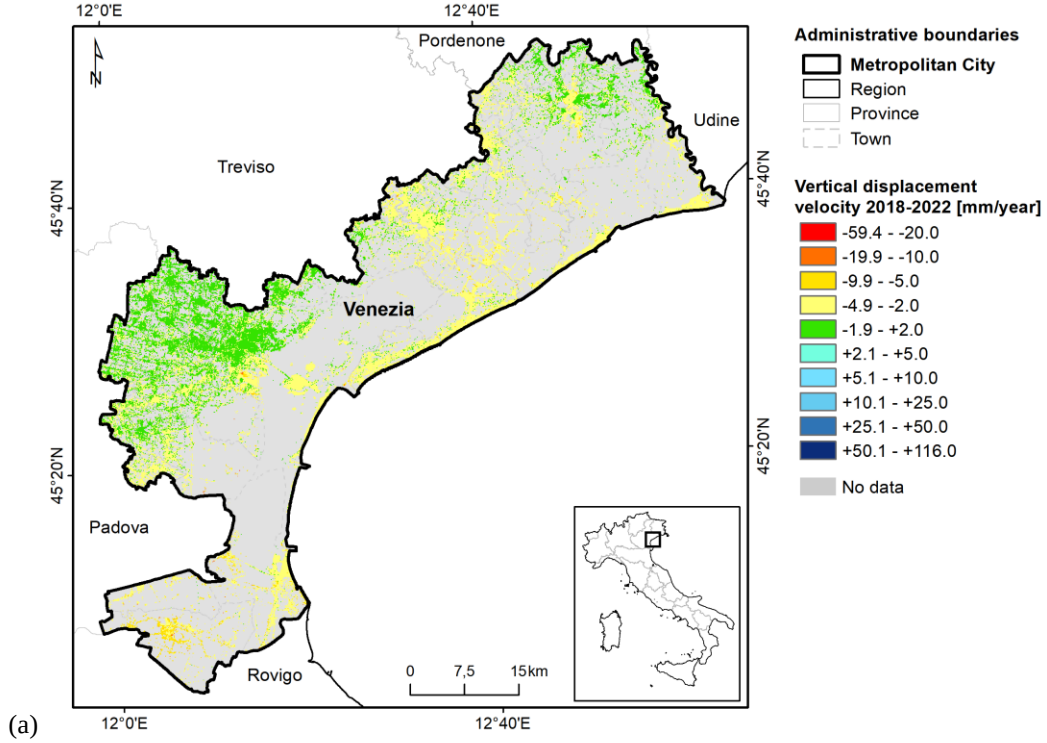

(a)

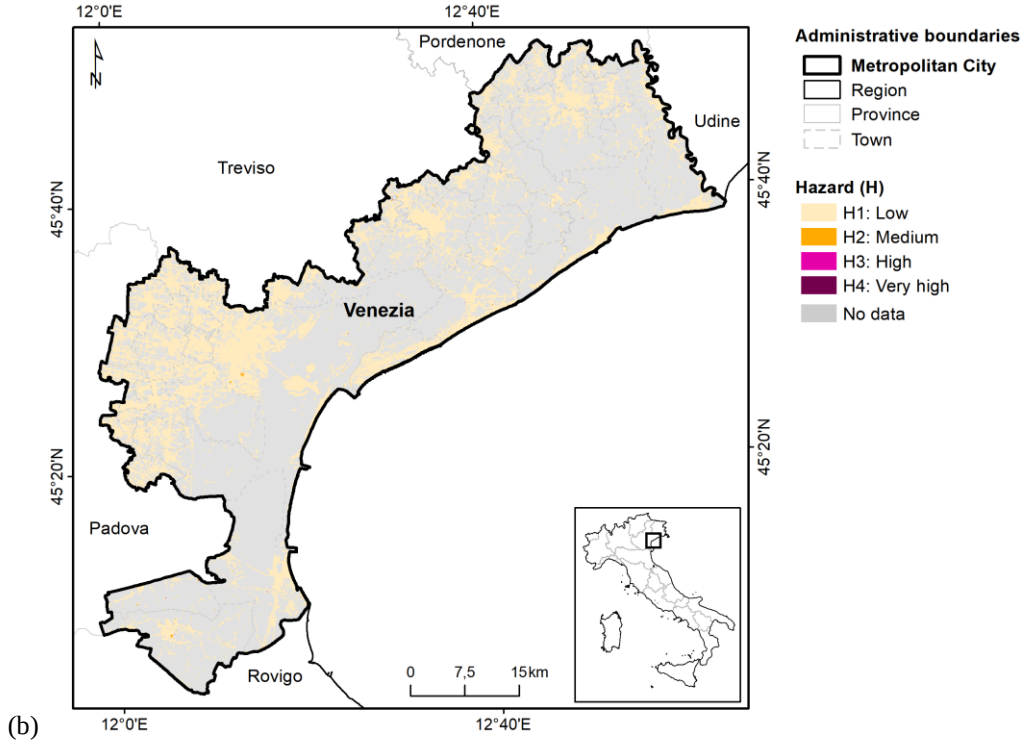

(b)

Figure 22 – Differential displacement hazard mapping in the metropolitan city of Venezia: (a) vertical ground displacement velocity in 2018–2022 based on EGMS Ortho InSAR datasets [5]*, and (b) resulting hazard map..*

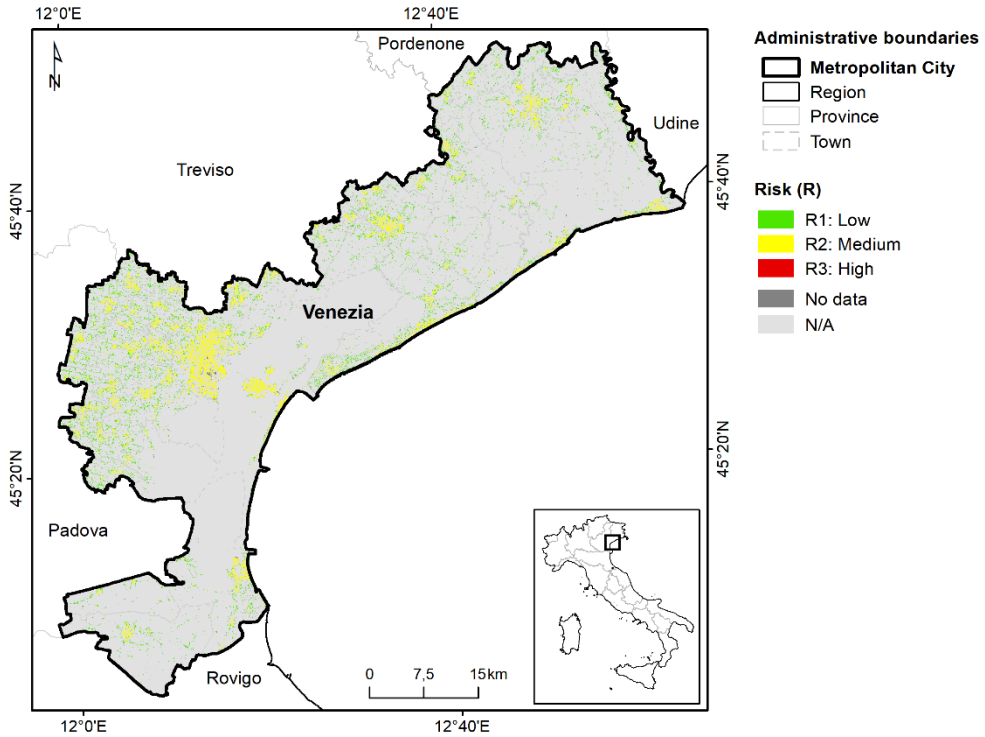

Figure 23 – Differential displacement risk mapping in the metropolitan city of Venezia, based on 2018–2022 satellite InSAR observations.

3.2.5 *Bologna*

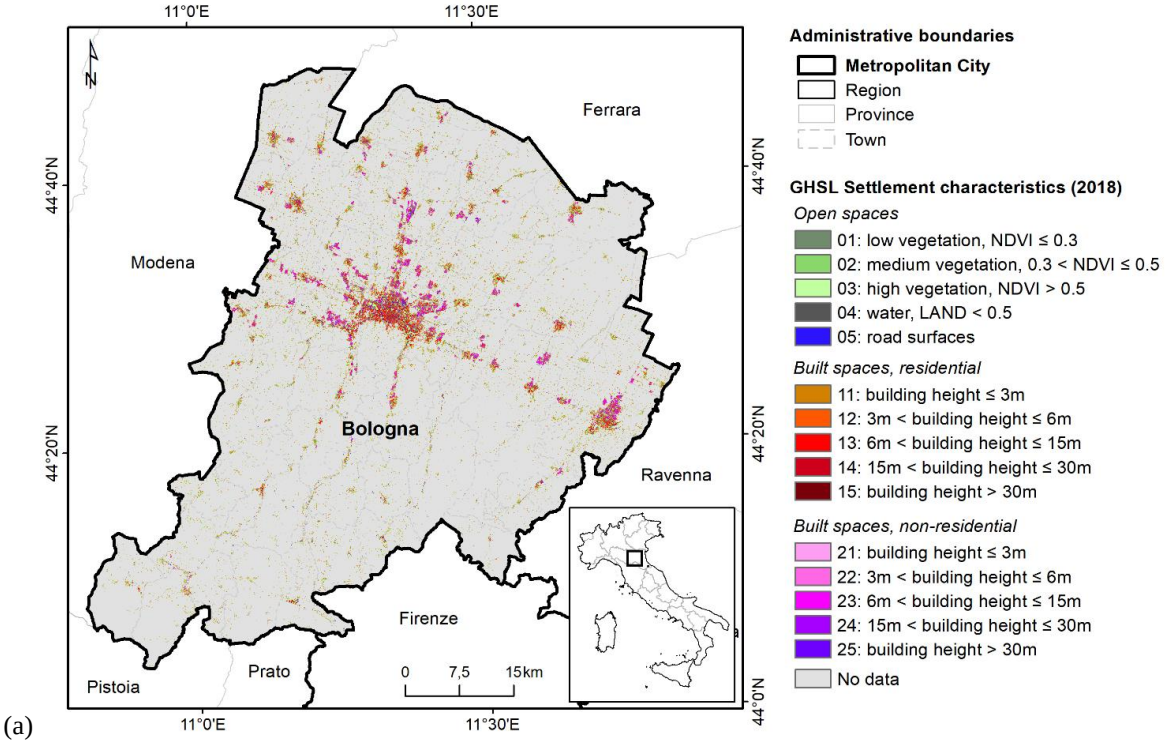

(a)

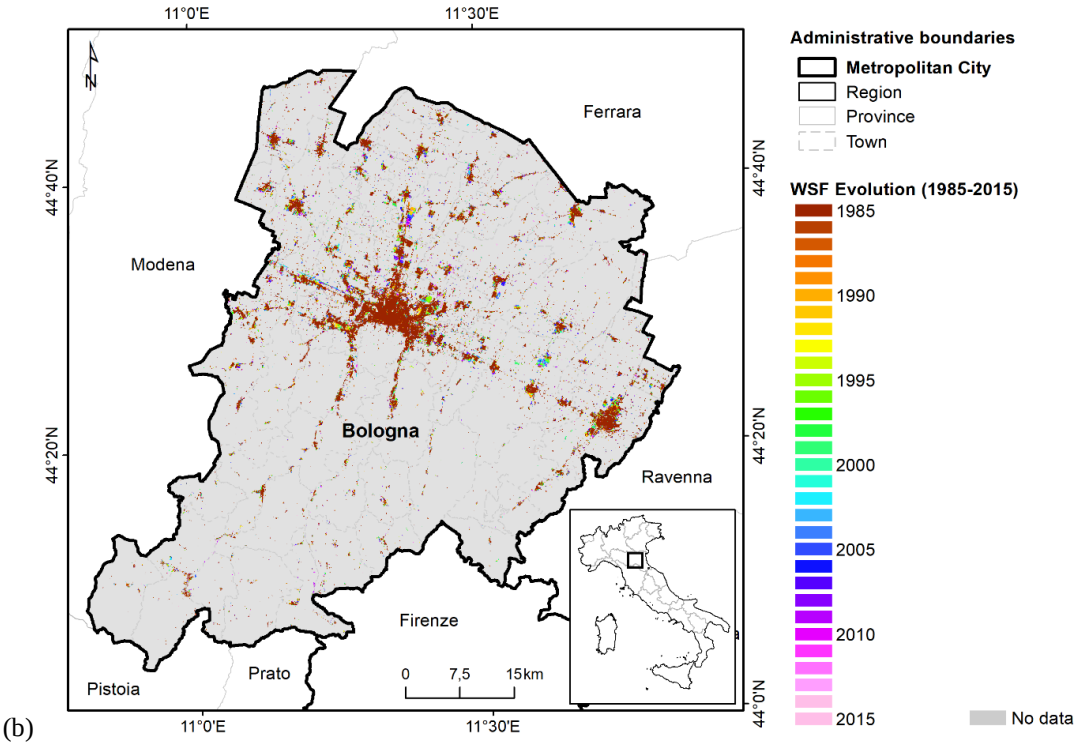

(b)

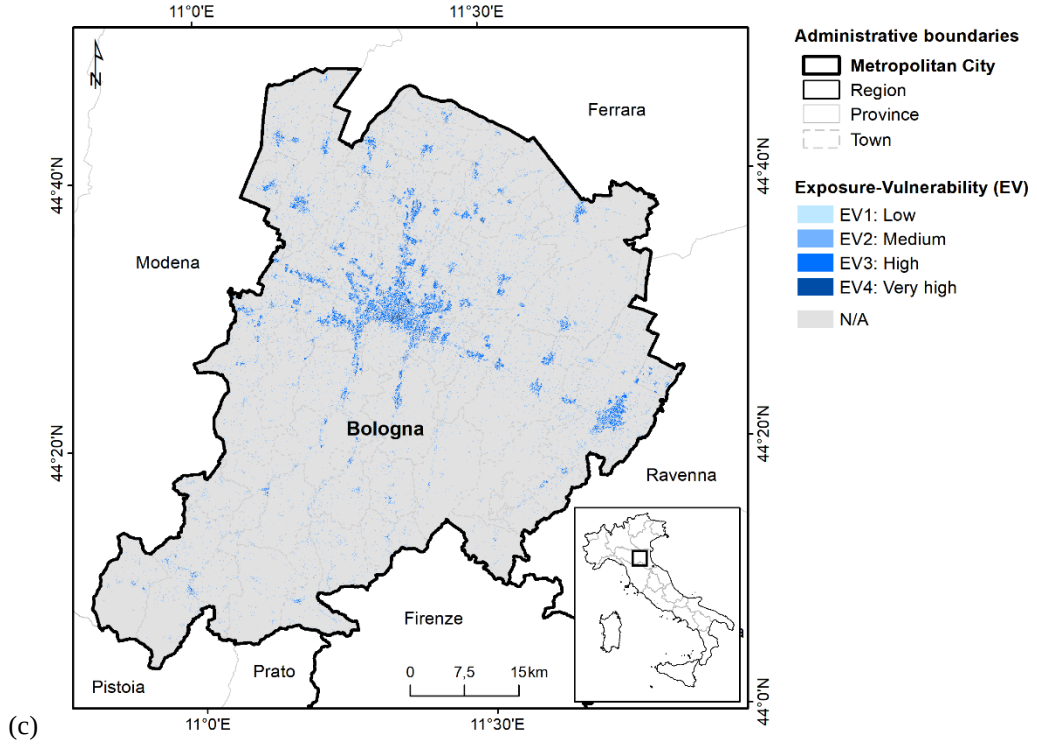

(c)

Figure 24 – Exposure-vulnerability mapping in the metropolitan city of Bologna: (a) GHS-BUILT-C R2023A - GHS Settlement Characteristics [1], (b) WSF Evolution 2015 [2]*, and (c) resulting exposure-vulnerability map.*

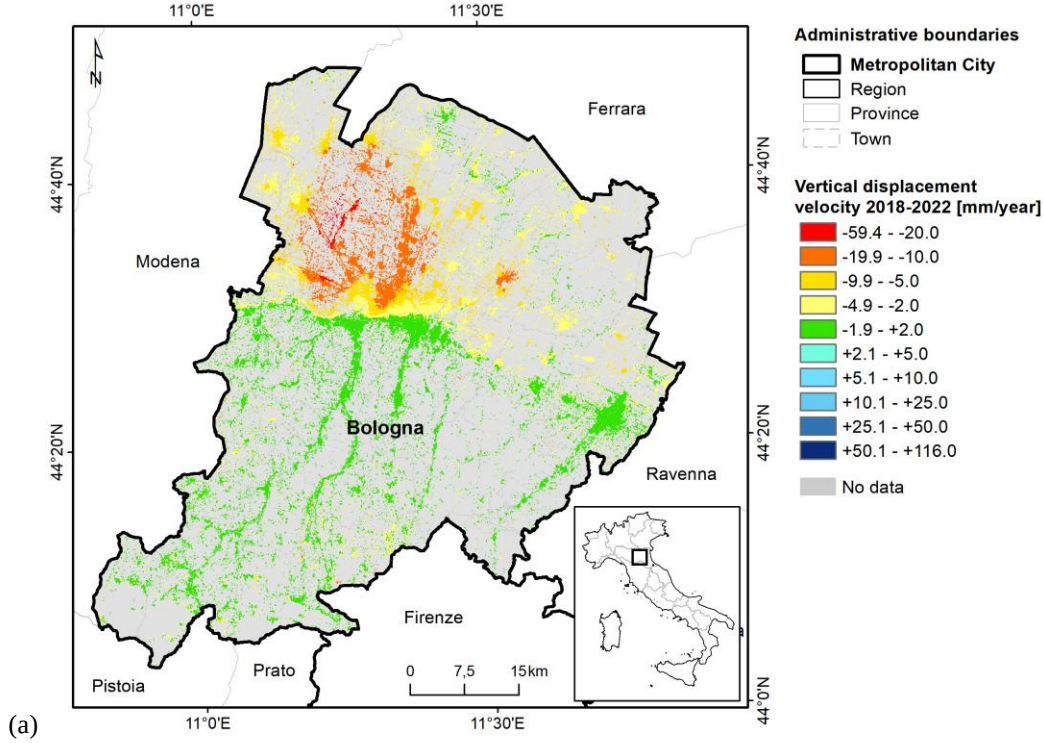

(a)

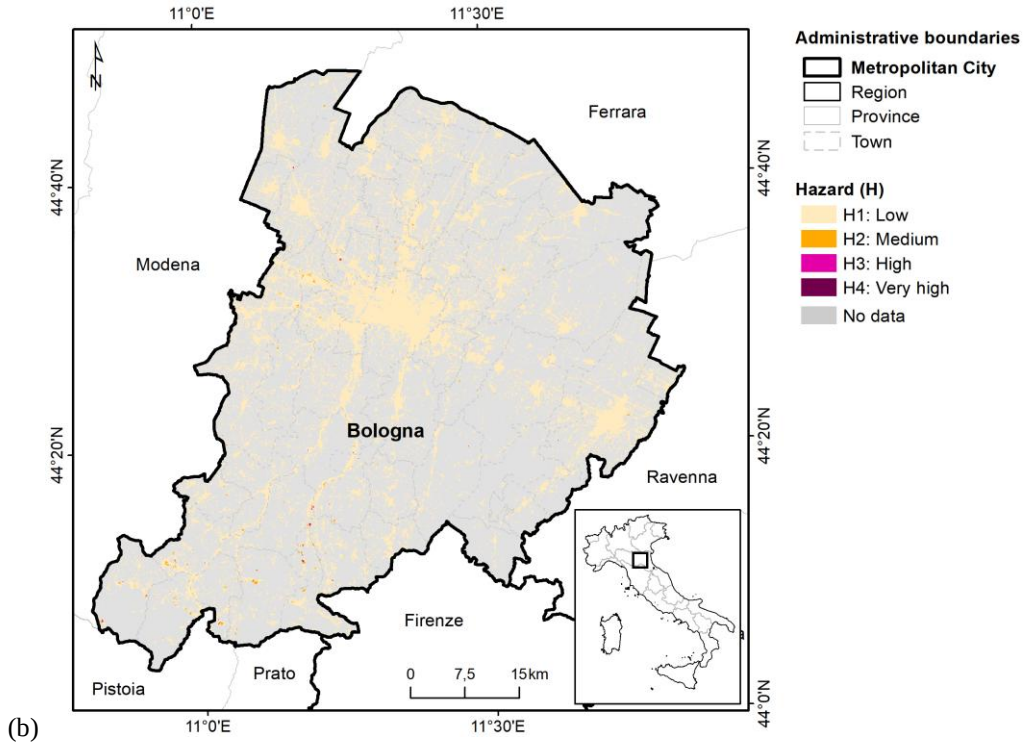

(b)

Figure 25 – Differential displacement hazard mapping in the metropolitan city of Bologna: (a) vertical ground displacement velocity in 2018–2022 based on EGMS Ortho InSAR datasets [5]*, and (b) resulting hazard map.*

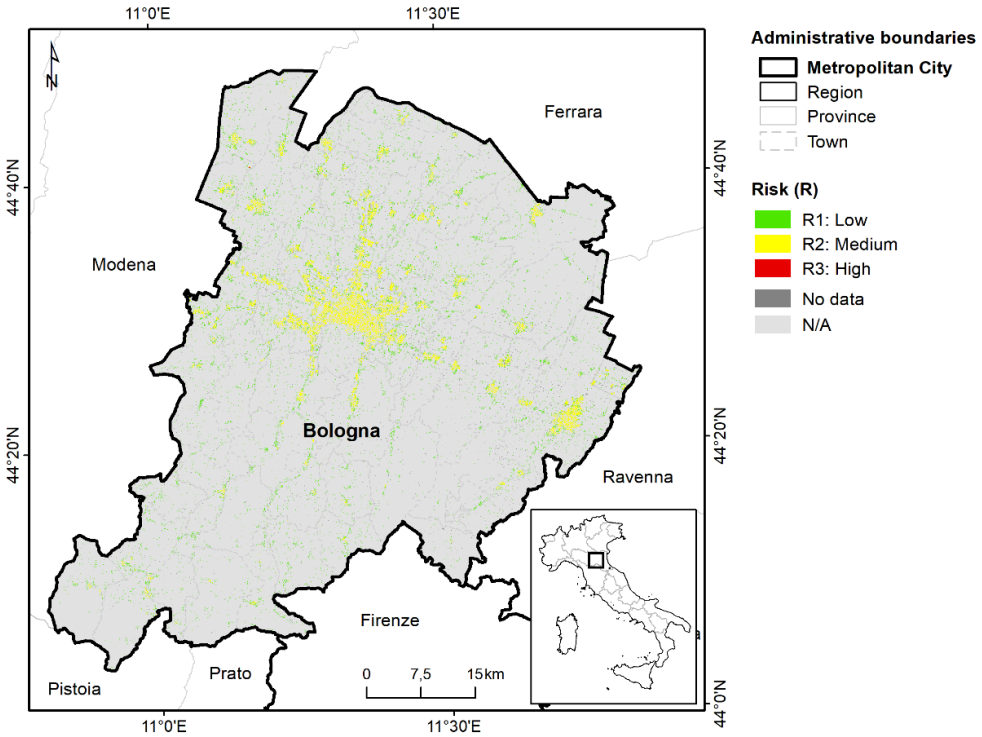

Figure 26 – Differential displacement risk mapping in the metropolitan city of Bologna, based on 2018–2022 satellite InSAR observations.

3.2.6 *Firenze*

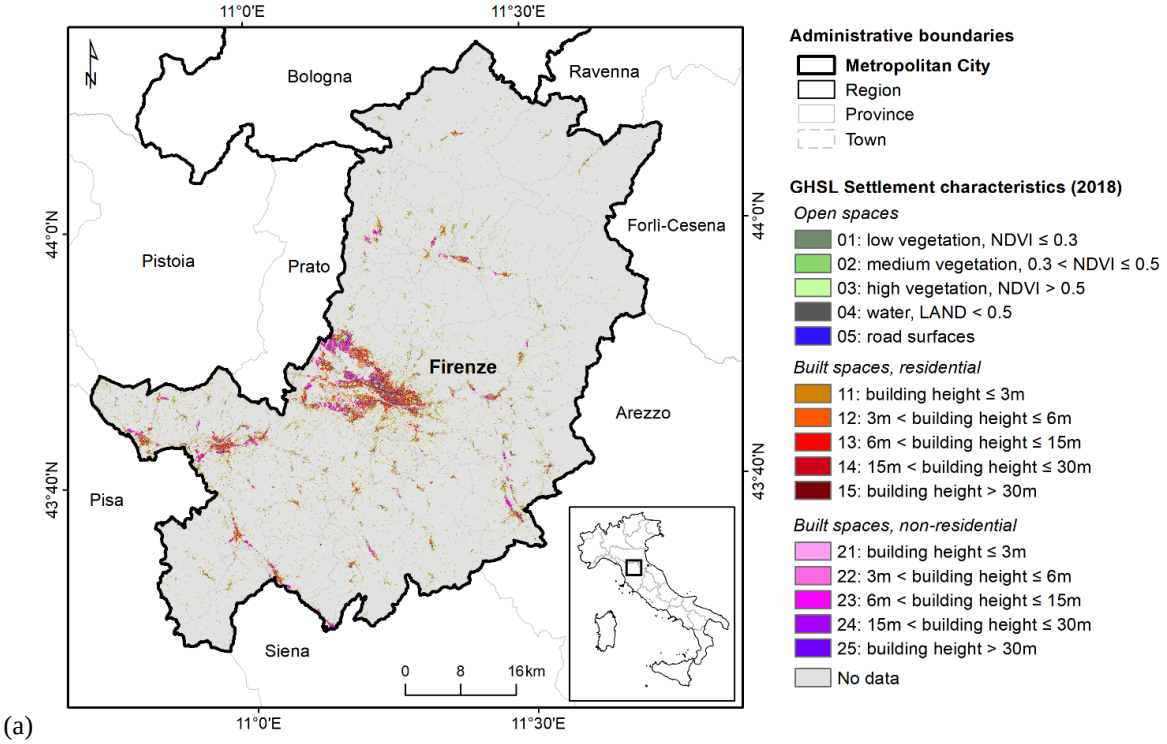

(a)

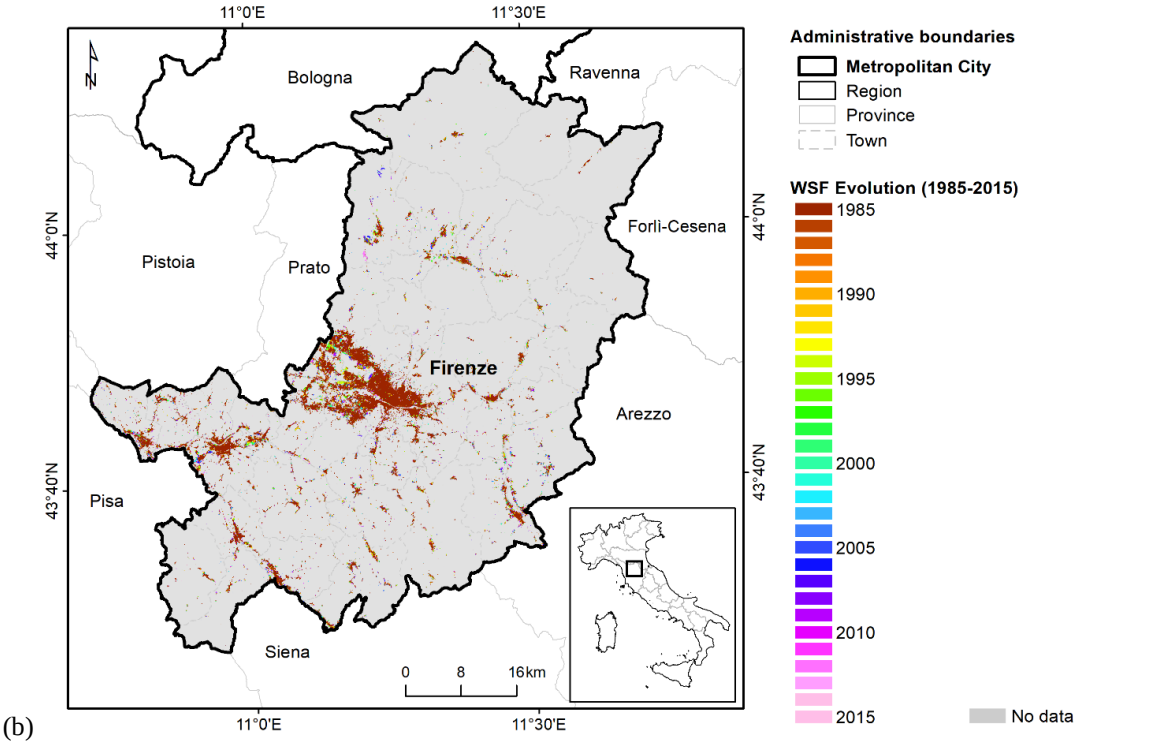

(b)

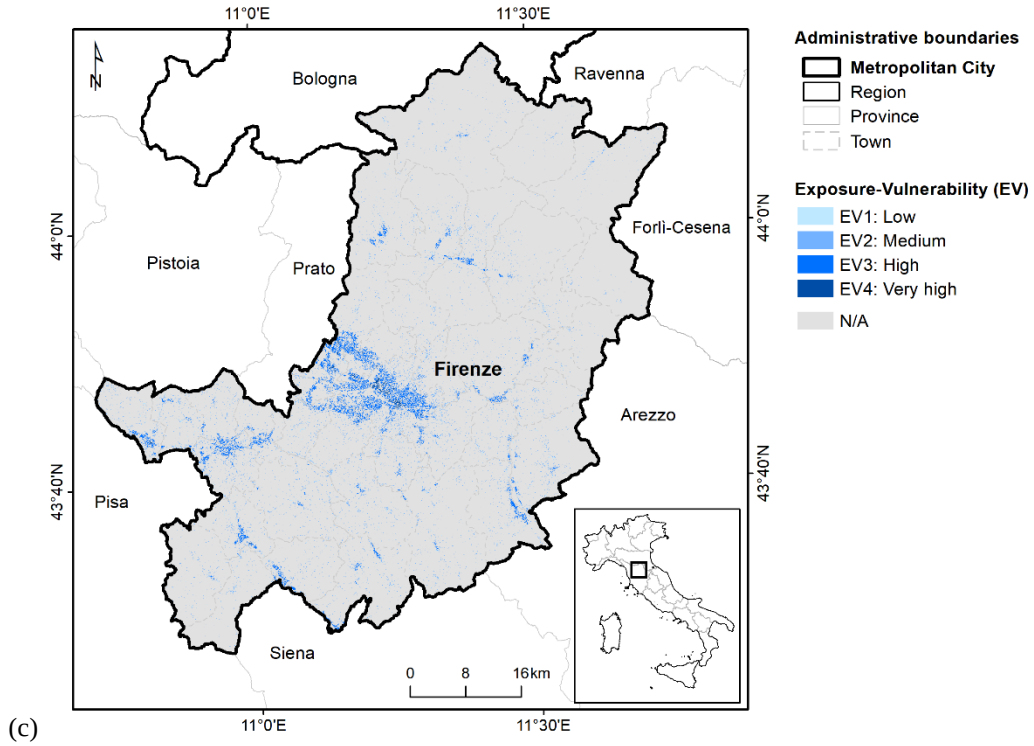

(c)

Figure 27 – Exposure-vulnerability mapping in the metropolitan city of Firenze: (a) GHS-BUILT-C R2023A - GHS Settlement Characteristics [1], (b) WSF Evolution 2015 [2]*, and (c) resulting exposure-vulnerability map.*

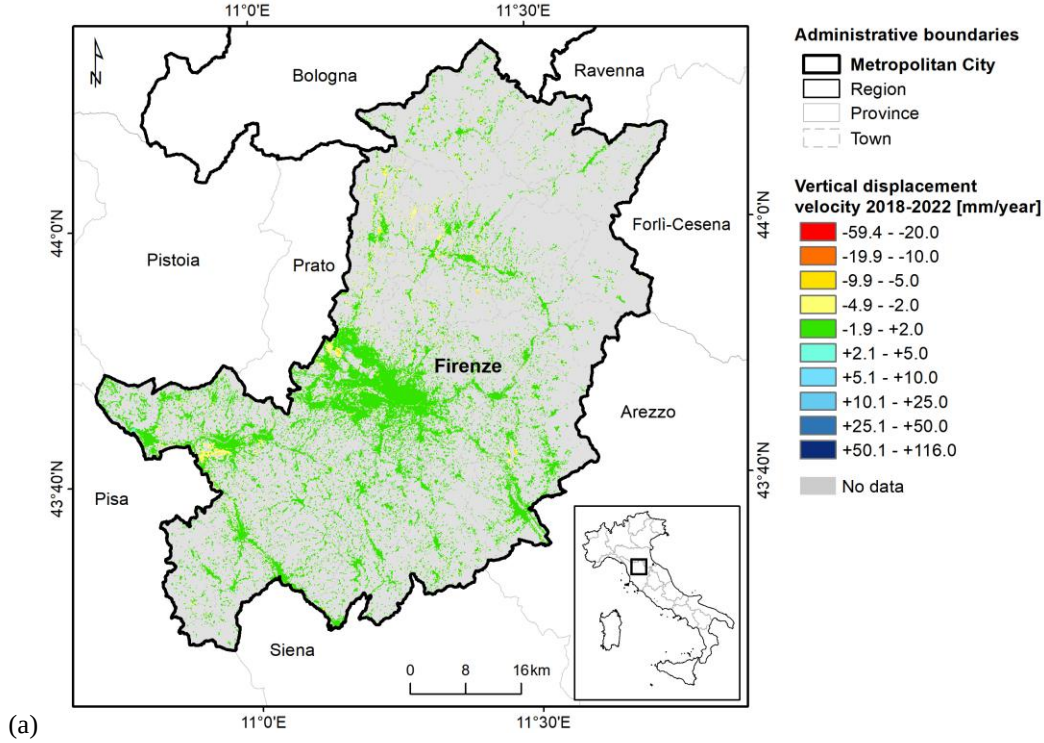

(a)

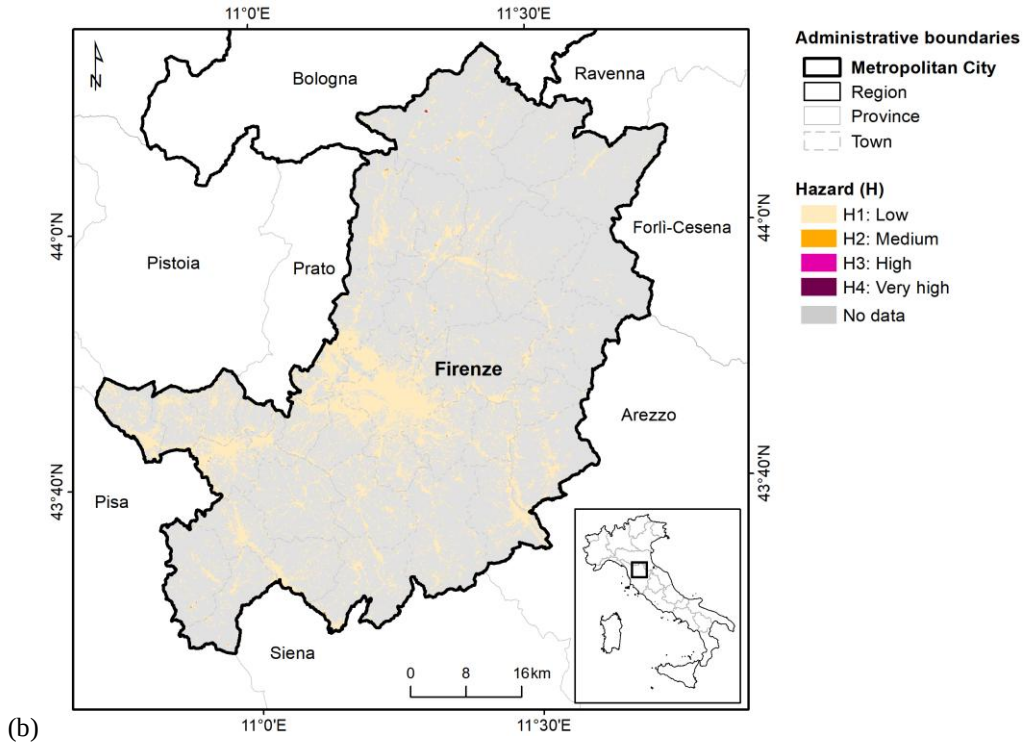

(b)

Figure 28 – Differential displacement hazard mapping in the metropolitan city of Firenze: (a) vertical ground displacement velocity in 2018–2022 based on EGMS Ortho InSAR datasets [5]*, and (b) resulting hazard map.*

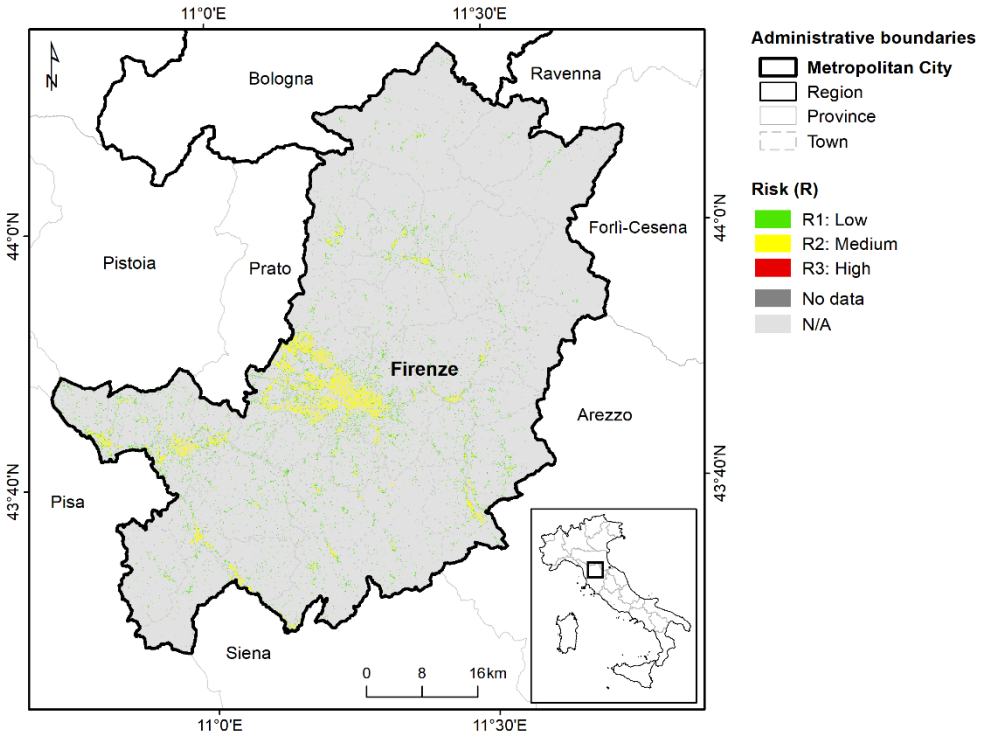

Figure 29 – Differential displacement risk mapping in the metropolitan city of Firenze, based on 2018–2022 satellite InSAR observations.

3.2.7 Roma

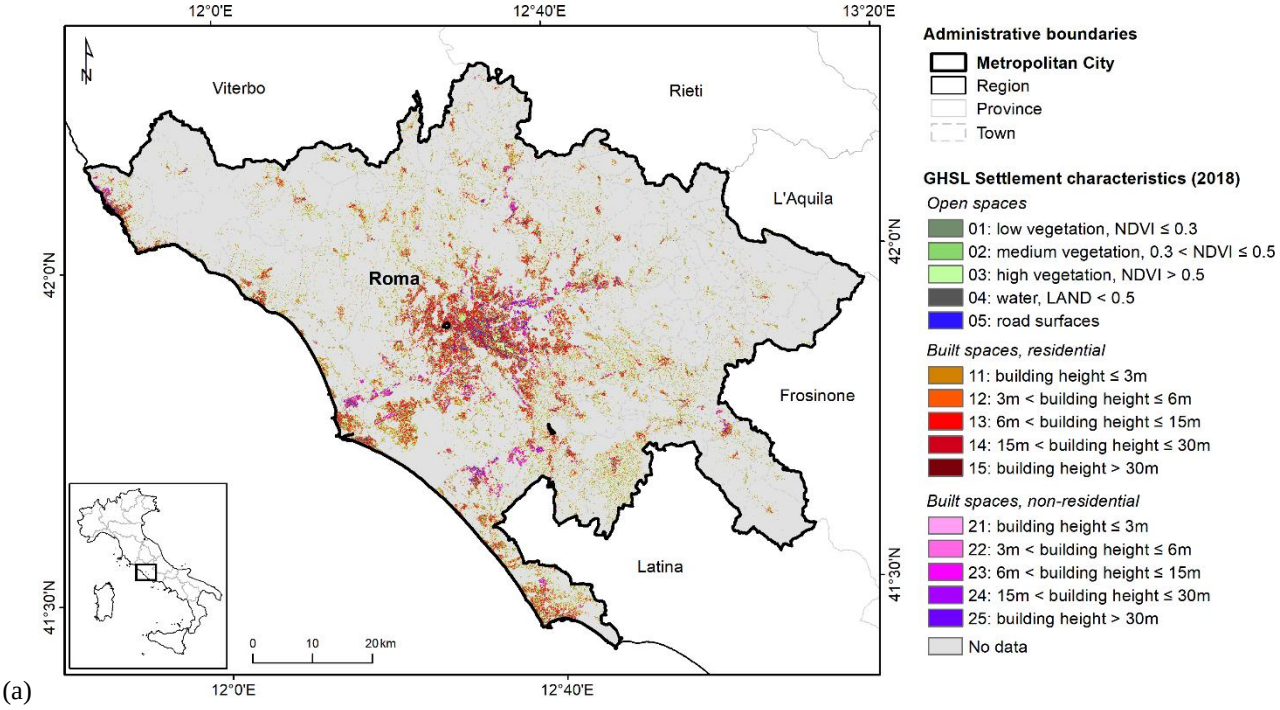
12°0'E
12°40'E
13°20'E
42°0'N
41°30'N
Viterbo
Rieti
L'Aquila
Roma
Frosinone
Latina
0 10 20km
Administrative boundaries
Metropolitan City
Region
Province
Town
GHSL Settlement characteristics (2018)
Open spaces
01: low vegetation, NDVI ≤ 0.3
02: medium vegetation, 0.3 < NDVI ≤ 0.5
03: high vegetation, NDVI > 0.5
04: water, LAND < 0.5
05: road surfaces
Built spaces, residential
11: building height ≤ 3m
12: 3m < building height ≤ 6m
13: 6m < building height ≤ 15m
14: 15m < building height ≤ 30m
15: building height > 30m
Built spaces, non-residential
21: building height ≤ 3m
22: 3m < building height ≤ 6m
23: 6m < building height ≤ 15m
24: 15m < building height ≤ 30m
25: building height > 30m
No data

(a)

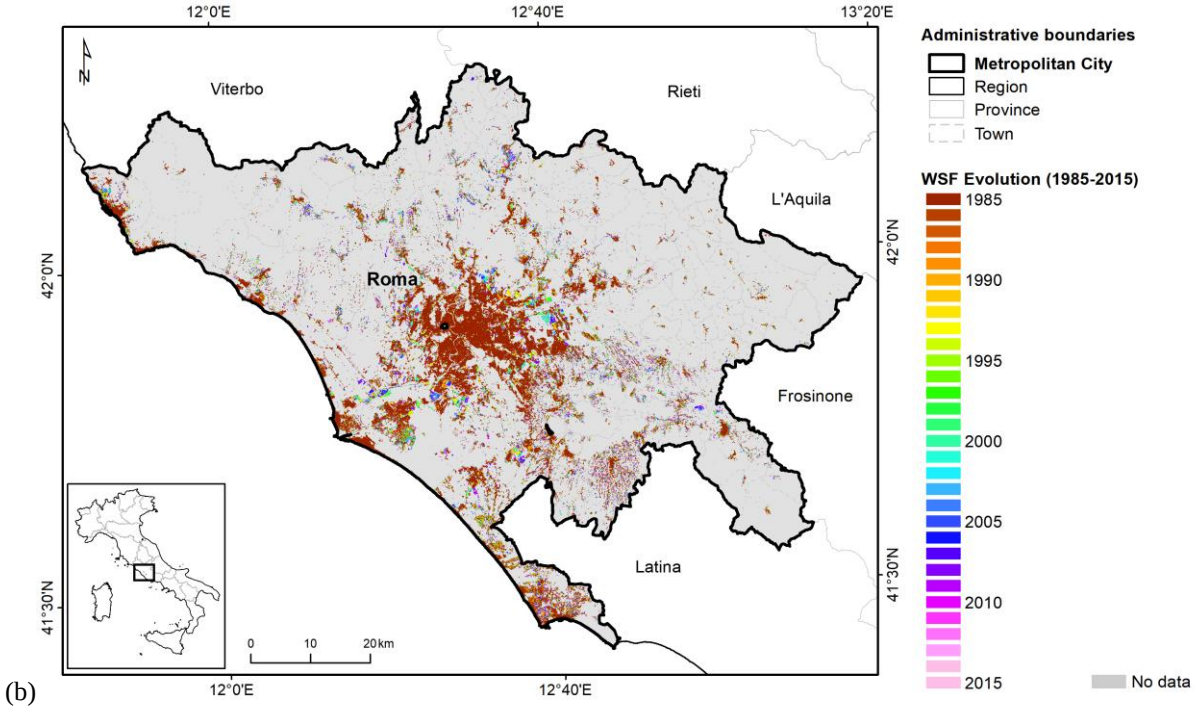
12°0'E
12°40'E
13°20'E
42°0'N
41°30'N
Viterbo
Rieti
L'Aquila
Roma
Frosinone
Latina
0 10 20km
Administrative boundaries
Metropolitan City
Region
Province
Town
WSF Evolution (1985-2015)
1985
1990
1995
2000
2005
2010
2015
No data

(b)

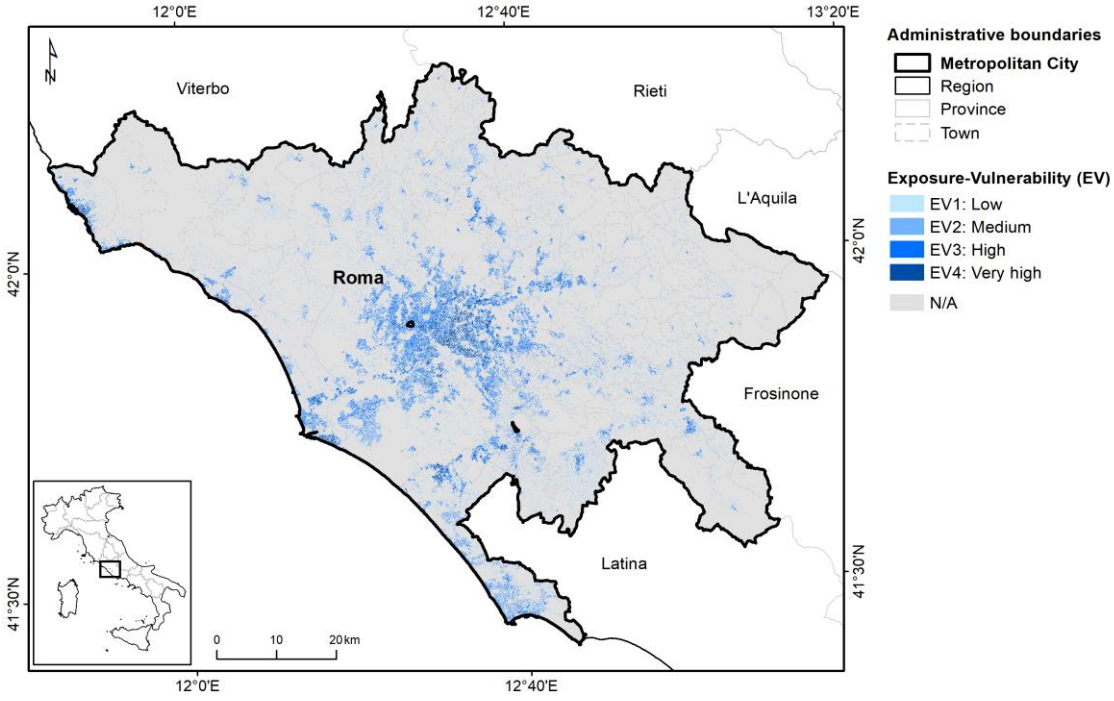

(c)

Figure 30 – Exposure-vulnerability mapping in the metropolitan city of Roma: (a) GHS-BUILT-C R2023A - GHS Settlement Characteristics [1], (b) WSF Evolution 2015 [2]*, and (c) resulting exposure-vulnerability map.*

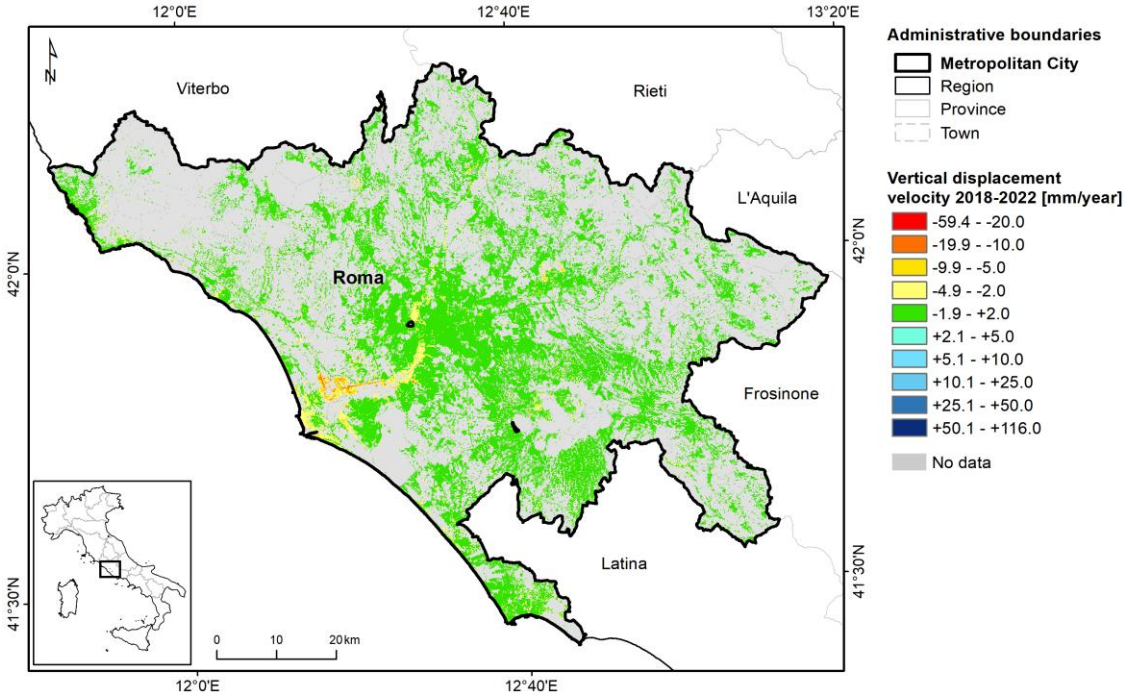

(a)

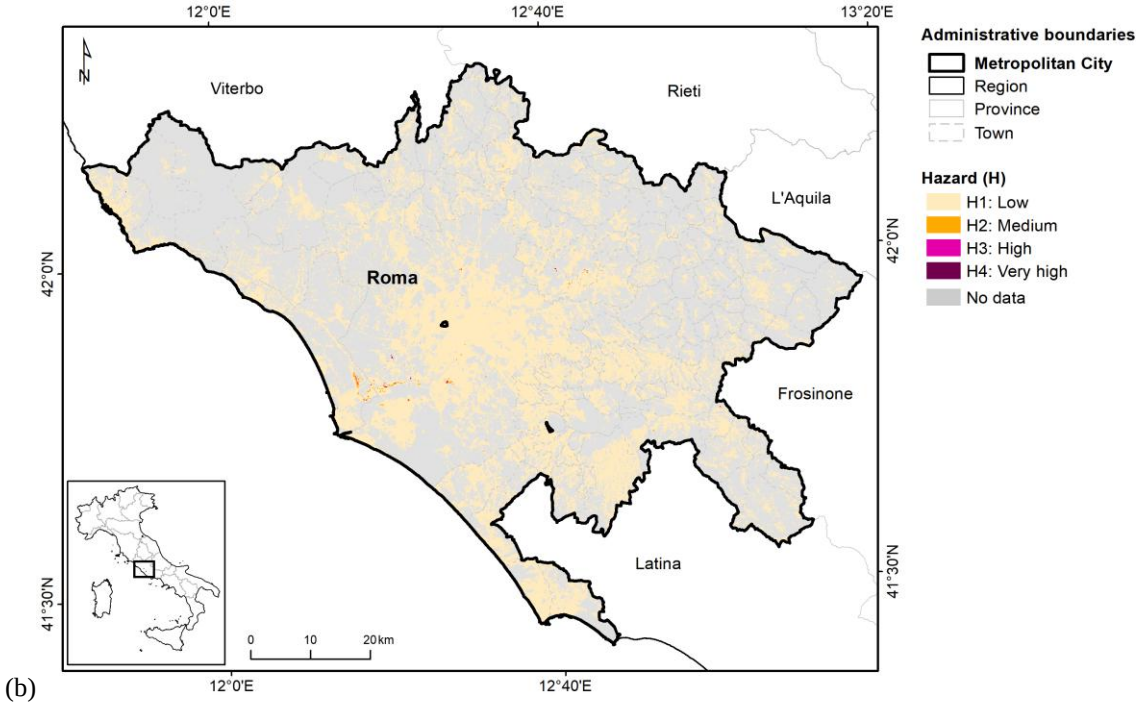

(b)

Figure 31 – Differential displacement hazard mapping in the metropolitan city of Roma: (a) vertical ground displacement velocity in 2018–2022 based on EGMS Ortho InSAR datasets [5]*, and (b) resulting hazard map.*

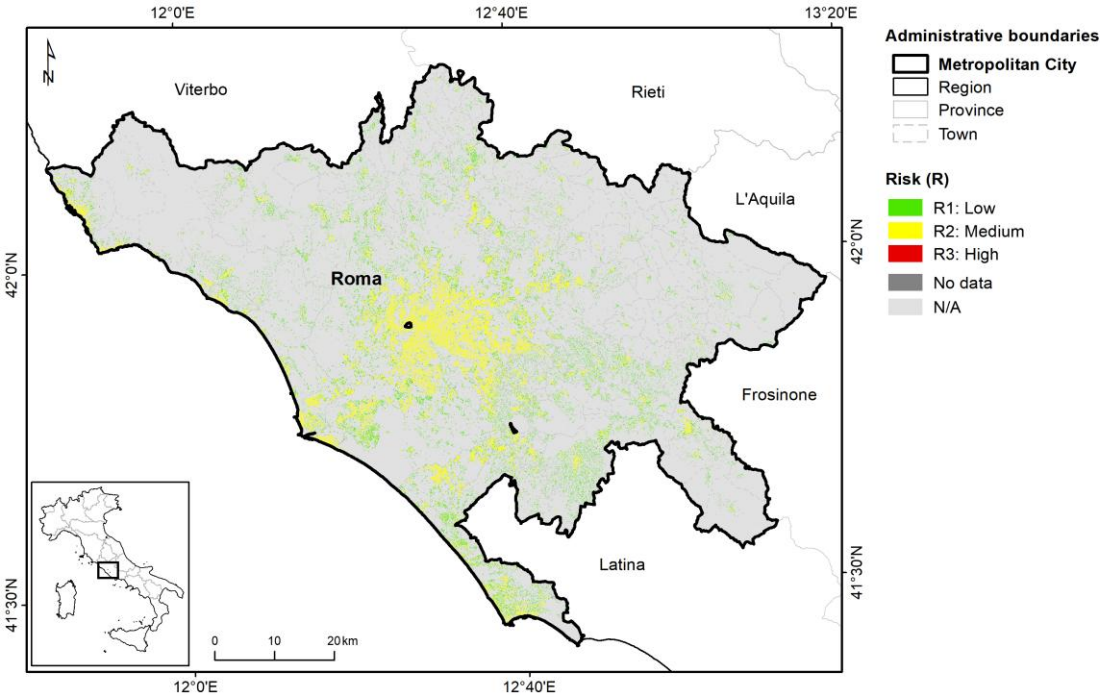

Figure 32 – Differential displacement risk mapping in the metropolitan city of Roma, based on 2018–2022 satellite InSAR observations.

3.2.8 Napoli

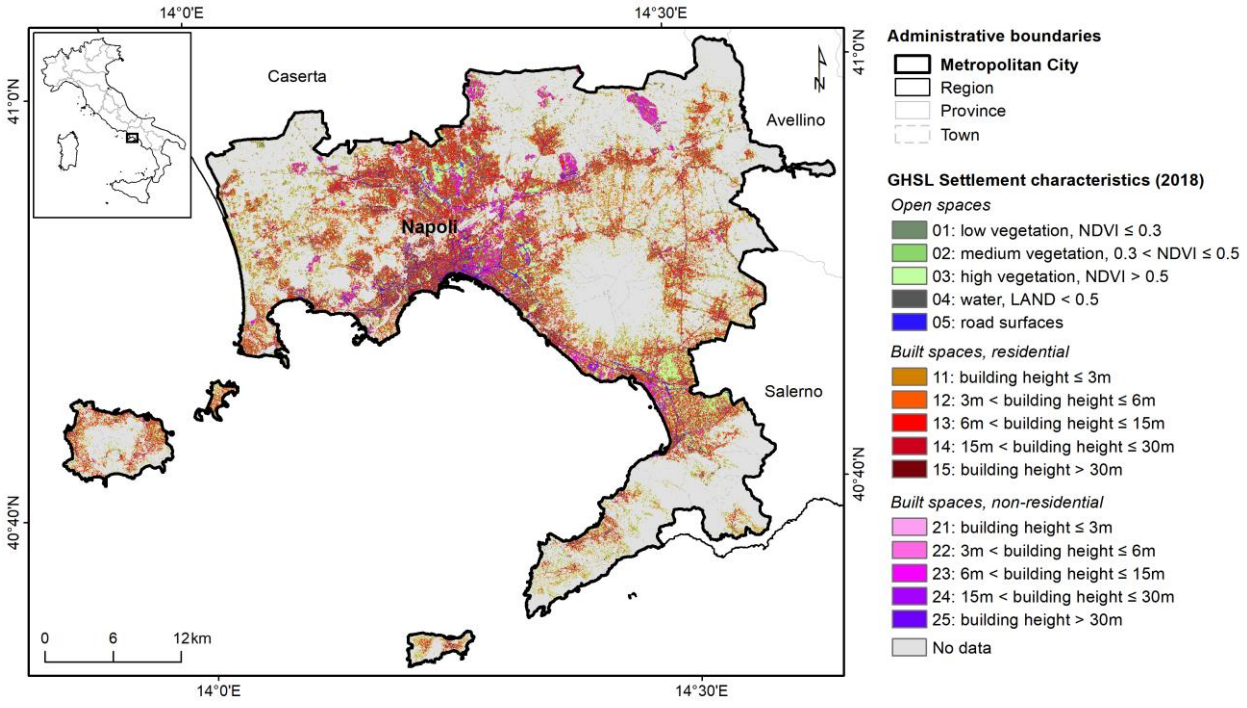

(a)

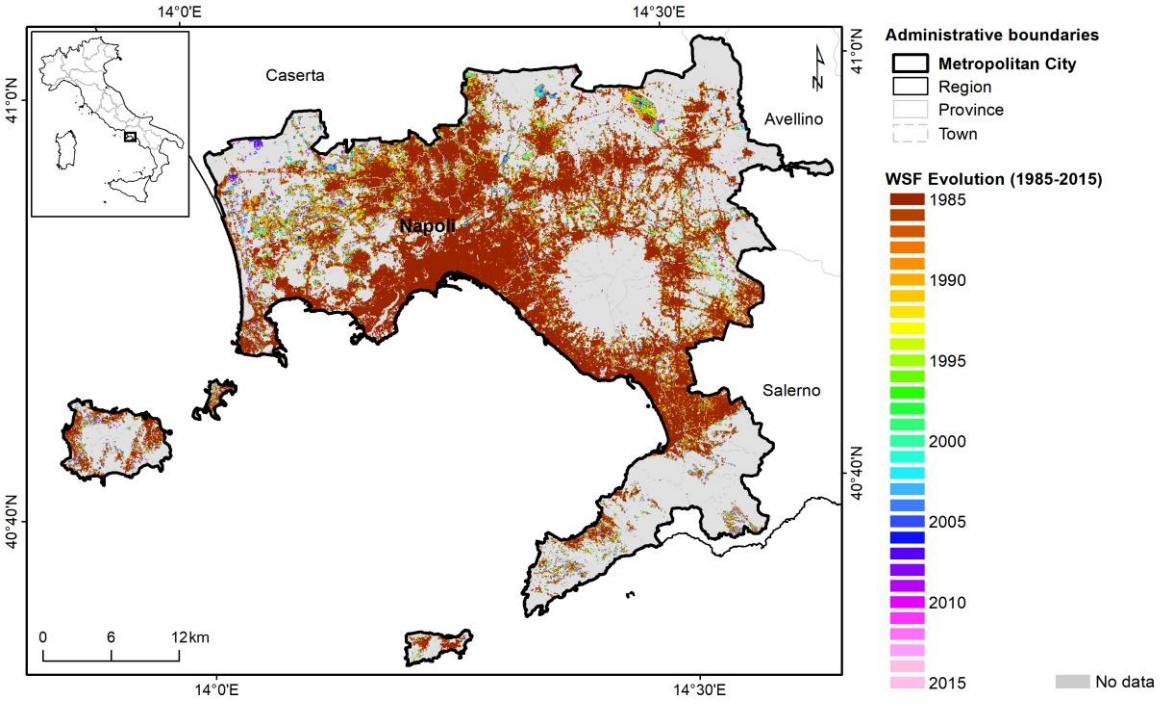

(b)

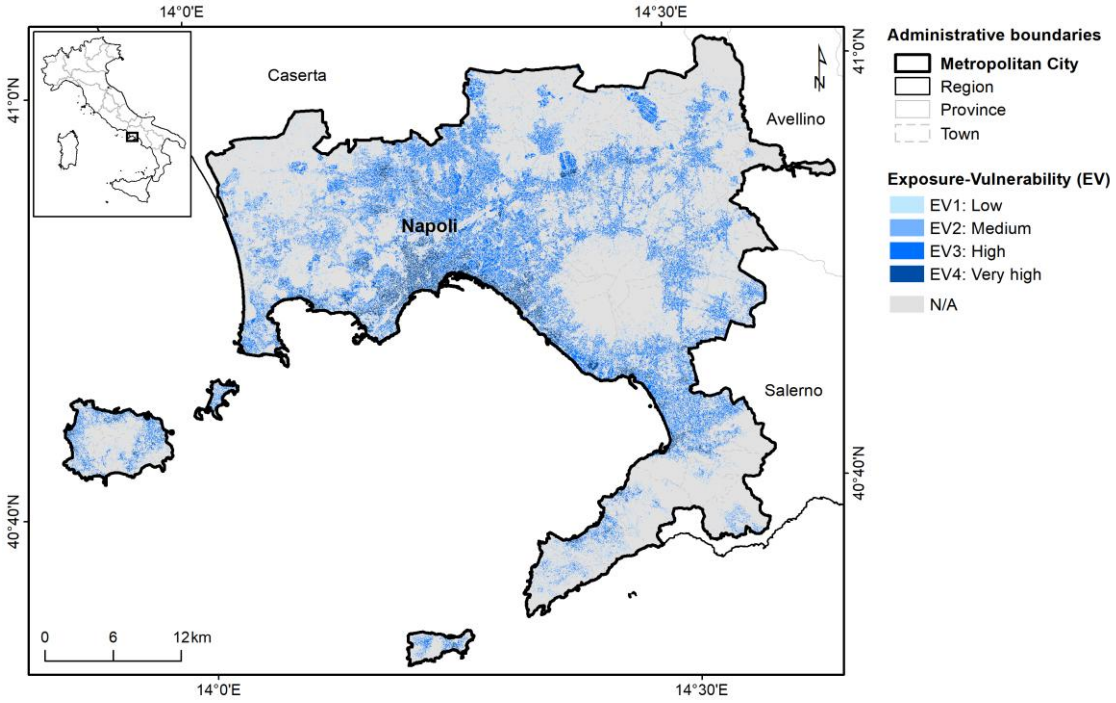

(c)

Figure 33 – Exposure-vulnerability mapping in the metropolitan city of Napoli: (a) GHS-BUILT-C R2023A - GHS Settlement Characteristics [1], (b) WSF Evolution 2015 [2]*, and (c) resulting exposure-vulnerability map.*

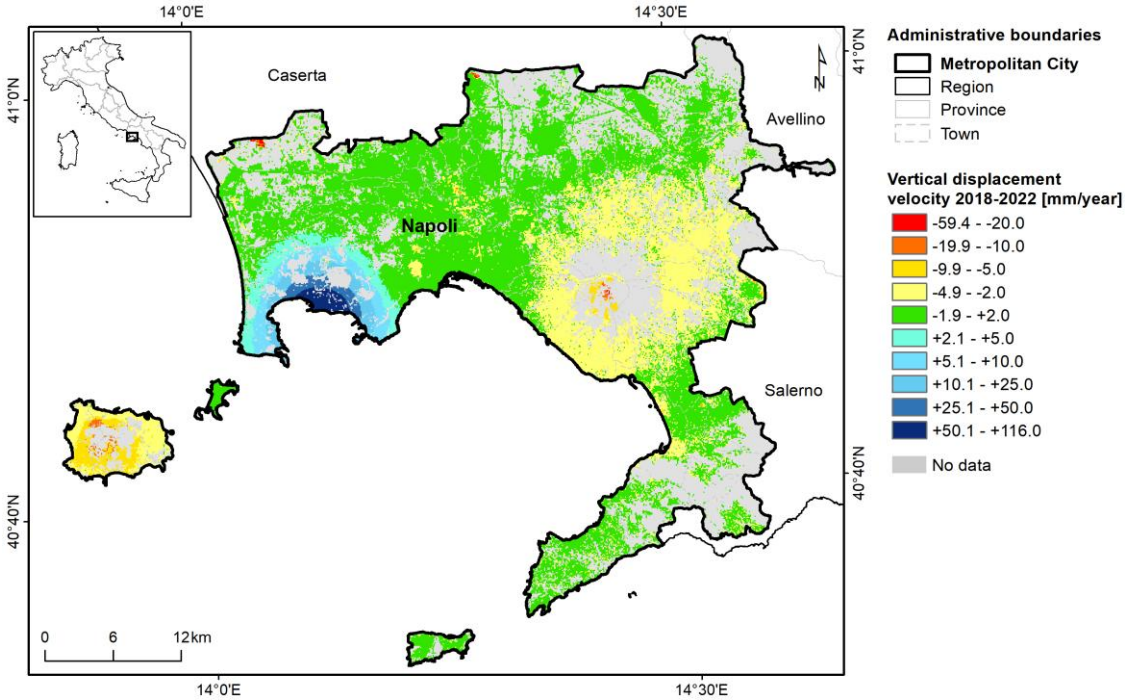

(a)

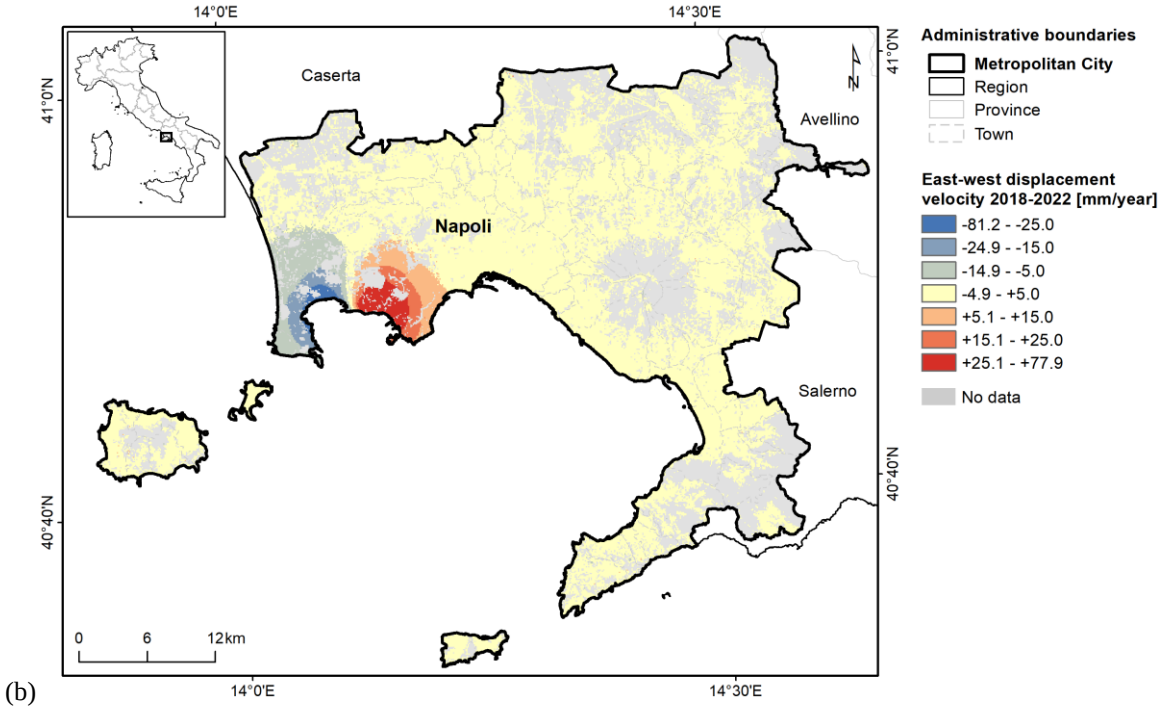

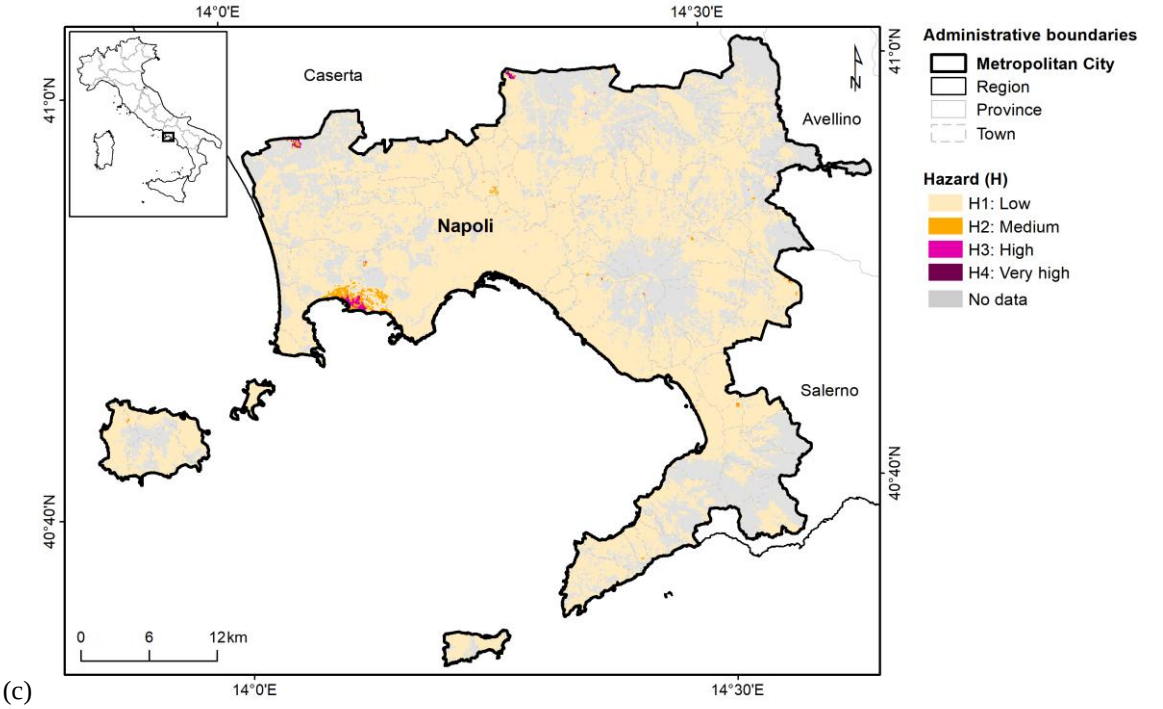

Figure 34 – Differential displacement hazard mapping in the metropolitan city of Napoli: (a) vertical and (b) east-west ground displacement velocity in 2018–2022 based on EGMS Ortho InSAR datasets [5,6]*, and (c) resulting hazard map.*

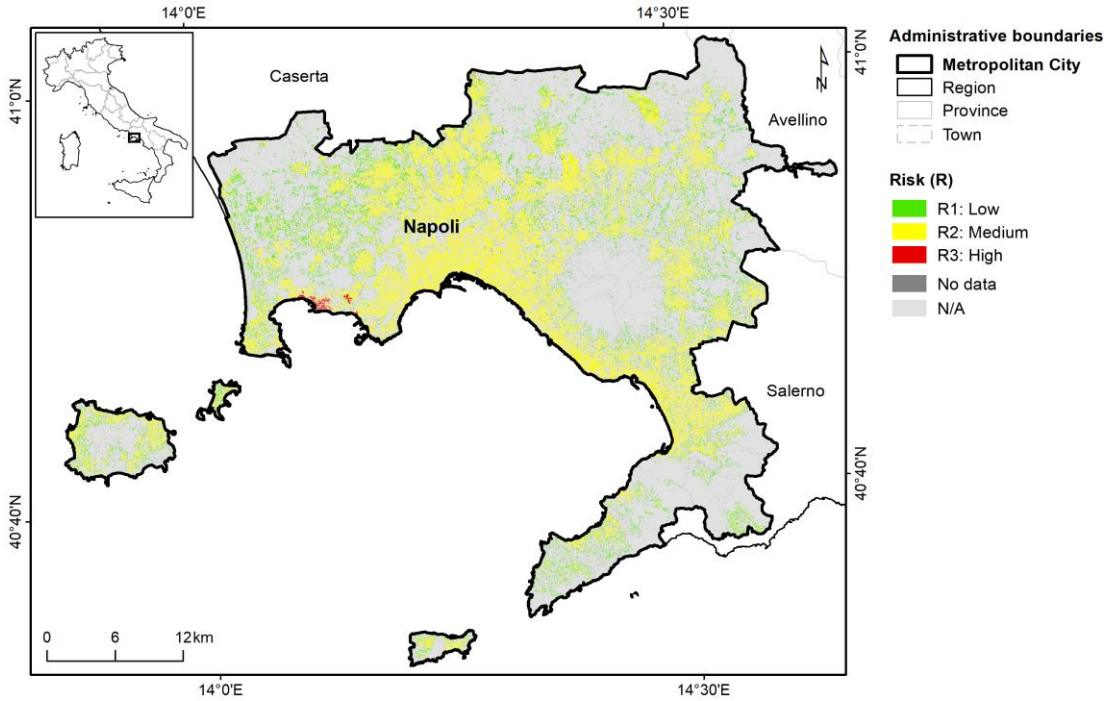

Figure 35 – Differential displacement risk mapping in the metropolitan city of Napoli, based on 2018–2022 satellite InSAR observations.

3.2.9 Bari

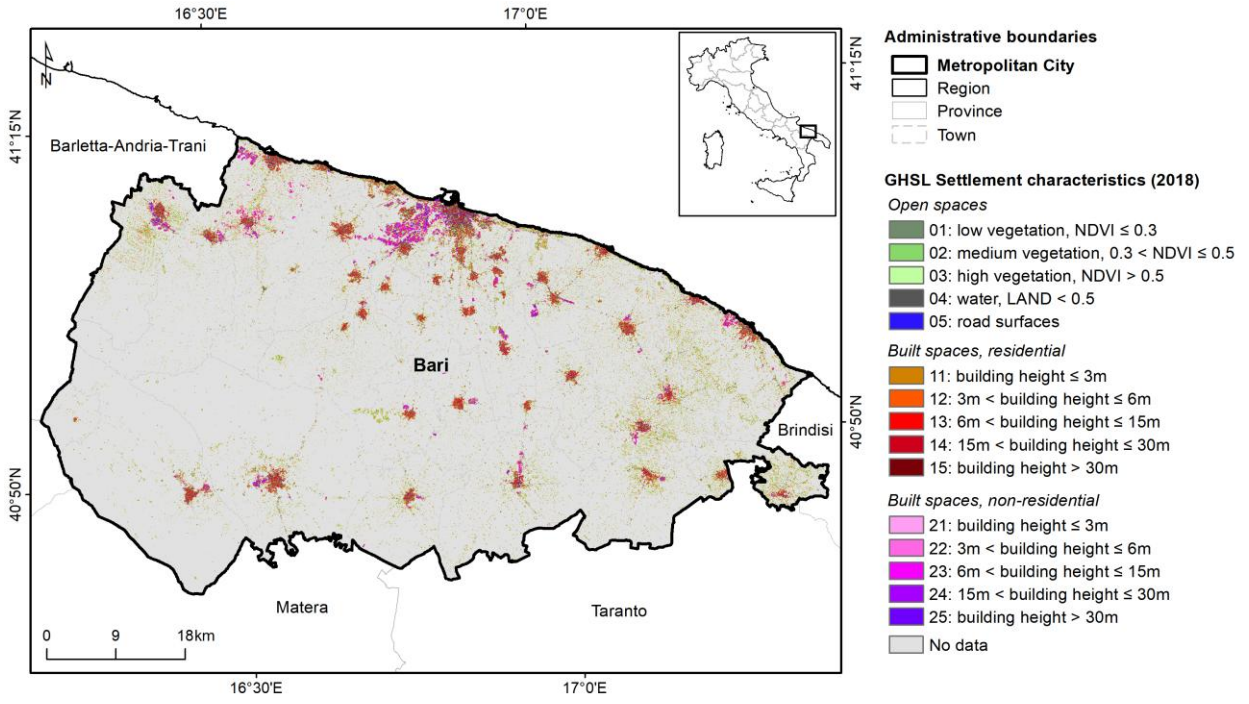

(a)

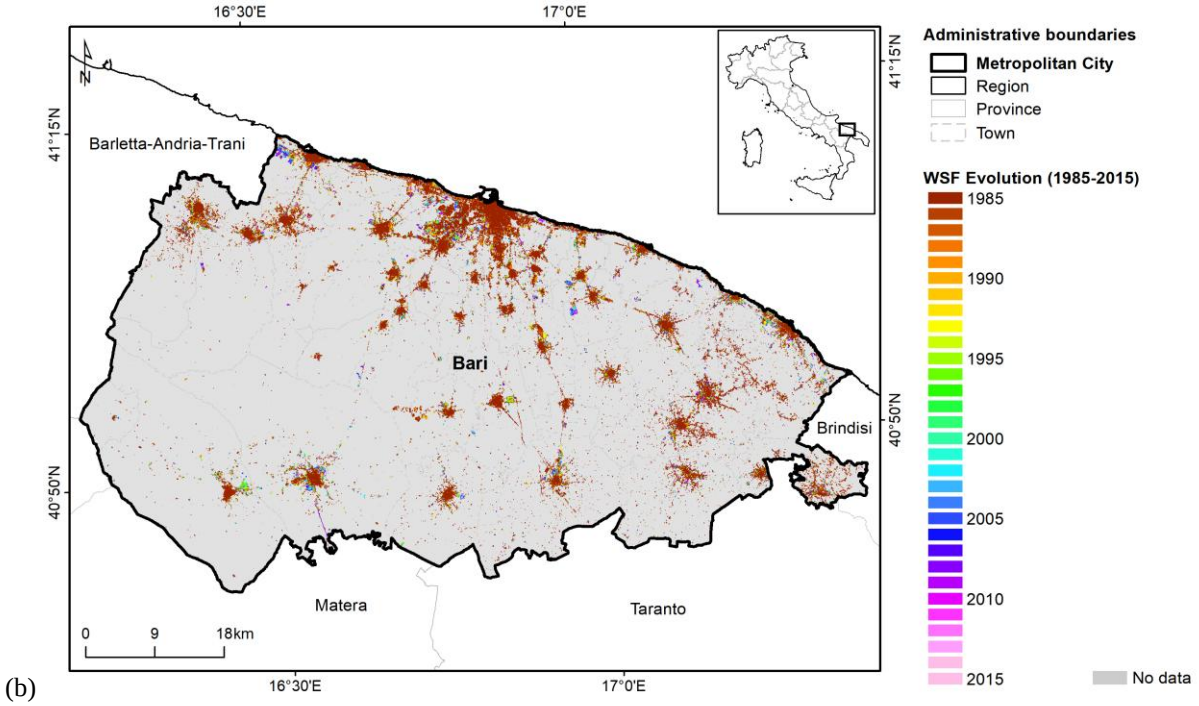

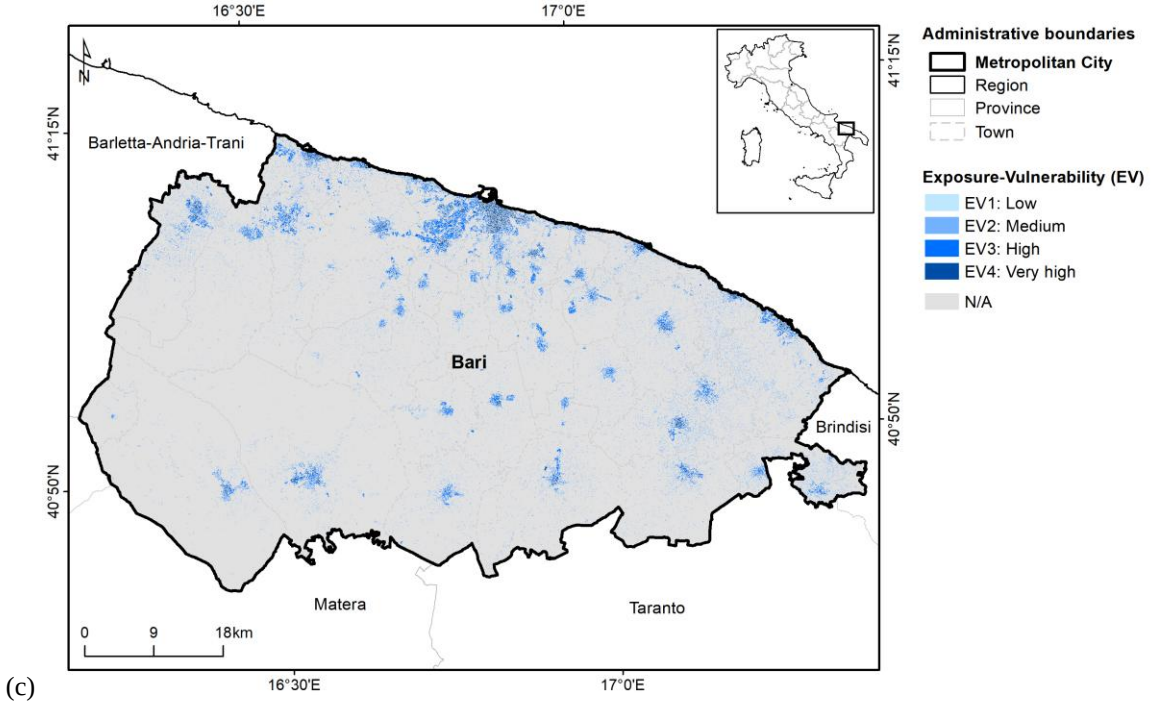

Figure 36 – Exposure-vulnerability mapping in the metropolitan city of Bari: (a) GHS-BUILT-C R2023A - GHS Settlement Characteristics [1], (b) WSF Evolution 2015 [2]*, and (c) resulting exposure-vulnerability map.*

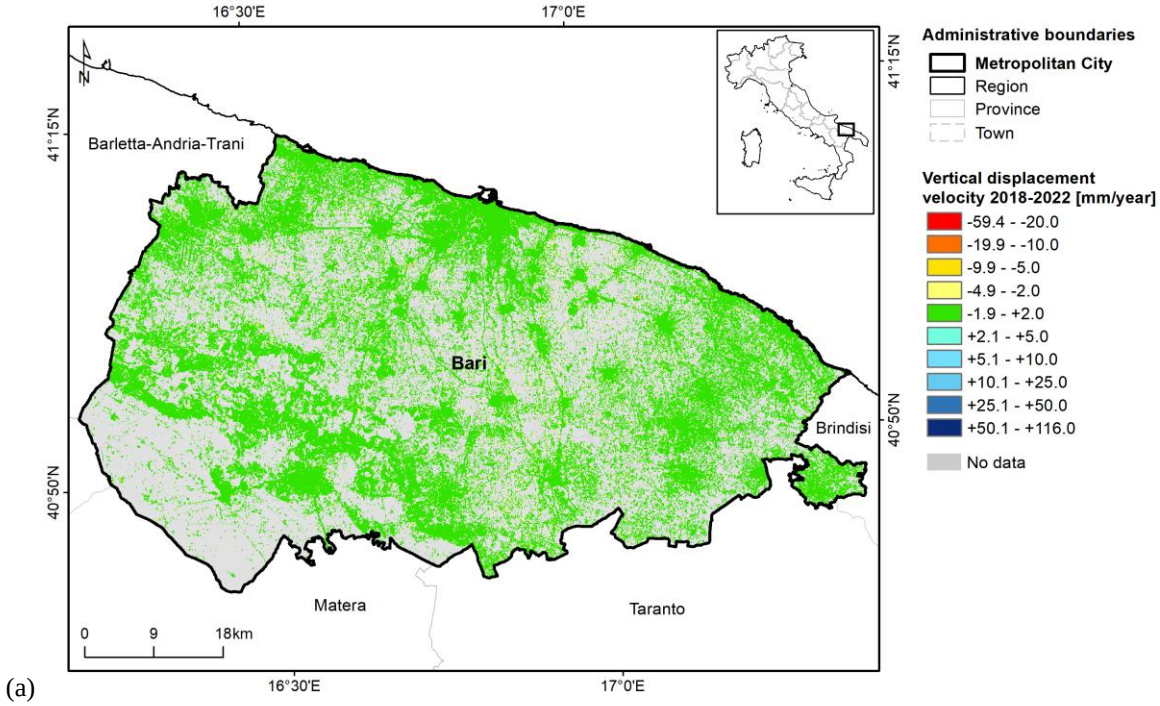

(a)

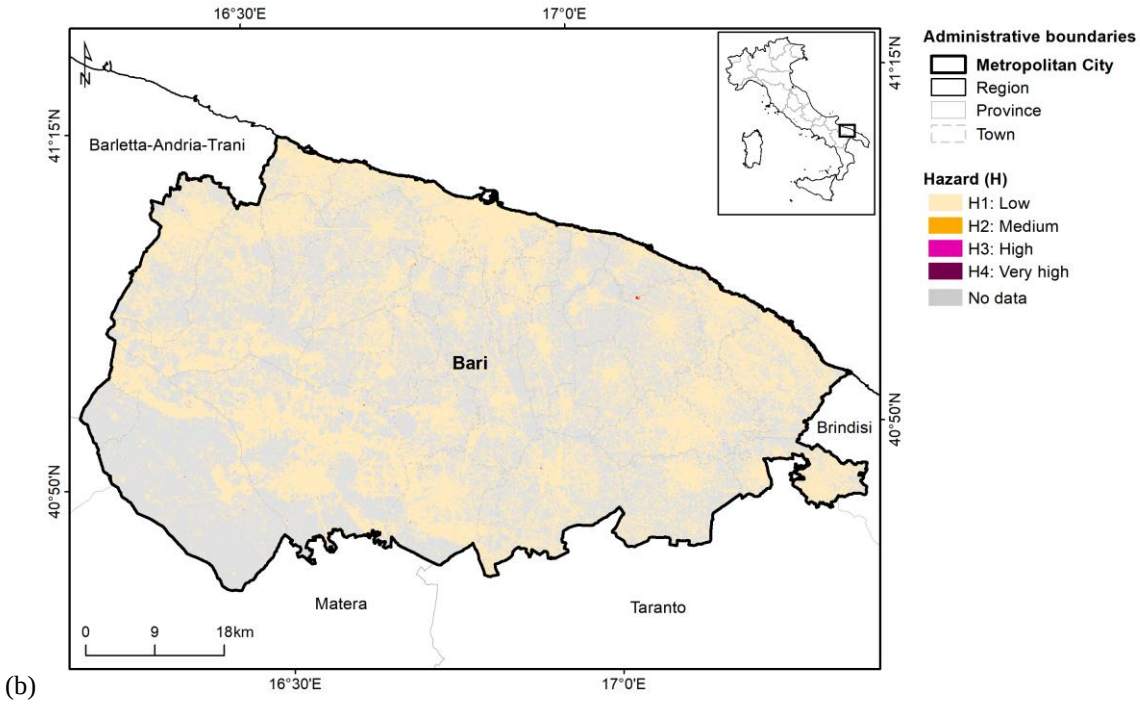

(b)

Figure 37 – Differential displacement hazard mapping in the metropolitan city of Bari: (a) vertical ground displacement velocity in 2018–2022 based on EGMS Ortho InSAR datasets [5]*, and (b) resulting hazard map.*

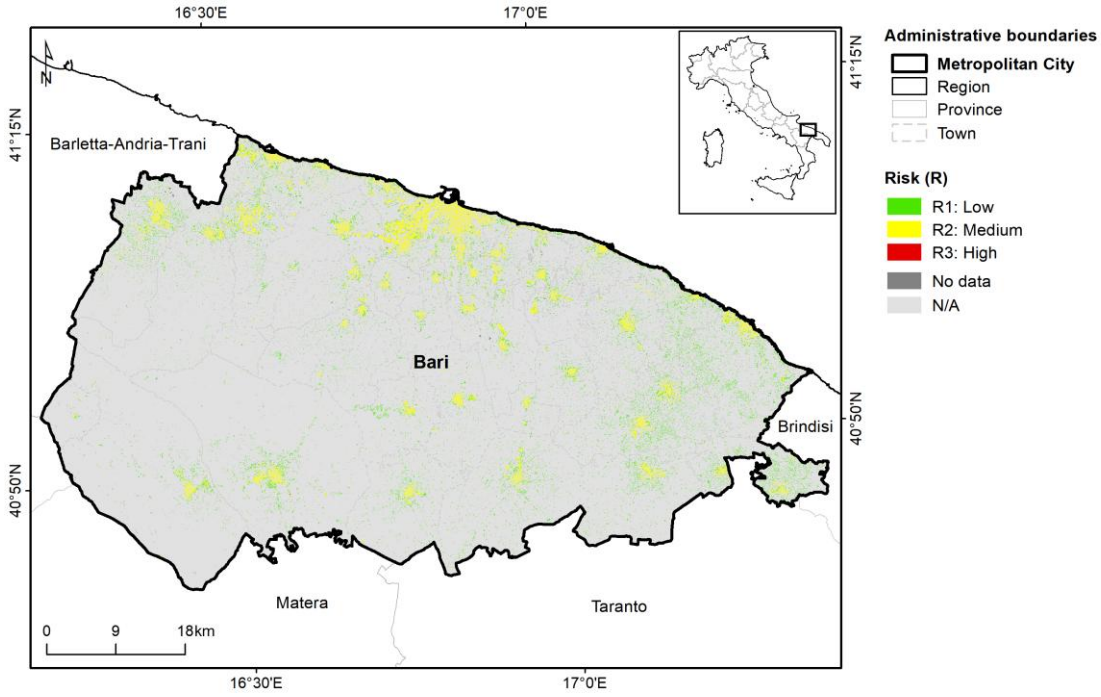

Figure 38 – Differential displacement risk mapping in the metropolitan city of Bari, based on 2018–2022 satellite InSAR observations.

3.2.10 Reggio Calabria

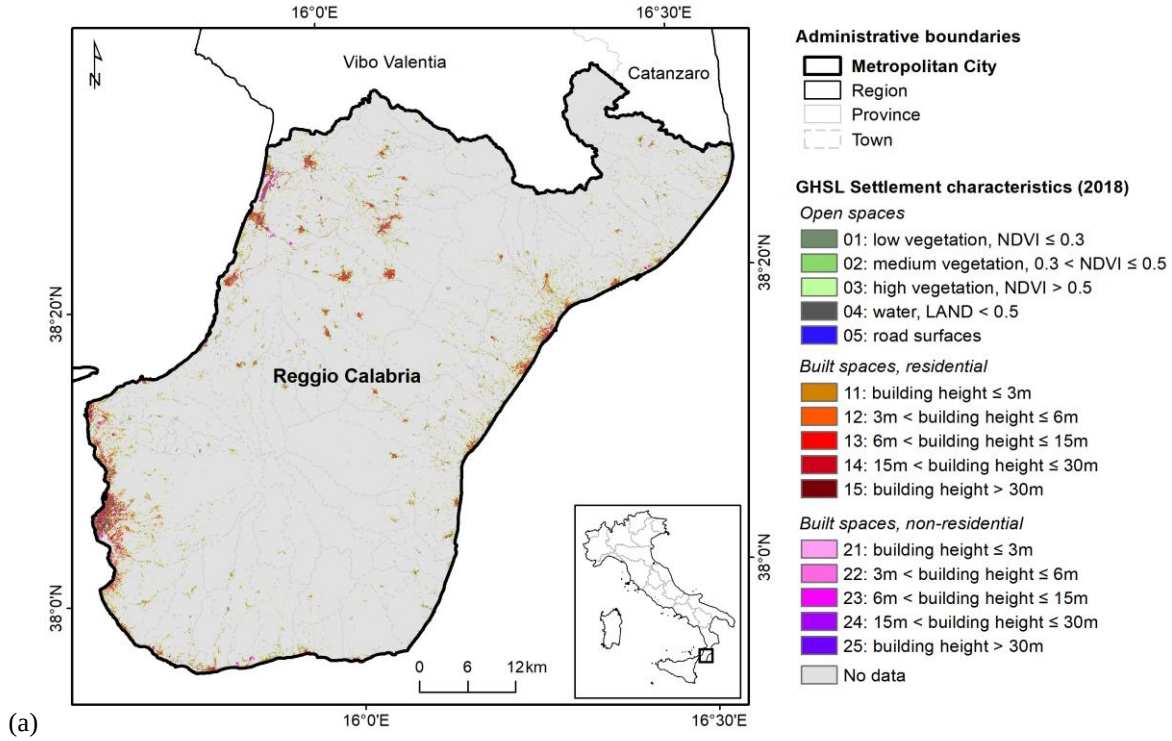

(a)

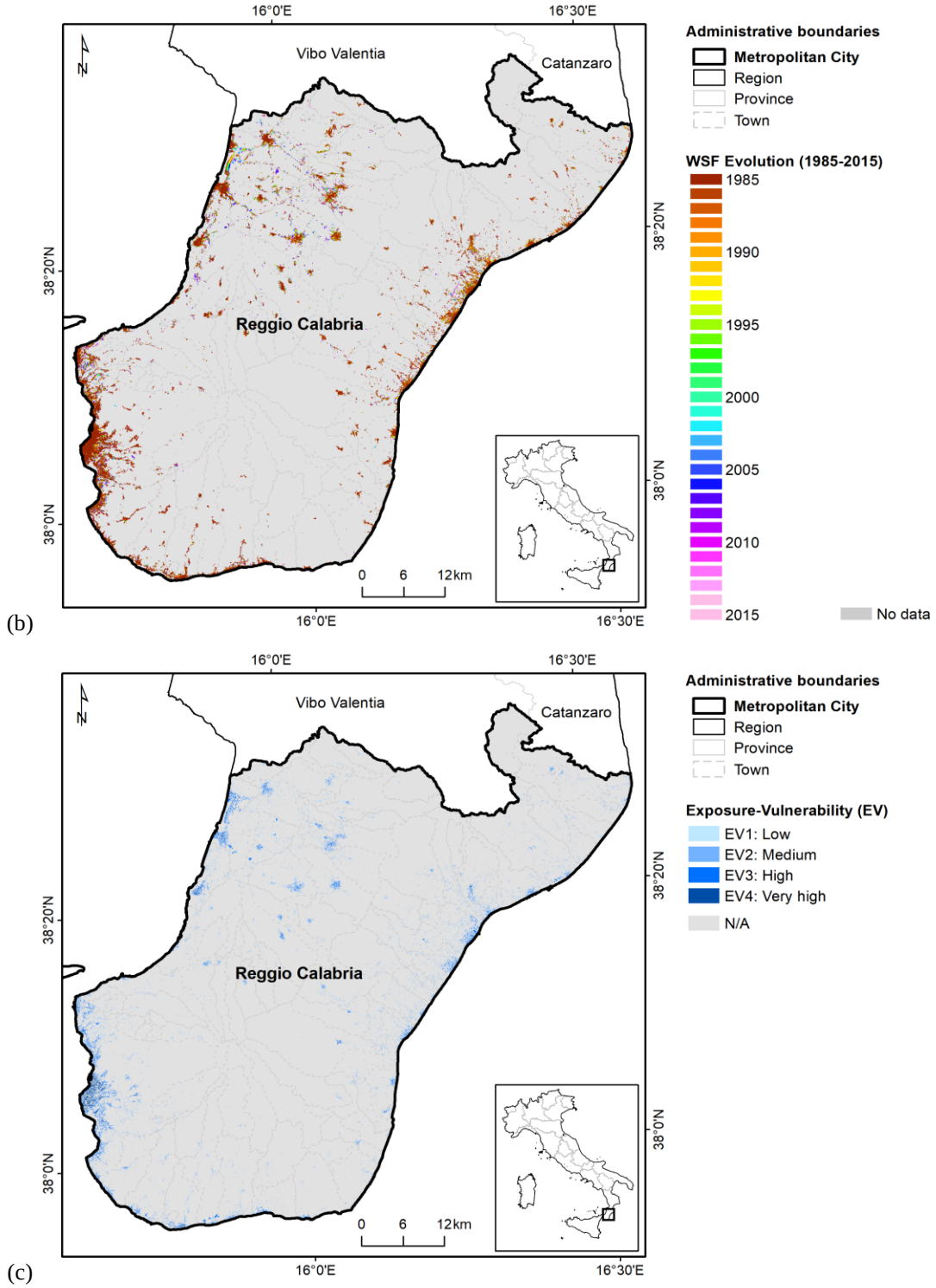

Figure 39 – Exposure-vulnerability mapping in the metropolitan city of Reggio Calabria: (a) GHS-BUILT-C R2023A - GHS Settlement Characteristics [1], (b) WSF Evolution 2015 [2]*, and (c) resulting exposure-vulnerability map.*

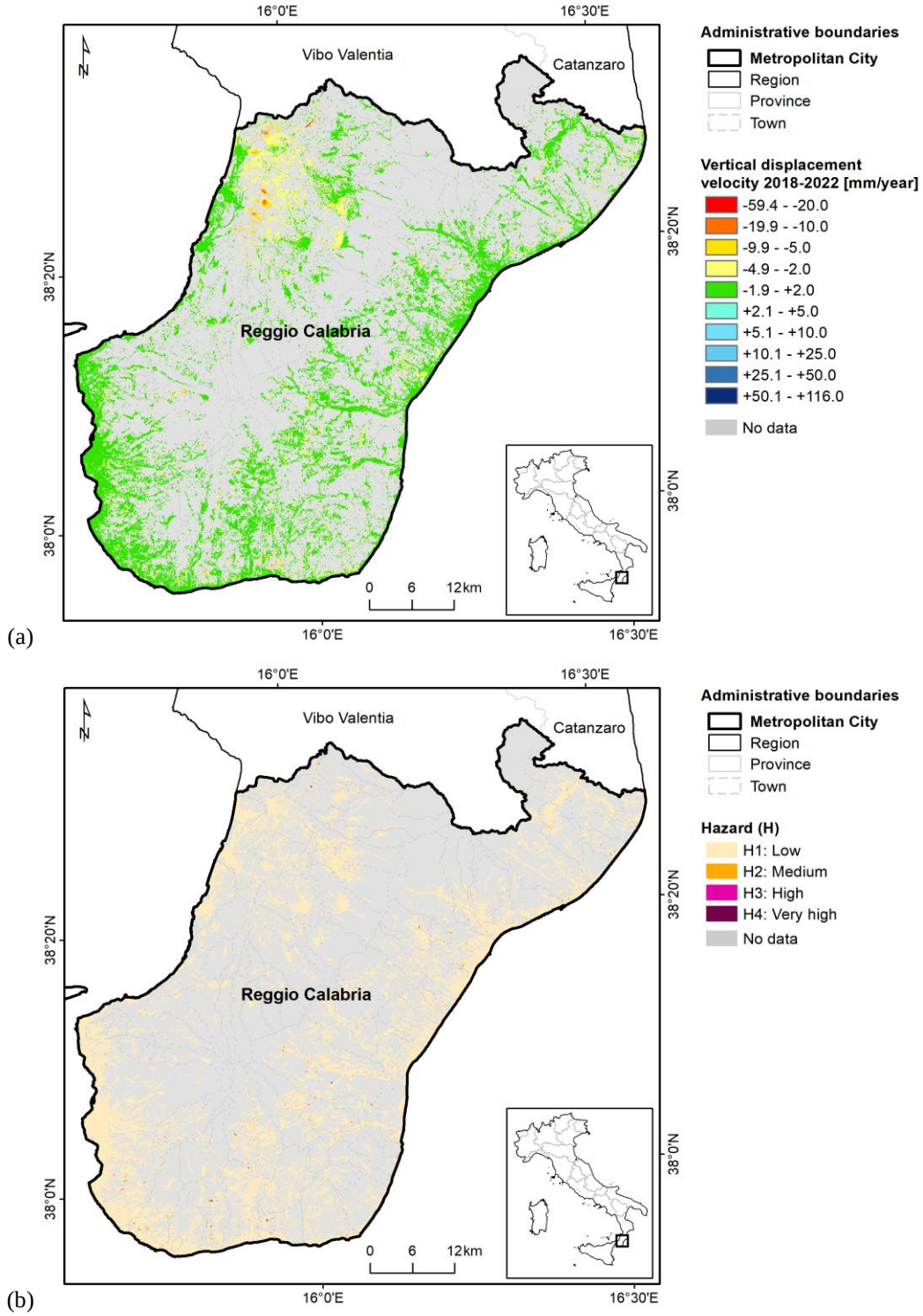

Figure 40 – Differential displacement hazard mapping in the metropolitan city of Reggio Calabria: (a) vertical ground displacement velocity in 2018–2022 based on EGMS Ortho InSAR datasets [5]*, and (b) resulting hazard map.*

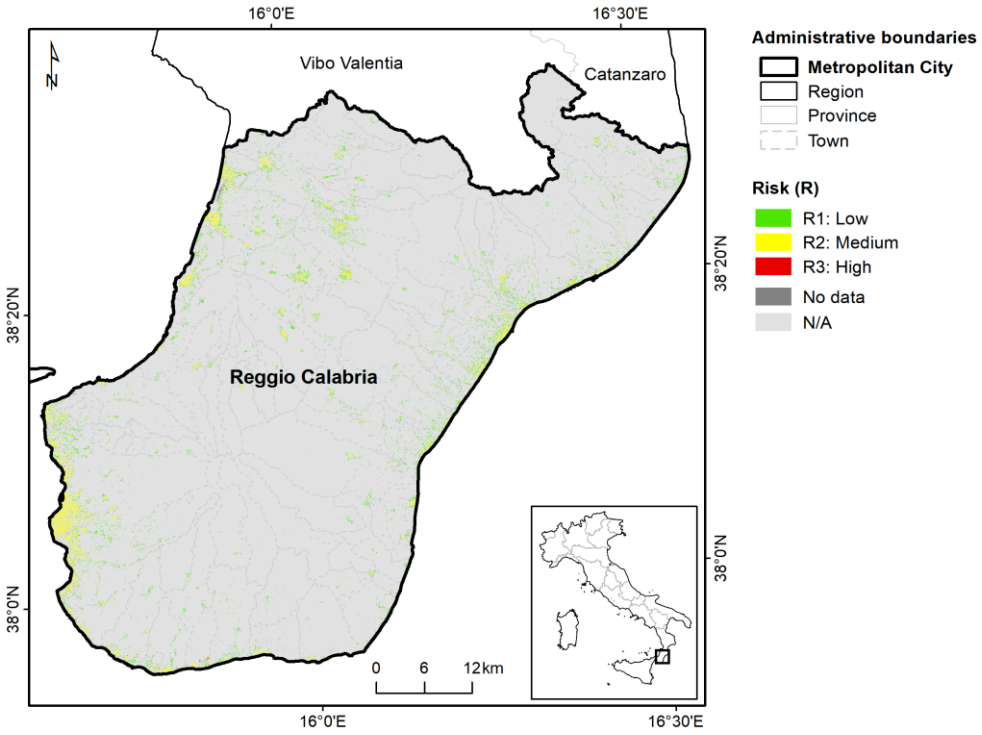

Figure 41 – Differential displacement risk mapping in the metropolitan city of Reggio Calabria, based on 2018–2022 satellite InSAR observations.

3.2.11 Palermo

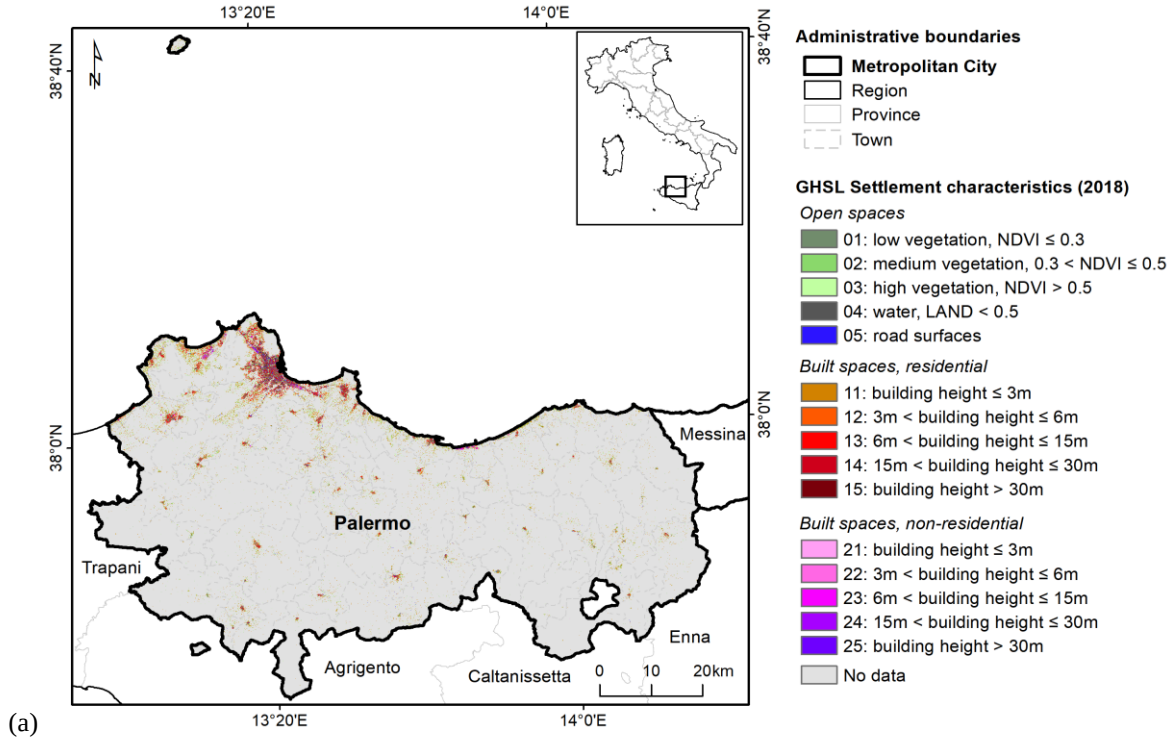

(a)

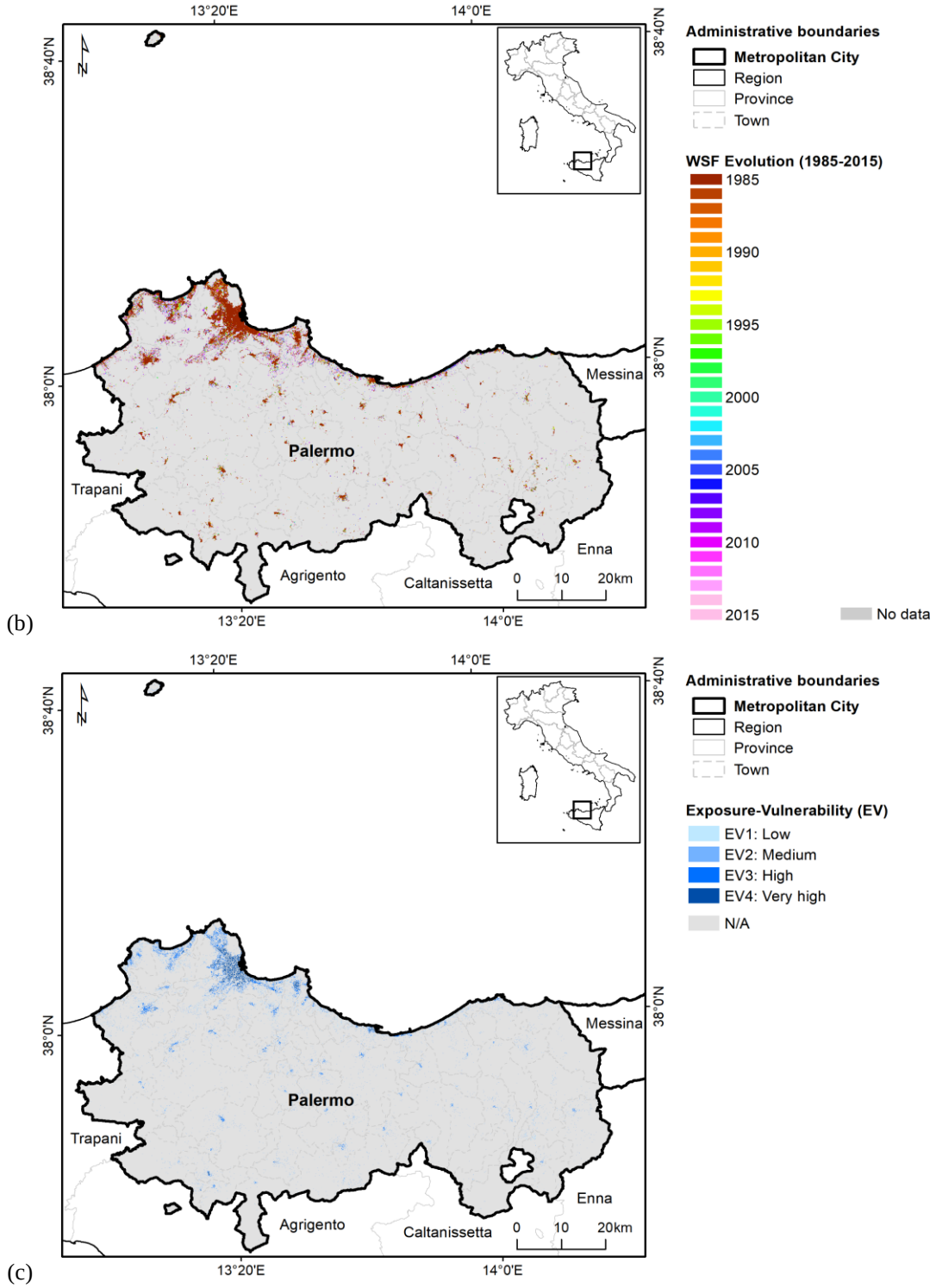

Figure 42 – Exposure-vulnerability mapping in the metropolitan city of Palermo: (a) GHS-BUILT-C R2023A - GHS Settlement Characteristics [1], (b) WSF Evolution 2015 [2]*, and (c) resulting exposure-vulnerability map.*

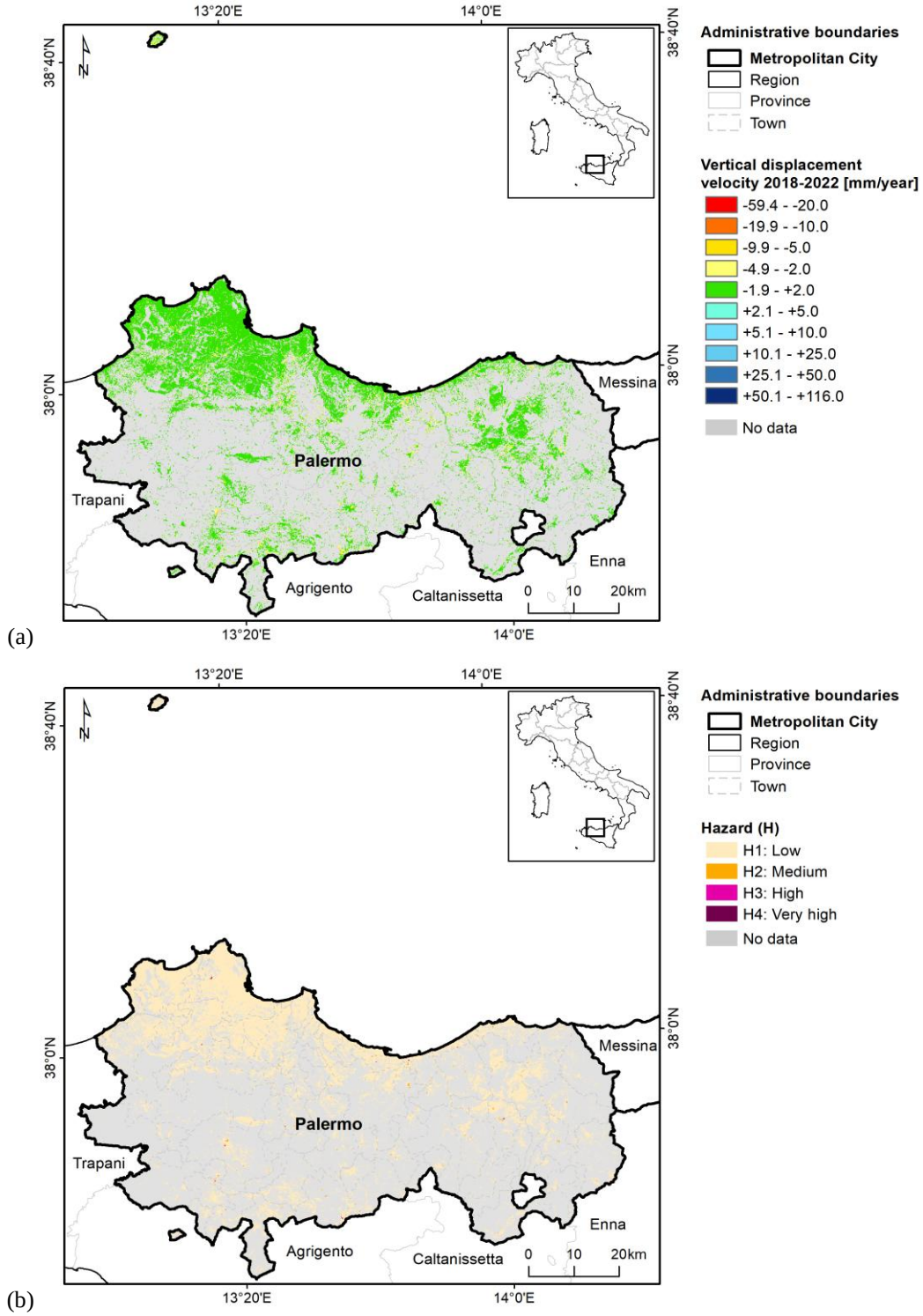

Figure 43 – Differential displacement hazard mapping in the metropolitan city of Palermo: (a) vertical ground displacement velocity in 2018–2022 based on EGMS Ortho InSAR datasets [5]*, and (b) resulting hazard map.*

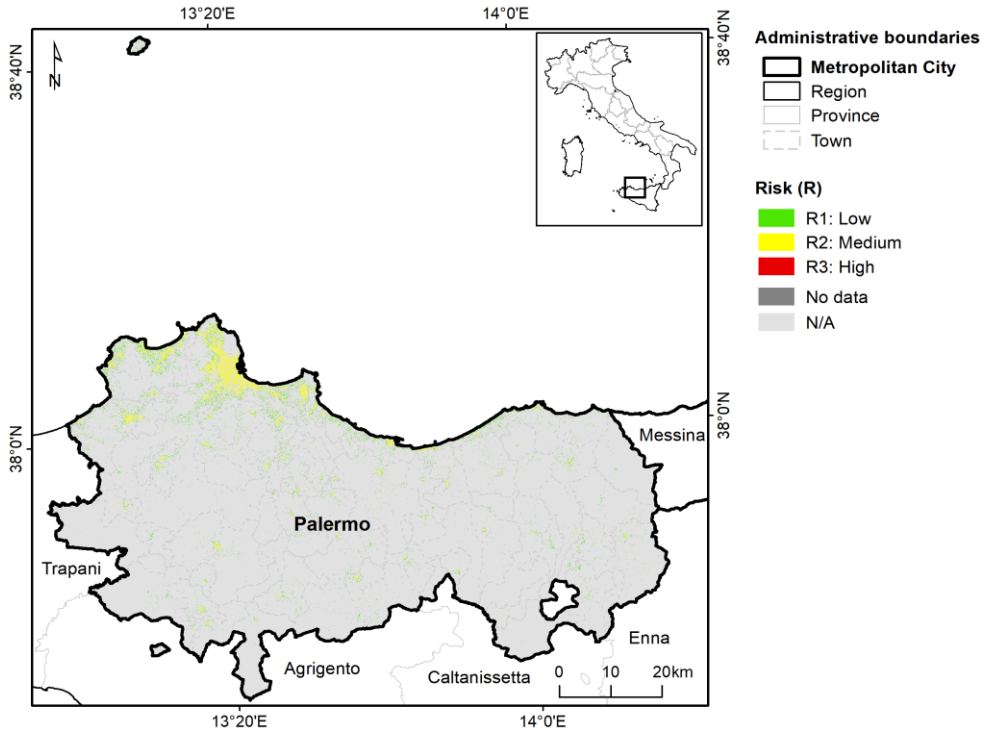

Figure 44 – Differential displacement risk mapping in the metropolitan city of Palermo, based on 2018–2022 satellite InSAR observations.

3.2.12 Messina

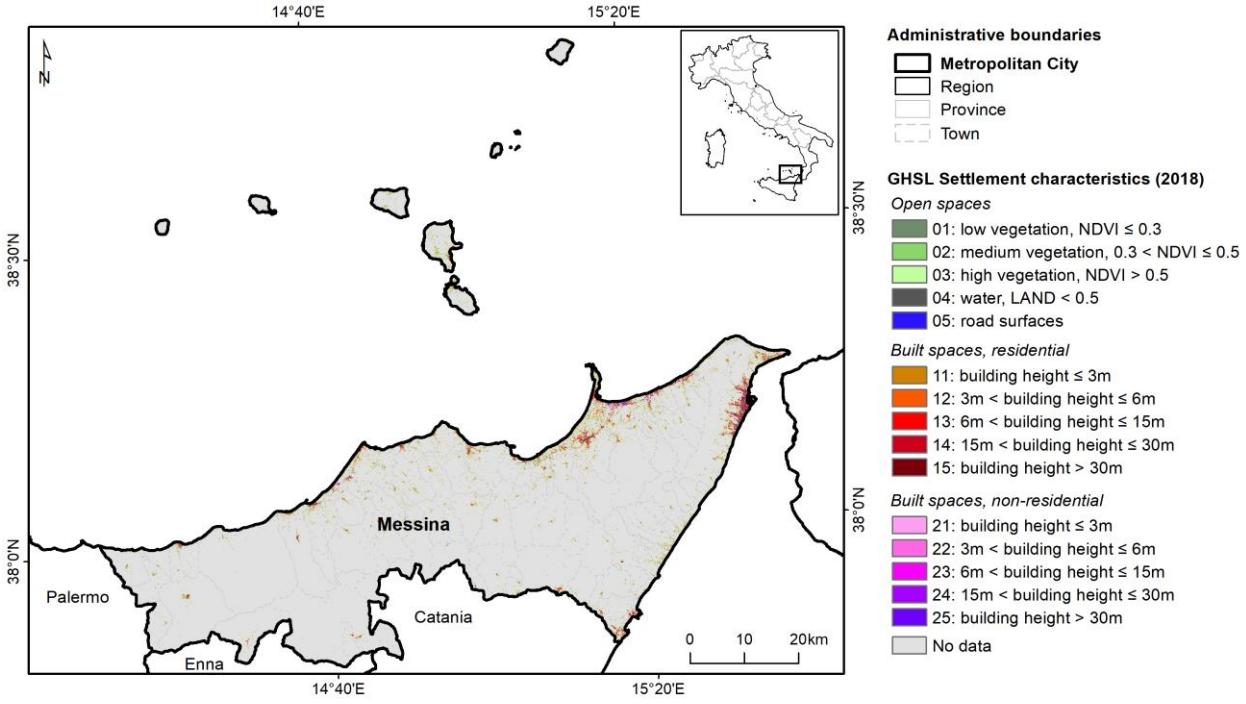

(a)

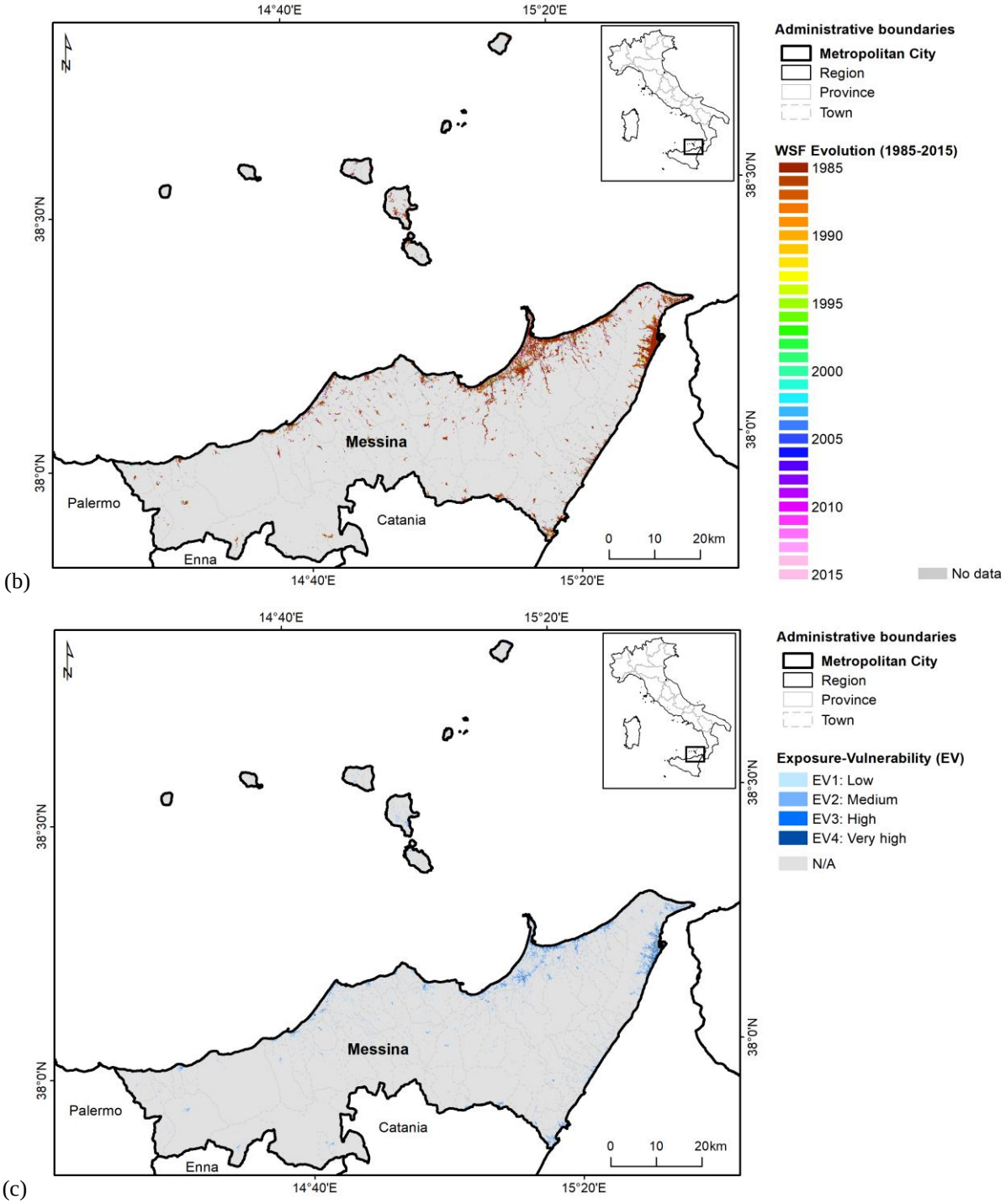

Figure 45 – Exposure-vulnerability mapping in the metropolitan city of Messina: (a) GHS-BUILT-C R2023A - GHS Settlement Characteristics [1], (b) WSF Evolution 2015 [2]*, and (c) resulting exposure-vulnerability map.*

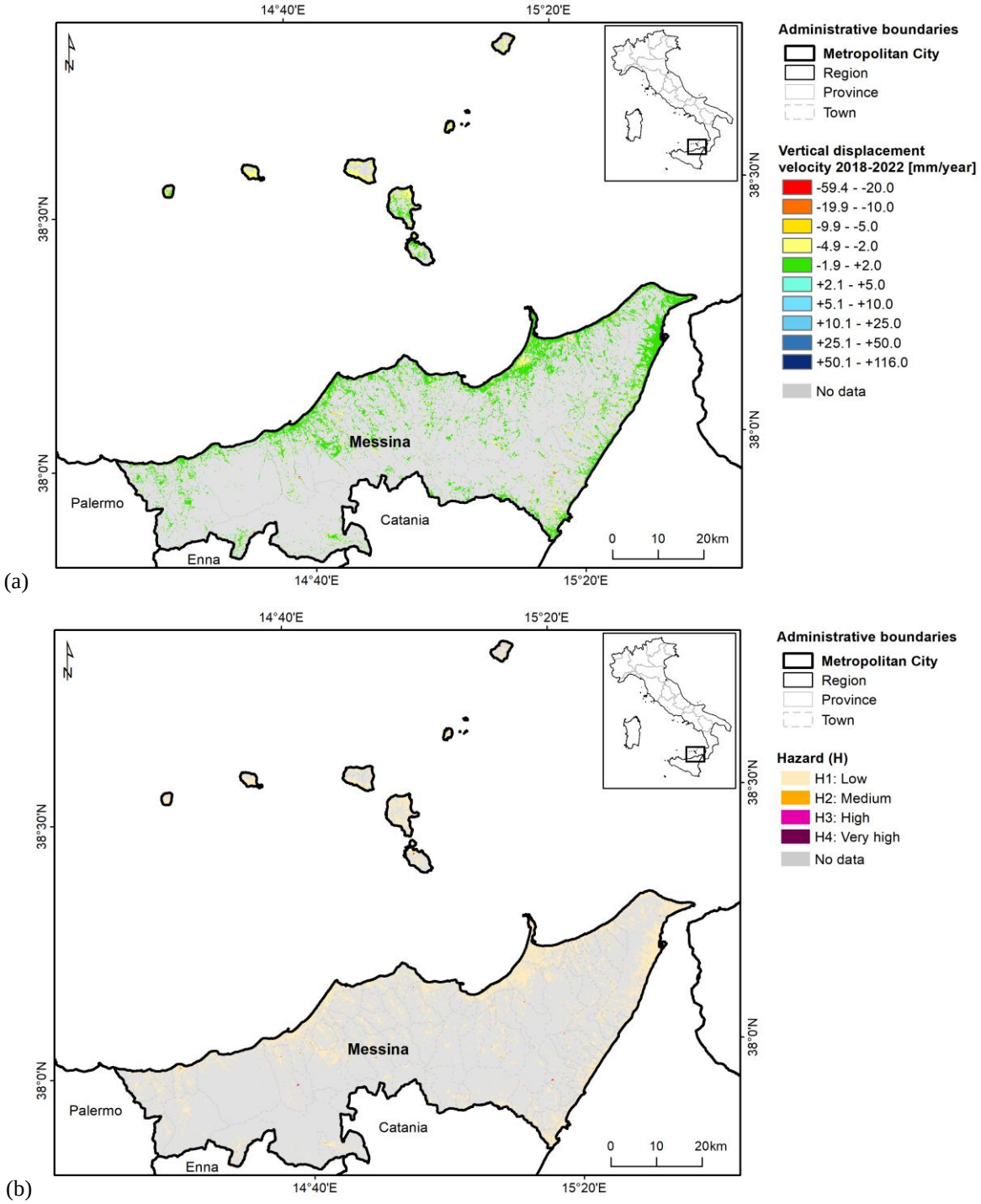

Figure 46 – Differential displacement hazard mapping in the metropolitan city of Messina: (a) vertical ground displacement velocity in 2018–2022 based on EGMS Ortho InSAR datasets [5]*, and (b) resulting hazard map.*

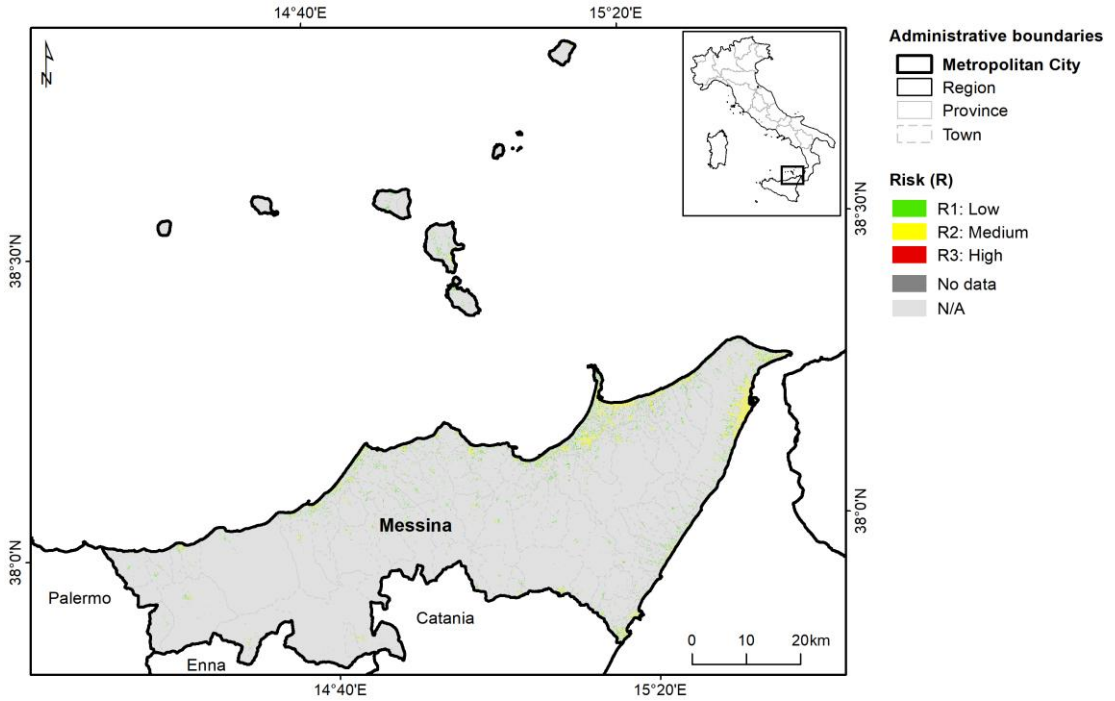

Figure 47 – Differential displacement risk mapping in the metropolitan city of Messina, based on 2018–2022 satellite InSAR observations.

3.2.13 Catania

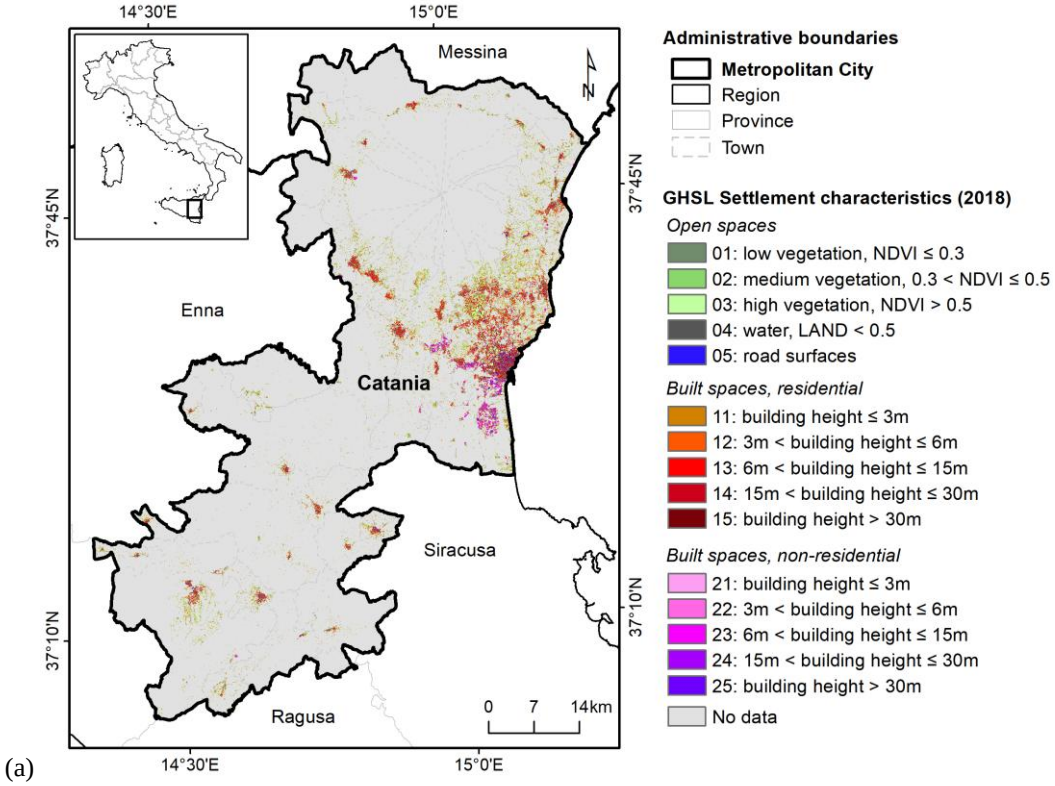

(a)

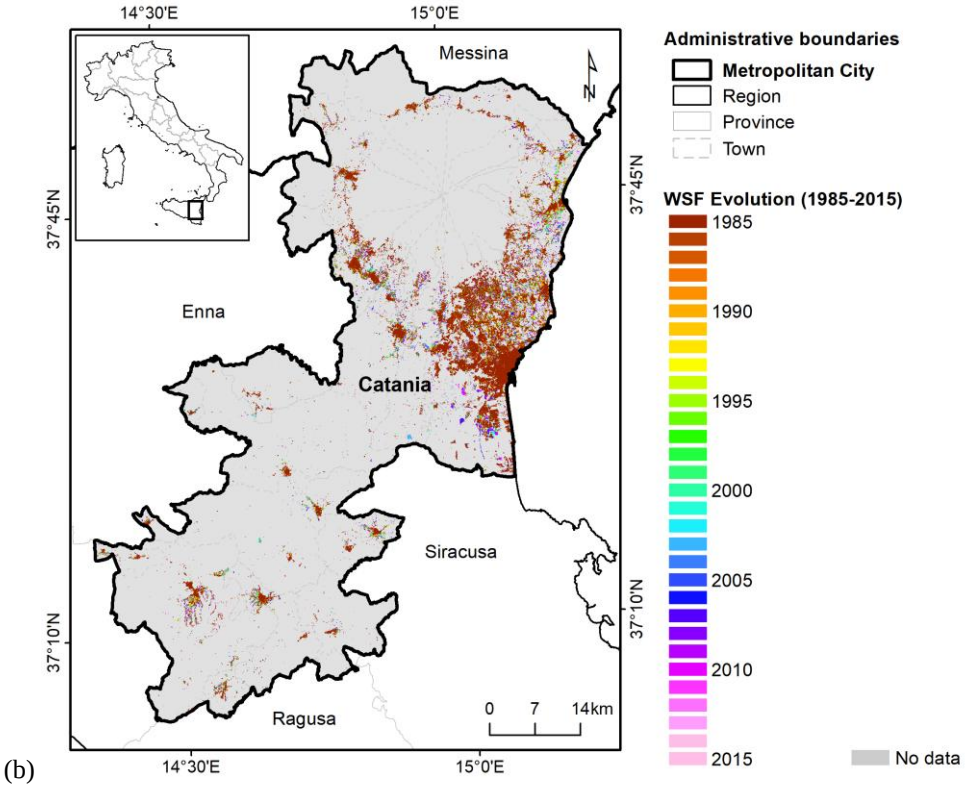

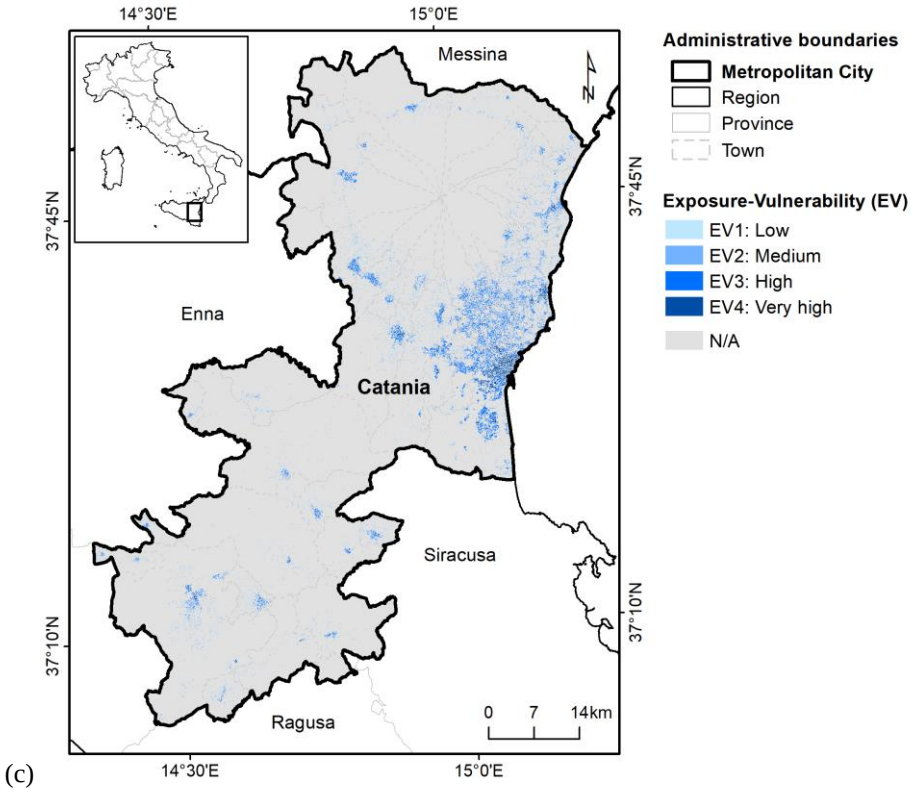

Figure 48 – Exposure-vulnerability mapping in the metropolitan city of Catania: (a) GHS-BUILT-C R2023A - GHS Settlement Characteristics [1], (b) WSF Evolution 2015 [2]*, and (c) resulting exposure-vulnerability map.*

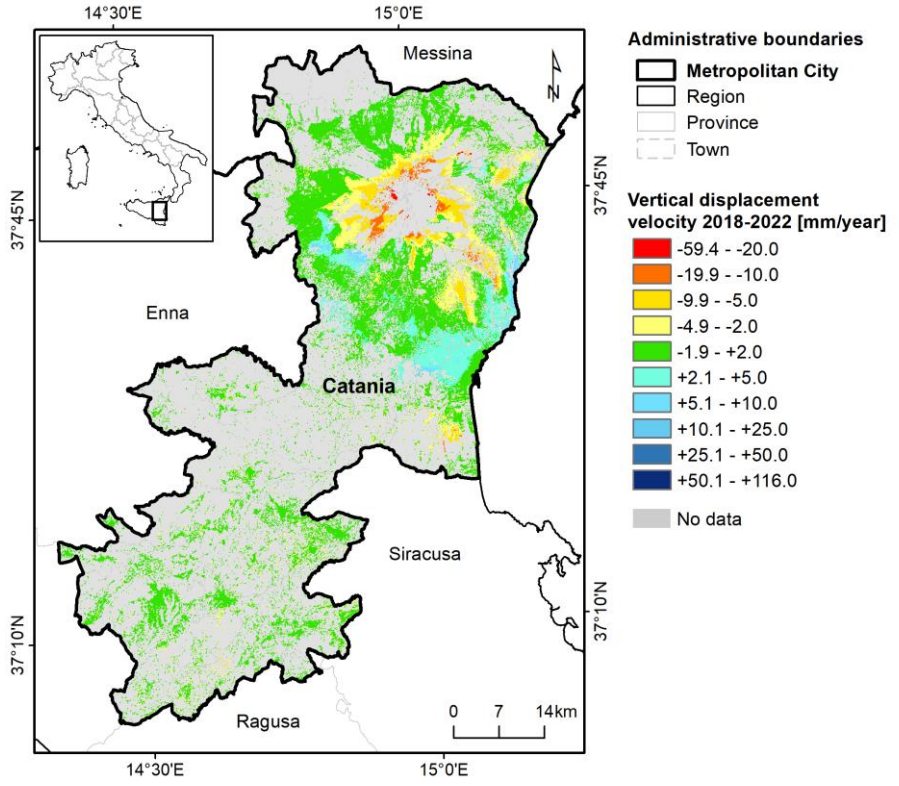
14°30'E
15°0'E
37°45'N
37°10'N
Messina
Enna
Catania
Siracusa
Ragusa
0 7 14km
Administrative boundaries
Metropolitan City
Region
Province
Town
Vertical displacement velocity 2018-2022 [mm/year]
-59.4 - -20.0
-19.9 - -10.0
-9.9 - -5.0
-4.9 - -2.0
-1.9 - +2.0
+2.1 - +5.0
+5.1 - +10.0
+10.1 - +25.0
+25.1 - +50.0
+50.1 - +116.0
No data

(a)

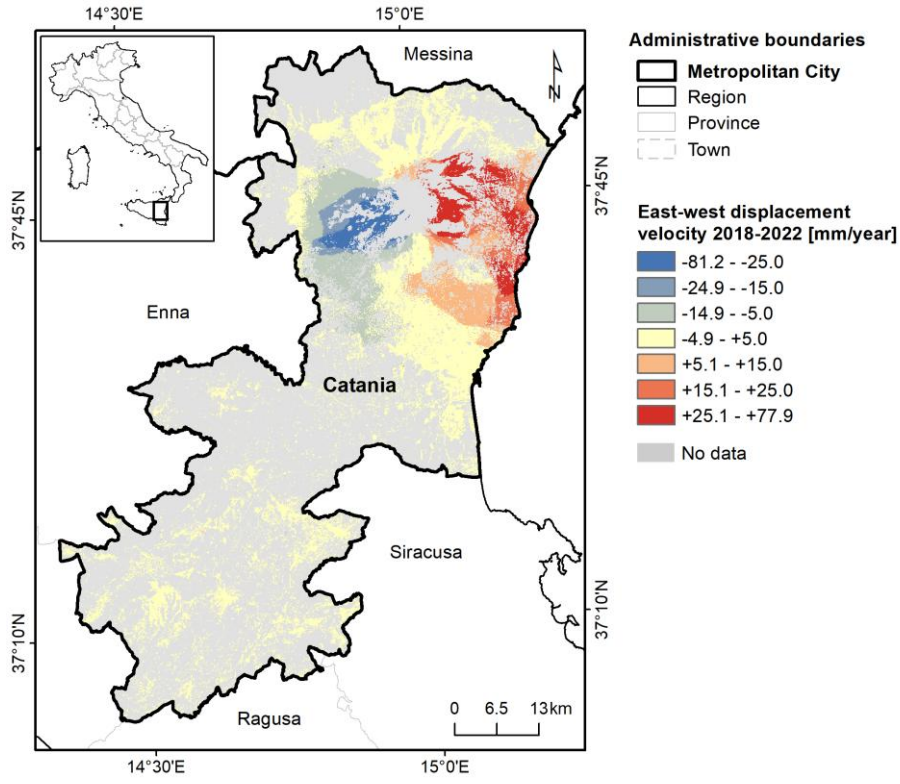
14°30'E
15°0'E
37°45'N
37°10'N
Messina
Enna
Catania
Siracusa
Ragusa
0 6.5 13km
Administrative boundaries
Metropolitan City
Region
Province
Town
East-west displacement velocity 2018-2022 [mm/year]
-81.2 - -25.0
-24.9 - -15.0
-14.9 - -5.0
-4.9 - +5.0
+5.1 - +15.0
+15.1 - +25.0
+25.1 - +77.9
No data

(b)

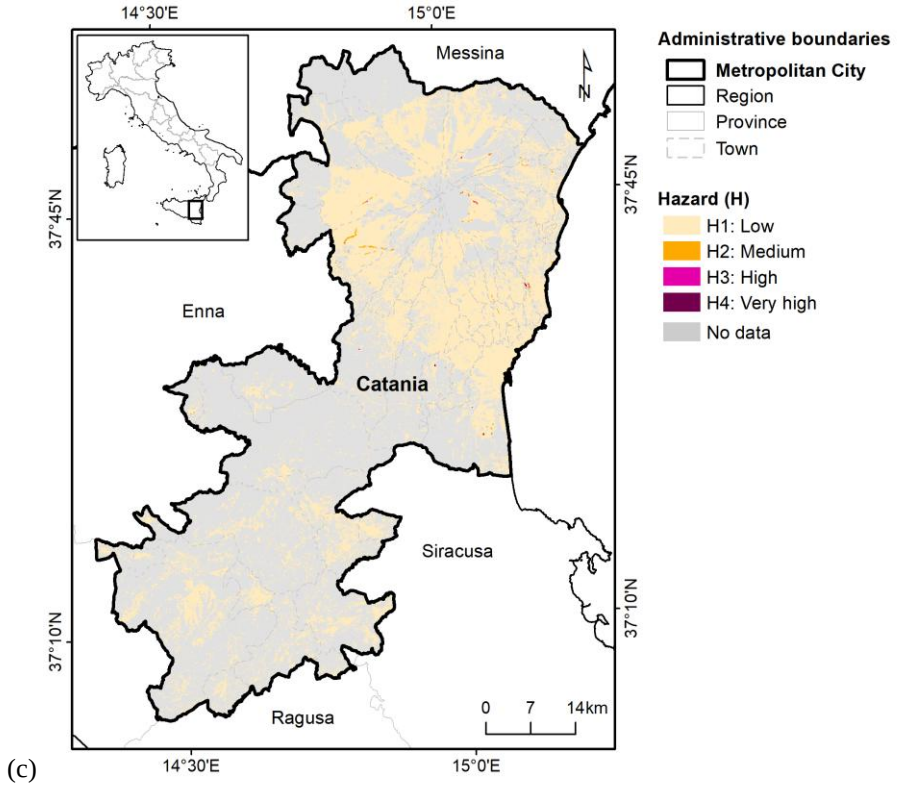

(c)

Figure 49 – Differential displacement hazard mapping in the metropolitan city of Catania: (a) vertical and (b) east-west ground displacement velocity in 2018–2022 based on EGMS Ortho InSAR datasets [5,6]*, and (c) resulting hazard map.*

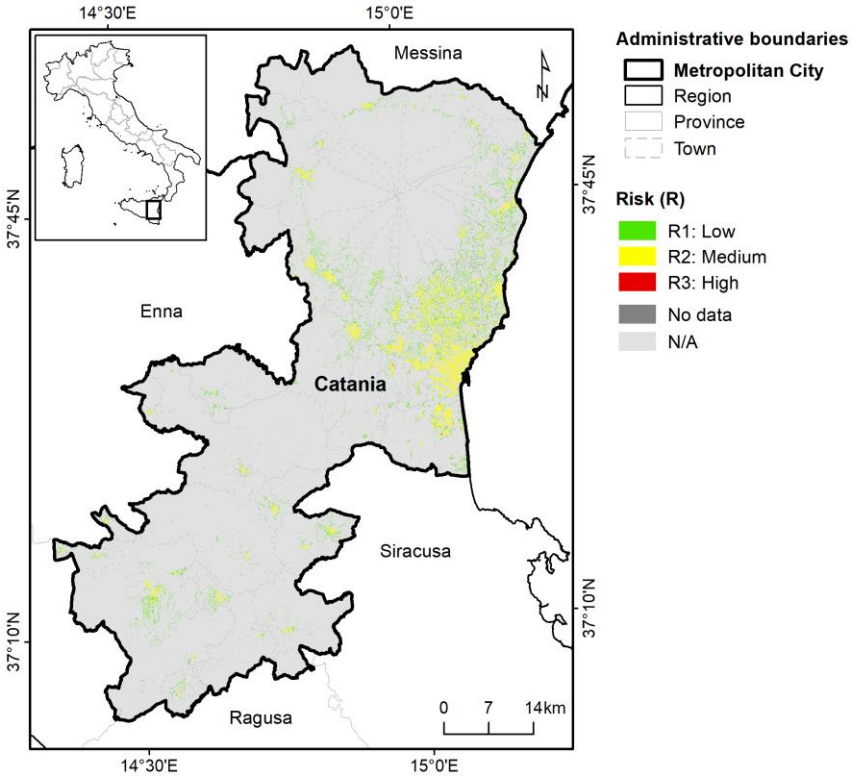

Figure 50 – Differential displacement risk mapping in the metropolitan city of Catania, based on 2018–2022 satellite InSAR observations.

3.2.14 Sassari

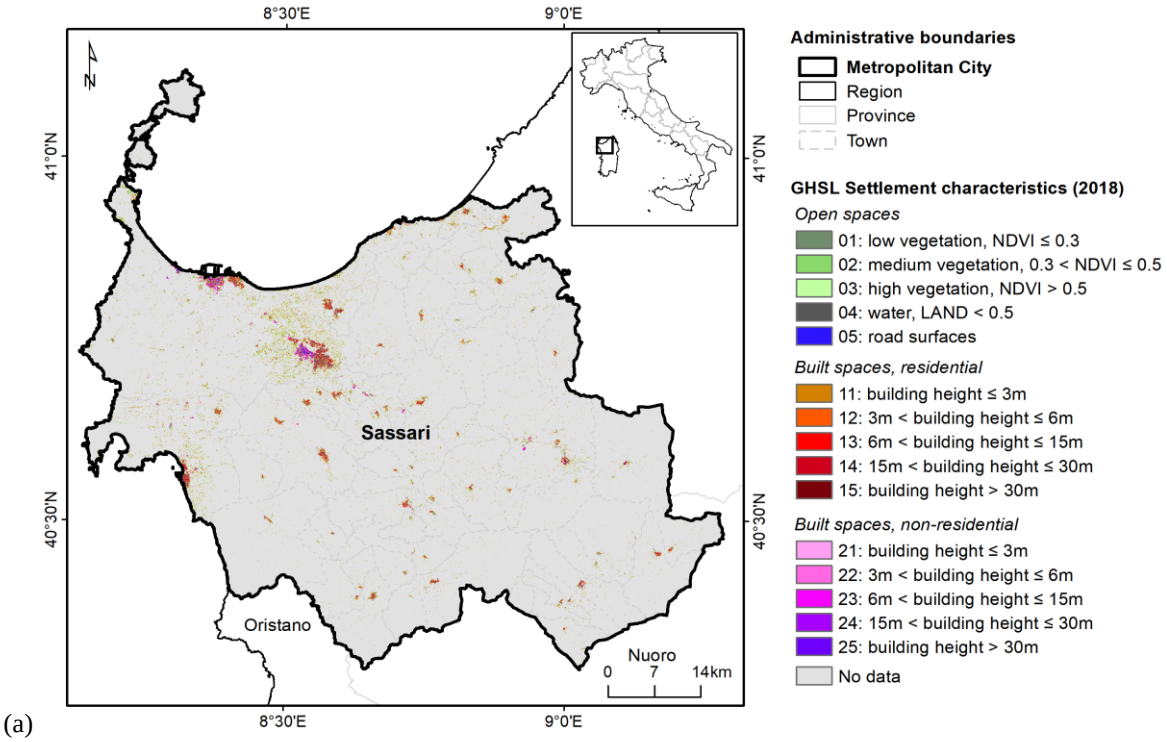

(a)

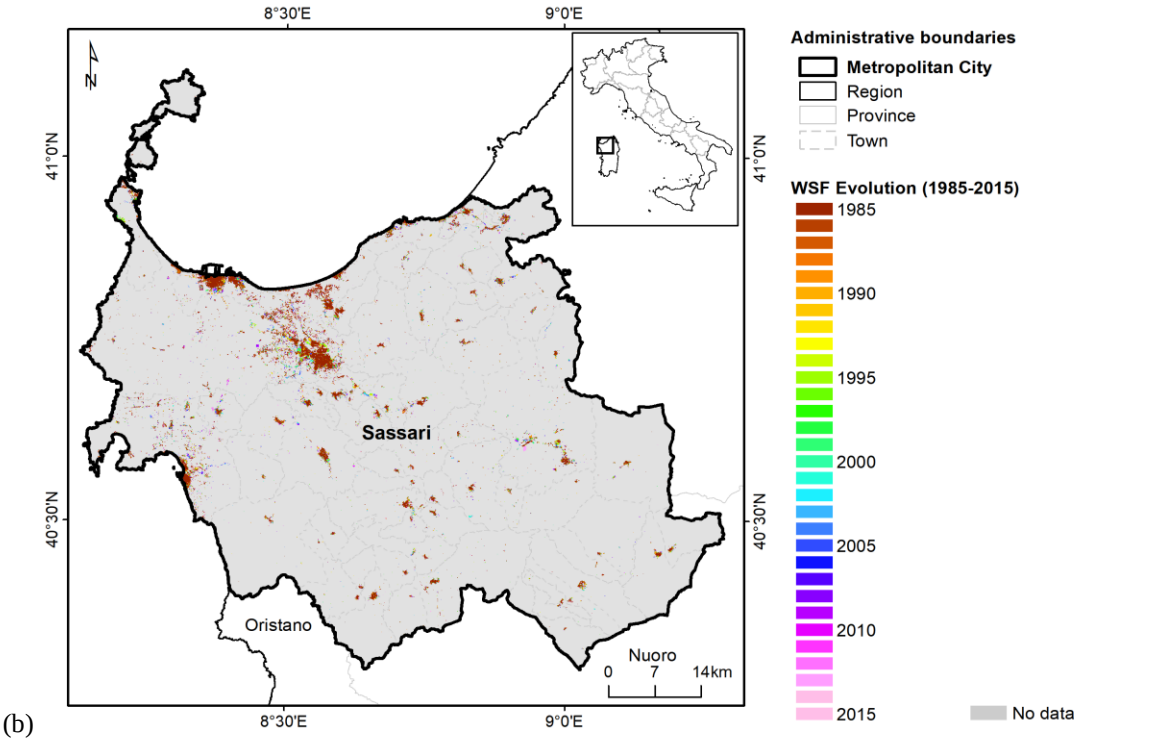

(b)

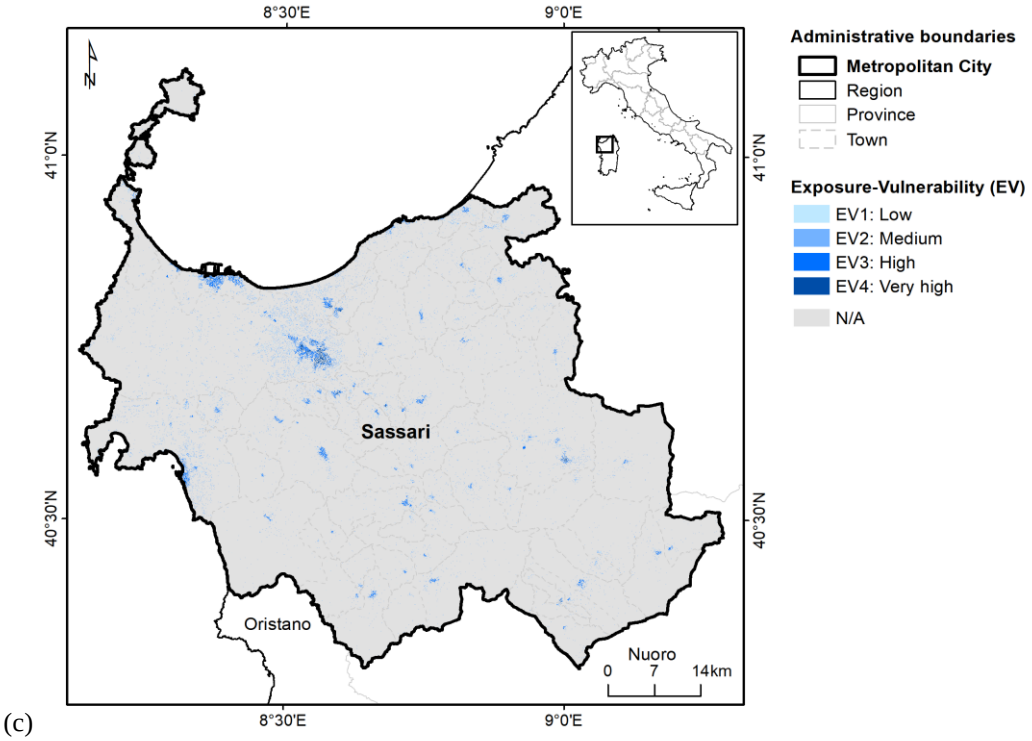

(c)

Figure 51 – Exposure-vulnerability mapping in the metropolitan city of Sassari: (a) GHS-BUILT-C R2023A - GHS Settlement Characteristics [1], (b) WSF Evolution 2015 [2]*, and (c) resulting exposure-vulnerability map.*

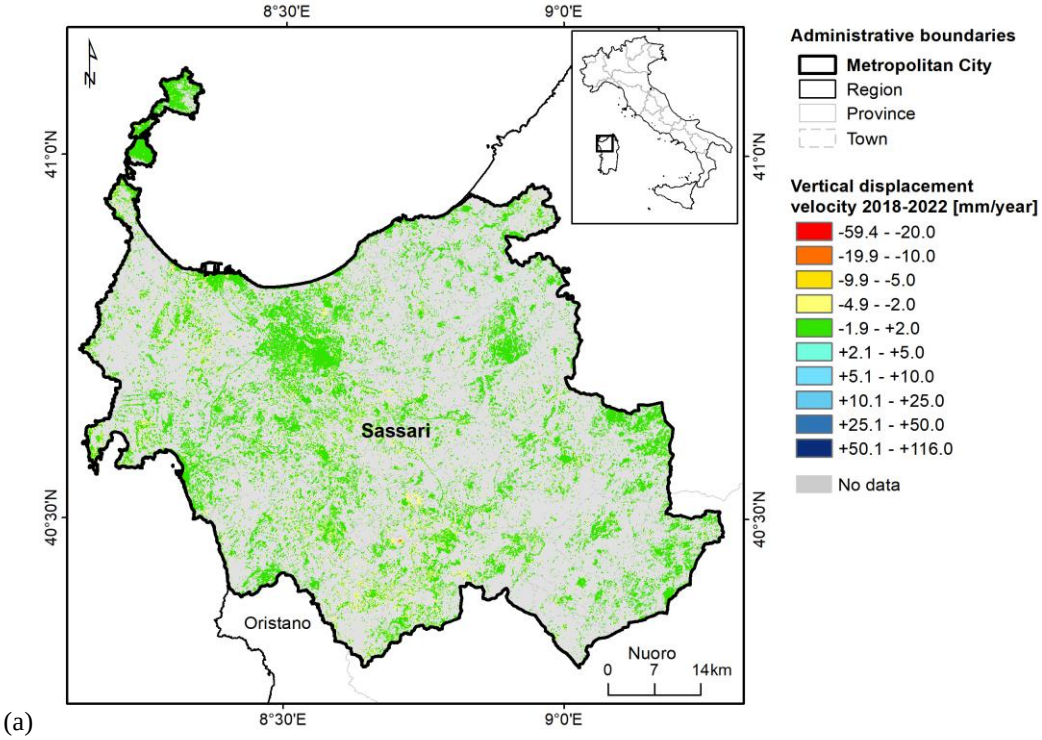

(a)

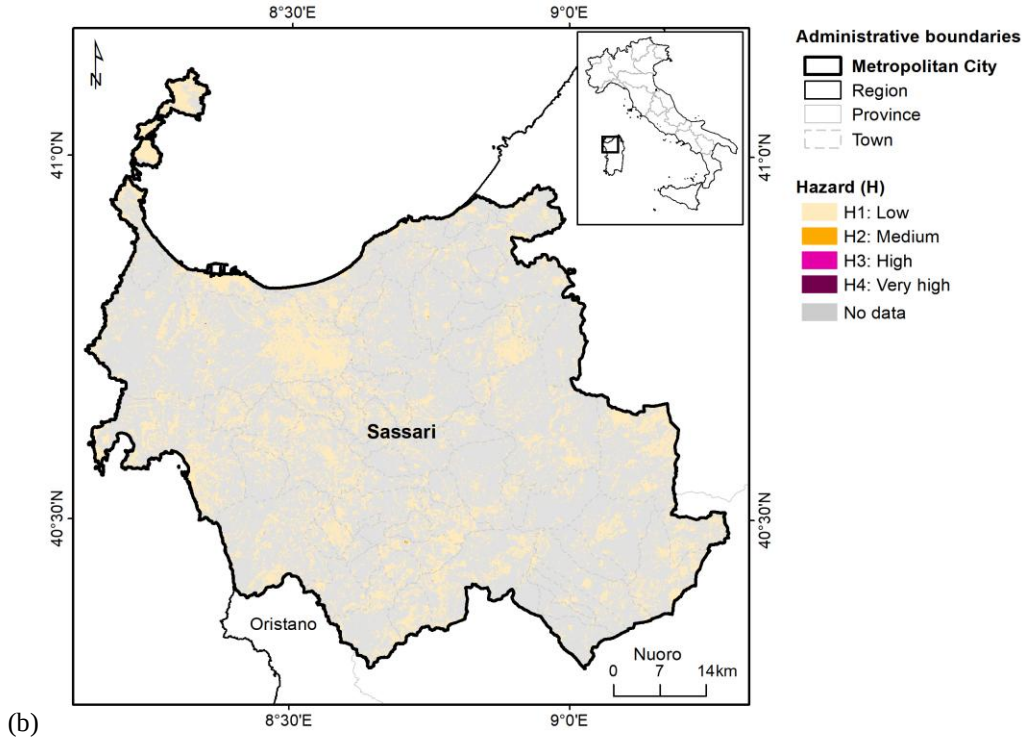

(b)

Figure 52 – Differential displacement hazard mapping in the metropolitan city of Sassari: (a) vertical ground displacement velocity in 2018–2022 based on EGMS Ortho InSAR datasets [5]*, and (b) resulting hazard map.*

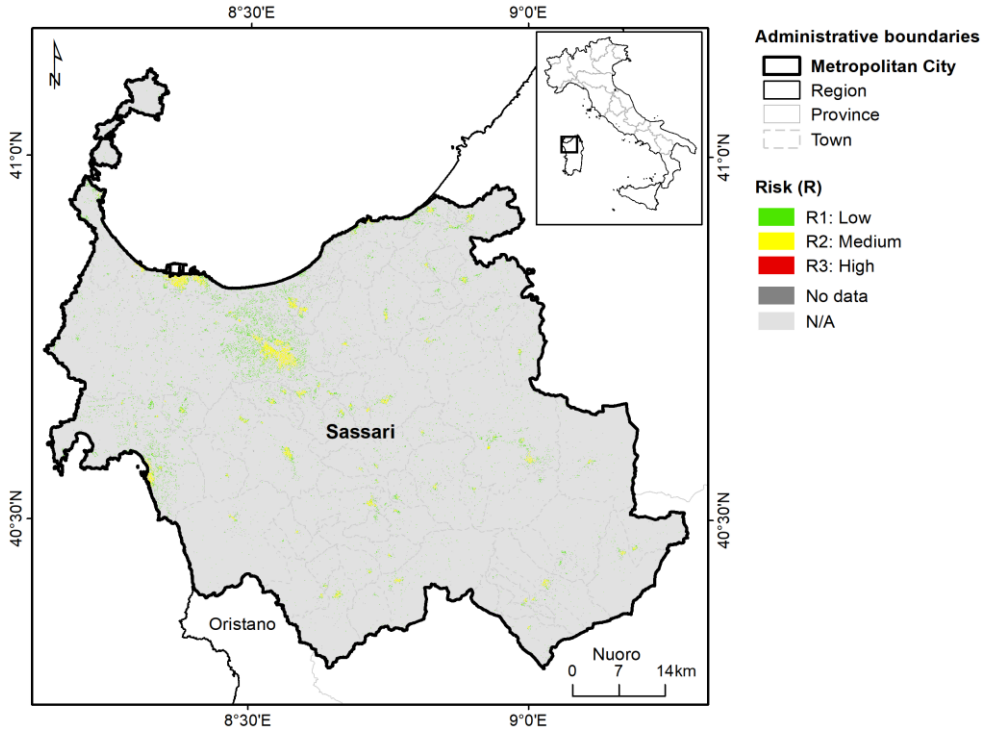

Figure 53 – Differential displacement risk mapping in the metropolitan city of Sassari, based on 2018–2022 satellite InSAR observations.

3.2.15 Cagliari

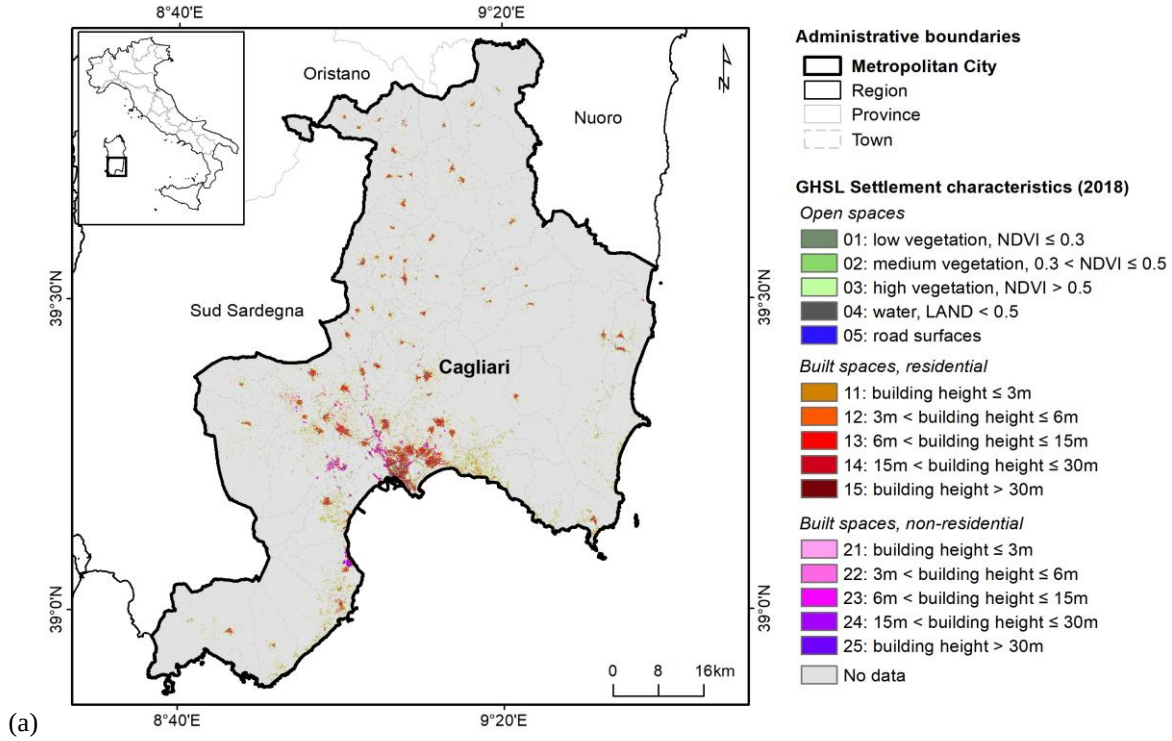

(a)

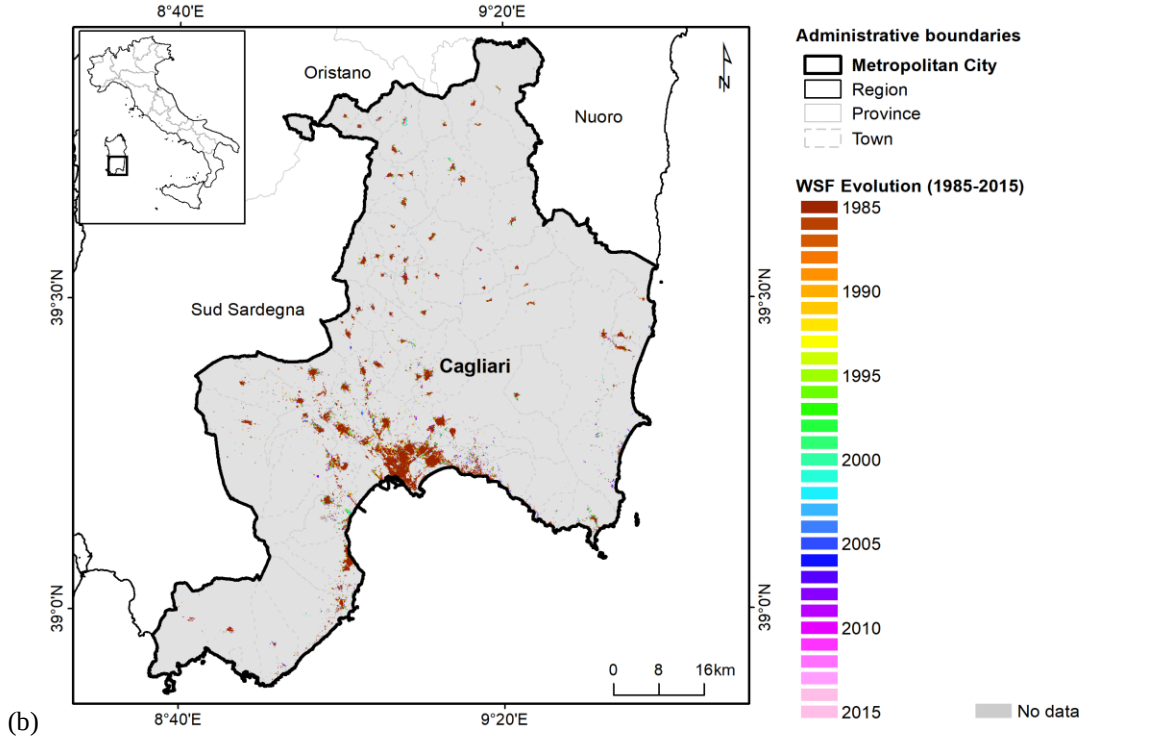

(b)

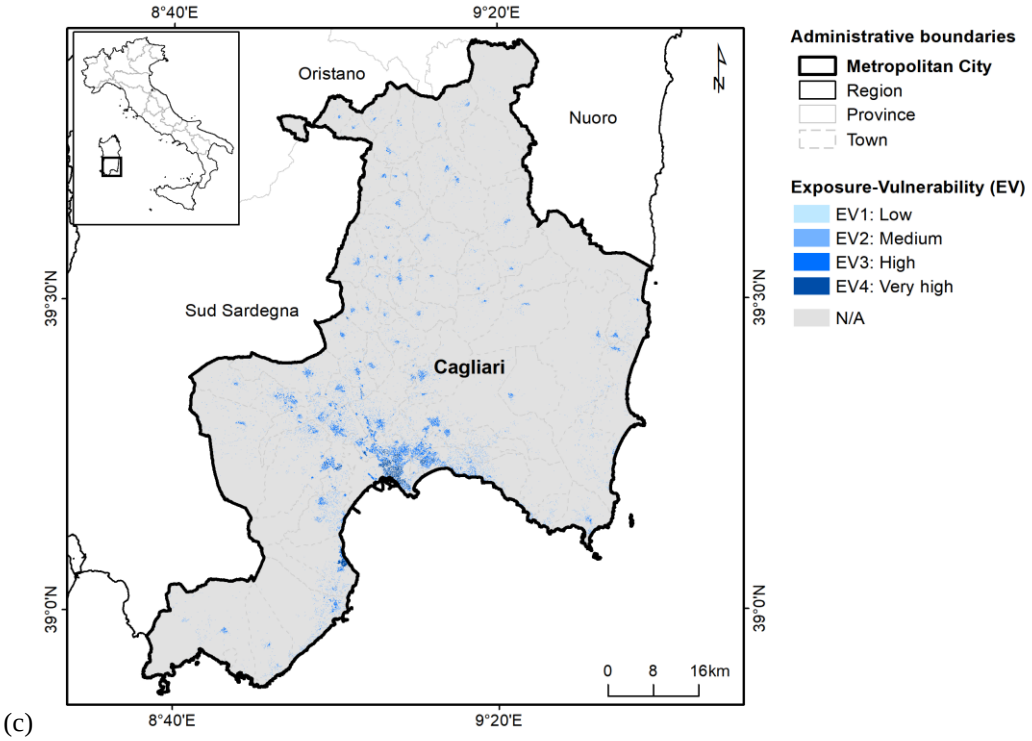

(c)

Figure 54 – Exposure-vulnerability mapping in the metropolitan city of Cagliari: (a) GHS-BUILT-C R2023A - GHS Settlement Characteristics [1], (b) WSF Evolution 2015 [2]*, and (c) resulting exposure-vulnerability map.*

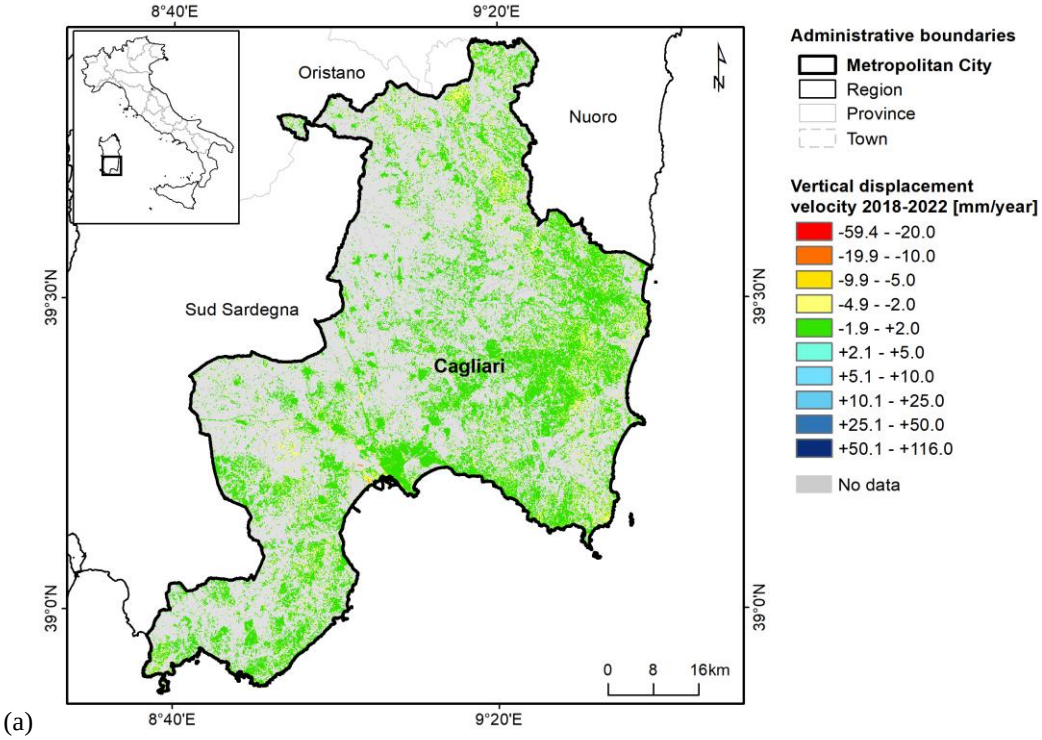

(a)

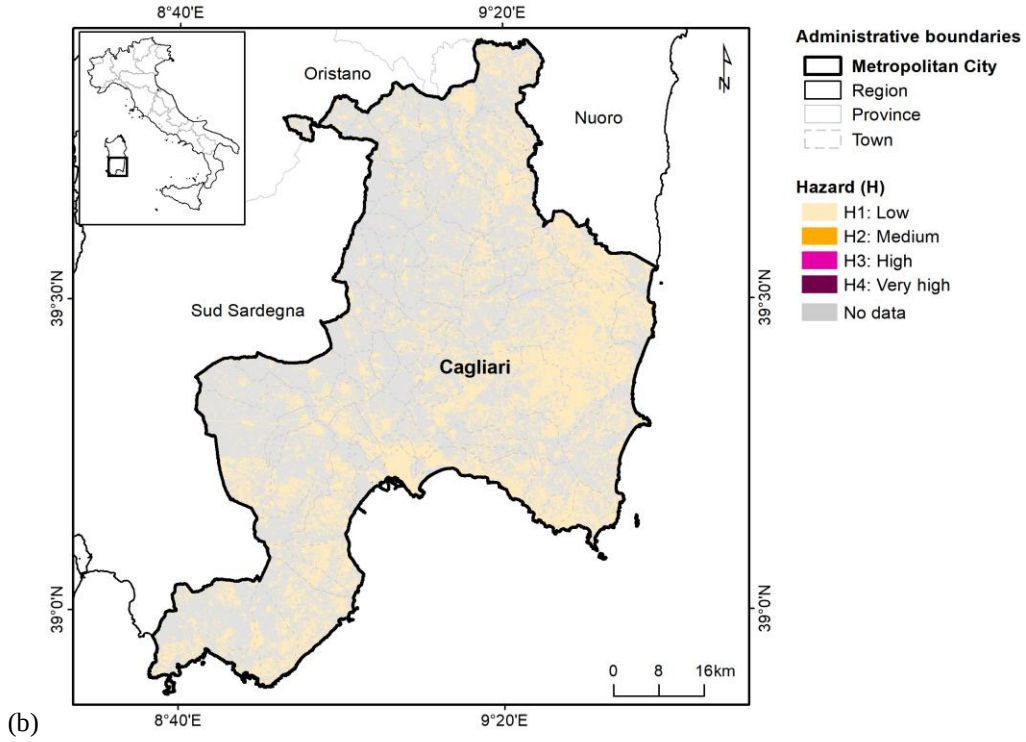

(b)

Figure 55 – Differential displacement hazard mapping in the metropolitan city of Cagliari: (a) vertical ground displacement velocity in 2018–2022 based on EGMS Ortho InSAR datasets [5]*, and (b) resulting hazard map.*

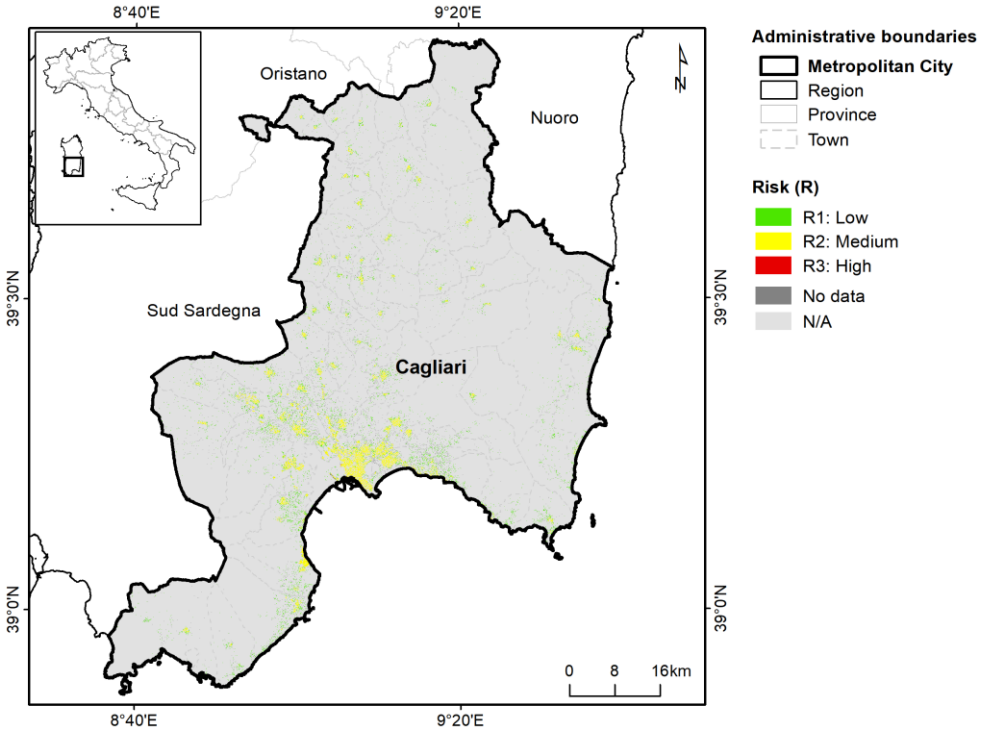

Figure 56 – Differential displacement risk mapping in the metropolitan city of Cagliari, based on 2018–2022 satellite InSAR observations.

4 CONCLUSIONS

The national scale risk assessment analysis provided an overview of the extent and location of the urban sectors of the 15 metropolitan cities of Italy where differential ground displacement is likely or might induce damage to urban infrastructure.

Over a cumulative investigated area of 54,378 km^2 for the 15 metropolitan cities of Italy and a total urbanized area amounting to 2,665 km^2, about 1.44 km^2 of land revealed high risk (R3) levels associated with differential displacement (either subsidence or uplift), mainly concentrated in narrow sectors exhibiting significant angular distortions (and, in some cases, an additive threat due to horizontal strain) occurring over very high exposure-vulnerability infrastructure (private/public buildings) within the cities of Napoli (e.g. Pozzuoli and Bagnoli), Catania, Roma and Messina. In these zones, there is a high likelihood of already occurred/incipient structural damage at urban infrastructure; site inspections to verify the structural health of the buildings and ad hoc mitigation measures are recommended at single-building scale.

On the other hand, a medium risk (R2) level was identified across the vast majority of the metropolitan areas' land (1351 km^2), where potential structural damage might occur at the urban infrastructure involved; in these areas, tailored monitoring of ground deformation and derived stress indices is recommended at the building block scale. Finally, low risk (R1) level is identified across the remaining 1133 km^2, where no specific actions are required.

When using information from the risk mapping products provided in this report and, in digital form through SubRISK+ *Control Room*, it is worth accounting for the following:

- Urban settlement data from the GHSL and WSF do not include information on foundations, maintenance status or other structural health parameters of the buildings that may influence their vulnerability; a detailed analysis of such parameters at building-block or building scale would be recommended to enhance the assessment at finer analysis scales.
- Satellite InSAR datasets do not provide information on N-S displacement that may occur, hence horizontal strain along the N-S direction is not accounted for, whilst it could be significant in structurally-controlled basins delimited by E-W oriented faults; in such cases, other geodetic data (e.g. levelling, or GPS/GNSS) might provide complementary data to enhance the hazard assessment.
- The hazard mapping approach assumes that the estimated ground displacement velocities for the 2018–2022 period have affected the observed areas for a total of 10 years (namely, during 2013–2022); this assumption may result in underestimation of hazard levels for cities that have been affected by subsidence processes for more than the selected 10 year-long interval (e.g. Bologna, that experienced anthropogenically-driven land subsidence since the 1960s; [23]), and overestimation of hazard levels for cities that have been affected for shorter periods.
- The spatial resolution of the risk maps is influenced by the resolution on the input datasets that are exploited to generate them, namely: hazard mapping is performed at the same 100 m resolution of the input EGMS Ortho layers, while exposure-vulnerability mapping is based on the 10 m resolution provided by GHSL. The latter is used as spatial reference for the risk assessment, meaning that the input hazard information associated to each pixel is homogeneous across 100 m by 100 m areas, hence smaller spatial granularities are not accounted for.

- The risk matrix is designed to output the same level of risk for different combinations of exposure-vulnerability and hazard pairs; for instance, medium risk (R2) is identified when low exposure-vulnerability (EV1) built-up spaces are affected by high (H3) or very high (H4) hazard, or also when high exposure-vulnerability (EV3) built-up spaces are affected by low (H1) or medium (H2) hazard, and so on. This results in homogeneous risk levels deriving from different input conditions. Evidence of this methodological aspect is provided by the large proportions of medium risk (R2) levels across metropolitan cities such as Milano and Florence, where land subsidence affects very limited spots of their built-up areas and hazard levels due to differential displacements are mostly low (H1), but exposure-vulnerability of urban structures is high or very high (EV3-EV4), resulting in the R2 category.
- Risk maps refer to the risk induced by differential ground displacement, and therefore do not account for land subsidence magnitude and increased development of topographic depressions, or the increased flood exposure, or the loss of land to water in coastal areas. This aspect also links with the point above, given that similar risk levels are found across metropolitan cities that appear as mostly stable according to satellite observations but are moderately/highly vulnerable (e.g. Milano, mostly mapped as R2), and cities that have been widely impacted by land subsidence over the last decades (e.g. Bologna); in the latter case, despite the large extent of the renown subsiding land, the amount and size of zones affected by differential displacement exceeding the adopted thresholds are relatively limited, hence most of the built-up area results in medium risk (R2) levels, same as for other cities.

References

1. Pesaresi, M.; Panagiotis, P. *GHS-BUILT-C R2023A - GHS Settlement Characteristics, derived from Sentinel2 composite (2018) and other GHS R2023A data. European Commission, Joint Research Centre (JRC)*; 2023;
2. Marconcini, M.; Metz-Marconcini, A.; Üreyen, S.; Palacios-Lopez, D.; Hanke, W.; Bachofer, F.; Zeidler, J.; Esch, T.; Gorelick, N.; Kakarla, A.; et al. Outlining where humans live, the World Settlement Footprint 2015. *Sci. Data* **2020**, *7*, 1–14, doi:10.1038/s41597-020-00580-5.
3. Rosen, P.A.; Hensley, S.; Joughin, I.R.; Li, F.K.; Madsen, S.N.; Rodriguez, E.; Goldstein, R.M. Synthetic aperture radar interferometry. *Proc. IEEE* **2000**, *88*, 333–380, doi:10.1109/5.838084.
4. Crosetto, M.; Solari, L.; Mróz, M.; Balasis-Levinsen, J.; Casagli, N.; Frei, M.; Oyen, A.; Moldestad, D.A.; Bateson, L.; Guerrieri, L.; et al. The evolution of wide-area DInSAR: From regional and national services to the European ground motion service. *Remote Sens.* 2020, *12*, 2043, doi:10.3390/RS12122043.
5. EEA *European Ground Motion Service: Ortho – Vertical Component 2018-2022 (vector), Europe, yearly, Oct. 2023*; 2023;
6. EEA *European Ground Motion Service: Ortho – East-West Component 2018-2022 (vector), Europe, yearly, Oct. 2023*; 2023;
7. EEA *European Ground Motion Service: Calibrated 2018-2022 (vector), Europe, yearly, Oct. 2023*; 2023;
8. Cigna, F.; Tapete, D. Urban growth and land subsidence: Multi-decadal investigation using human settlement data and satellite InSAR in Morelia, Mexico. *Sci. Total Environ.* **2022**, *811*, 152211, doi:10.1016/j.scitotenv.2021.152211.
9. Cigna, F.; Tapete, D. Present-day land subsidence rates, surface faulting hazard and risk in Mexico City with 2014–2020 Sentinel-1 IW InSAR. *Remote Sens. Environ.* **2021**, *253*, 1–19, doi:10.1016/j.rse.2020.112161.
10. Cigna, F.; Tapete, D. Satellite InSAR survey of structurally-controlled land subsidence due to groundwater exploitation in the Aguascalientes Valley, Mexico. *Remote Sens. Environ.* **2021**, *254*, 1–23, doi:10.1016/j.rse.2020.112254.
11. Ohenhen, L.O.; Shirzaei, M.; Barnard, P.L. Slowly but surely: Exposure of communities and infrastructure to subsidence on the US east coast. *PNAS Nexus* **2024**, *3*, pgad426, doi:10.1093/pnasnexus/pgad426.
12. Ohenhen, L.O.; Shirzaei, M. Land Subsidence Hazard and Building Collapse Risk in the Coastal City of Lagos, West Africa. *Earth's Futur.* **2022**, *10*, e2022EF003219, doi:https://doi.org/10.1029/2022EF003219.
13. Garg, S.; Motagh, M.; Indu, J.; Karanam, V. Tracking hidden crisis in India's capital from space: implications of unsustainable groundwater use. *Sci. Rep.* **2022**, *12*, 651, doi:10.1038/s41598-021-04193-9.
14. CEN *Eurocode 7: Geotechnical design - Part 1: General rules [EN 1997-1]. Authority: The European Union Per Regulation 305/2011, Directive 98/34/EC, Directive 2004/18/EC.*; 2004;

15. Bouwer, H. Land Subsidence and Cracking Due to Ground-Water Depletion. *Groundwater* **1977**, *15*, 358–364, doi:10.1111/j.1745-6584.1977.tb03180.x.

16. Skempton, A.W.; McDonalds, D.H. Allowable settlements of buildings. In Proceedings of the Proc. ICE, London, 5; 1956; pp. 727–768.

17. Tandanand, S.; Powell, L.R. *Determining horizontal displacement and strains due to subsidence. Report of Investigations n.9358*; U.S. Department of the Interior, Bureau of Mines, 1991;

18. Burland, J.B.; Wroth, C.P. Settlement of Buildings and Associated Damage. In Proceedings of the SOA Review, Proc. Conf. Settlement of Structures, Pentech Press, Cambridge, London; 1974; pp. 611–654.

19. Peduto, D.; Nicodemo, G.; Maccabiani, J.; Ferlisi, S. Multi-scale analysis of settlement-induced building damage using damage surveys and DInSAR data: A case study in The Netherlands. *Eng. Geol.* **2017**, *218*, 117–133, doi:10.1016/j.enggeo.2016.12.018.

20. Sanabria, M.P.; Guardiola-Albert, C.; Tomás, R.; Herrera, G.; Prieto, A.; Sánchez, H.; Tessitore, S. Subsidence activity maps derived from DInSAR data: Orihuela case study. *Nat. Hazards Earth Syst. Sci.* **2014**, *14*, 1341–1360, doi:10.5194/nhess-14-1341-2014.

21. Zhu, M.; Wan, X.; Fei, B.; Qiao, Z.; Ge, C.; Minati, F.; Vecchioli, F.; Li, J.; Costantini, M. Detection of Building and Infrastructure Instabilities by Automatic Spatiotemporal Analysis of Satellite SAR Interferometry Measurements. *Remote Sens.* **2018**, *10*, 1816, doi:10.3390/rs10111816.

22. Qu, F.; Zhang, Q.; Lu, Z.; Zhao, C.; Yang, C.; Zhang, J. Land subsidence and ground fissures in Xi'an, China 2005–2012 revealed by multi-band InSAR time-series analysis. *Remote Sens. Environ.* **2014**, *155*, 366–376, doi:10.1016/J.RSE.2014.09.008.

23. Zuccarini, A.; Giacomelli, S.; Severi, P.; Berti, M. Long-term spatiotemporal evolution of land subsidence in the urban area of Bologna, Italy. *Bull. Eng. Geol. Environ.* **2023**, *83*, 35, doi:10.1007/s10064-023-03517-5.